NTNU

Norwegian University of
Science and Technology

# Producing Steel Fiber Reinforced Polymer Composite Pipes

Daniel Tran

Materials Technology
Submission date: June 2016
Supervisor: Andreas Echtermeyer, IPM
Co-supervisor: Nils Petter Vedvik, IPM

Norwegian University of Science and Technology
Department of Engineering Design and Materials

NTNU - NORWEGIAN UNIVERSITY
OF SCIENCE AND TECHNOLOGY
DEPARTMENT OF ENGINEERING DESIGN
AND MATERIALS

# MASTER THESIS SPRING 2016
# FOR
# STUD.TECHN. DANIEL TRAN

**Producing Steel-Fiber-Reinforced Polymer Composite Pipes**

***Produksjon av kompositt rør i stål armert plast***

Pipes are major components used in the offshore and processing industry. This project shall investigate novel ways to make composite pipes. Pipes will be made with steel fibers on a filament winding machine. New production methods and winding patterns shall be explored. The properties and performance will be tested of the finished products.

**Formal requirements:**

Three weeks after start of the thesis work, an A3 sheet illustrating the work is to be handed in. A template for this presentation is available on the IPM's web site under the menu "Masteroppgave" (https://www.ntnu.edu/web/ipm/master-thesis). This sheet should be updated one week before the master's thesis is submitted.

Risk assessment of experimental activities shall always be performed. Experimental work defined in the problem description shall be planed and risk assessed up-front and within 3 weeks after receiving the problem text. Any specific experimental activities which are not properly covered by the general risk assessment shall be particularly assessed before performing the experimental work. Risk assessments should be signed by the supervisor and copies shall be included in the appendix of the thesis.

The thesis should include the signed problem text, and be written as a research report with summary both in English and Norwegian, conclusion, literature references, table of contents, etc. During preparation of the text, the candidate should make efforts to create a well arranged and well written report. To ease the evaluation of the thesis, it is important to cross-reference text, tables and figures. For evaluation of the work a thorough discussion of results is appreciated.

The thesis shall be submitted electronically via DAIM, NTNU's system for Digital Archiving and Submission of Master's theses.

Torgeir Welo
Head of Division

Andreas Echtermeyer
Professor/Supervisor

NTNU
Norges teknisk-naturvitenskapelige universitet
Institutt for produktutvikling og materialer

# Abstract

This study has introduced a novel non-annealed stainless steel fiber with 8 $\mu m$ diameter to make a steel fiber reinforced polymer composite pipe. The primary objective was to make the pipes by the filament winding method. The aim was to report on the mechanical properties, and failure modes of these stainless steel fiber reinforced polymer composite pipes with a ductile epoxy resin system and to evaluate their performance for potential applications in the offshore industry.

The mechanical behavior under quasi-static compression was evaluated experimentally in both axial and radially to the hoop directions, along with the in-plane shear properties. The in-plane mechanical properties were determined by use of resistance strain gauge measurements bonded to the axial and hoop directions of the test samples. Also, their buckling behavior under external pressure was evaluated experimentally to understand their buckling behavior. Microscopy, burn-off test, and thickness measurements were performed on the produced test samples to determine the volume fraction of fiber, void content, and thickness.

Stainless steel fiber reinforced polymer composite cylindrical pipes with $\pm 55^{\circ}$ layup, and different thickness (three and six layers) were successfully made by the filament winding method. Test results indicate that the steel fiber reinforced polymer composites exhibit a much higher strain-to-failure than a typical UD carbon fiber composite (almost three times) combined with a high stiffness (about 80 $GPa$). Also, the SFRP composites exhibit similar ductile deformation behavior to that of the dry UD continuous steel fiber, i.e., an initial elastic response, a definite yield point and consecutive plastic and strain hardening behavior.



*Keywords*: Polymer-matrix composites (PMCs), Stainless steel fiber, Filament winding, Quasi-static compression testing, External pressure testing

# Sammendrag

Hovedmålet med denne oppgaven var å undersøke potensialet for en ny fibertype for anvendelse i vikling av plastkomposittrør. I denne oppgaven er det blitt brukt en-retnings kontinuerlige rustfritt stålfiber med en diameter på 8 $\mu m$ for å utvikle en stålfiberarmert plastkomposittrør. Målet var å rapportere om rørenes mekaniske egenskaper og skadeutvikling. Et annet mål var å evaluere ytelsen til rørene for finne potensielle deres potensielle bruksområder i offshore industrien.

Rørene ble testet for ytre trykk, og kvasistatiske kompresjonsbelastningsforhold. De mekaniske egenskapene ble bestemt ved bruk av strekklapper limt til i den aksiale- og bøyleretningen av the sylindriske testprøvene. Data i form av spenninger og belastninger fra disse strekklappene ble registrert underveis av testene og stress- belastningskurver ble beregnet for å finne de elastiske og styrkeegenskapene til materialet. Mikroskopi, burn-off test, og tykkelsesmålinger ble gjennomført for å vurdere kvaliteten av de produserte prøvene for å bestemme volumfraksjon fiber, hulromsinnhold og tykkelse.

Rustfritt stålfiberarmert plastkomposittrør med $\pm 55°$ opplegg, og forskjellig tykkelse (tre og seks lag) lagd med viklemetoden har blitt vellykket. Testresultatene viser at de stålfiberarmerte plastkomposittrørene har en mye høyere strekkbelastning enn et typisk UD karbonfiberkompositt (nesten tre ganger) kombinert med en høy stivhet (omtrent 80 $GPa$). De stålfiberarmerte komposittrørene viser lignende duktil oppførsel som for stålfiberen, dvs. først en elastisk reaksjon, etterfulgt av et bestemt flytepunkt og plastisk oppførsel.

*Nøkkelord*: Polymerekompositter, Rustfritt stålfiber, Vikling, Kvasistatisk kompresjonstesting, Eksternt trykktesting

# Table of Contents

# Preface

This master's thesis in TMM4911 Materials was written spring semester 2016 at the Norwegian University of Science and Technology, as part of the specialization course TMM4511 Materials, TMM4175 Polymers and Composites and TMT4242 Steel Offshore.

The motivation for this thesis is first and foremost my interest for both metals and composites. The idea to combine the two fields was proposed by Professor Andreas Echtermeyer when I was struggling to find an interesting topic for my thesis. During this thesis, I was part of the composite group at the Department of Engineering Design and Materials (IPM) where I have attempted to produce a stainless steel fiber reinforced polymer composite made by filament winding. This master's thesis is a continuation of my work done during my project thesis autumn semester 2015.

Since steel fibers are a new type of fibers, they are really hard to get a hold of as a student. Although frustrating at times, having spent my whole project thesis waiting for the steel fibers it was a relief to finally see them arrive at the office of IPM late december and ready for use in my master's thesis. Hopefully, with all its ups and downs this master's thesis will describe my long journey and dedication to filament wind steel fiber reinforced polymer composite pipes.

I would like to thank my supervisor Professor Andreas T. Echtermeyer for all the help and guidance along the way, and helping me find an interesting topic to explore. This work would not have been feasible without him. I would also like to express my gratitude to the people supporting this thesis such as my co-supervisor Nils Petter Vedvik, Kaspar Lasn for with the filament winding machine. Carl Magnus Midtbø for assistance in the workshop and instrumentation. The staff of IPM for friendly and professional help with papers and contracts. Last but not least, I would like to thank co-students at room A-447 for the pleasant working environment at the office.

Trondheim, June 10th 2016

.....

Daniel Tran
Stud.Techn.

# List of Figures

# List of Tables

# Symbols and Abbreviations

### Symbols

| | |
|---|---|
| $E$ | Young's modulus. |
| $E_1$ | Young's modulus in the longitudinal direction of the composite |
| $E_2$ | Young's modulus in the transverse direction of the composite |
| $\theta$ | Winding angle |
| $\sigma_{axial}$ | Axial stress |
| $\sigma_{hoop}$ | Hoop stress |
| $\tau_{12}$ | In-plane shear stress |
| $\gamma_{12}$ | In-plane shear strain |
| $\alpha$ | Winding angle |
| $\sigma$ | Stress |
| $\epsilon$ | Strain |
| $\epsilon_{axial}$ | Failure strain in axial direction |
| $\epsilon_{hoop}$ | Failure strain in hoop direction |
| $\epsilon^f_{axial}$ | Axial failure strain |
| $\epsilon^f_{hoop}$ | Hoop failure strain |
| $d_f$ | Diameter of filaments |
| $L$ | Unsupported length of cylinder |
| $L_o$ | Overall length of cylinder |
| $P$ | External pressure |
| $P_{cr}$ | Critical buckling pressure |
| $P_{exp}$ | Experimental buckling pressure |
| $A_f$ | Cross-sectional area of fiber |
| $A_o$ | Original cross-sectional area of the sample |
| $a$ | Mean shell radius |
| $n$ | Number of circumferential lobes formed |
| $D$ | Diameter of cylinder pipe |
| $D_i$ | Inner diameter of cylinder pipe |
| $X_1$ | Axial strength |
| $Y_2$ | Hoop strength |
| $S_{12}$ | Shear strength |

# Symbols and Abbreviations (Continued)

### Symbols

| | |
|---|---|
| $t$ | Wall thickness of pipe |
| $\nu$ | Poisson's ratio |
| $\nu_f$ | Poisson's ratio of fiber |
| $\nu_m$ | Poisson's ratio of matrix |
| $\nu_{12}$ | In-plane Poisson's ratio |
| $V_f$ | Volume fraction of fiber |
| $V_m$ | Matrix volume fraction |
| $m_f$ | Mass of fibers |
| $m_c$ | Mass of composite |
| $W_f$ | Weight fraction of fiber |
| $W_c$ | Weight fraction of composite |
| $\rho_{composite}$ | Density of composite |
| $\rho_{ct}$ | Theoretical density of composite |
| $\rho_{ce}$ | Experimental density of composite |
| $\rho_f$ | Density of fiber |
| $\rho_m$ | Density of matrix |
| $G$ | Shear modulus. |
| $G_f$ | Shear modulus of fiber |
| $G_m$ | Shear modulus of matrix |
| $G_{12}$ | In-plane shear modulus |
| $E_{1f}$ | Modulus of elasticity in the longitudinal direction of the fiber. |
| $E_{1m}$ | Modulus of elasticity in the longitudinal direction of the matrix |
| $V_v$ | Void fraction of composite |
| $R$ | Radius of cylinder pipe |
| $\epsilon_{ULT}$ | Ultimate failure strain |
| $\sigma_{UTS}$ | Ultimate tensile strength |

# Symbols and Abbreviations (Continued)

### Abbreviations

| | |
|---|---|
| NTNU | Norwegian University of Science and Technology |
| IPM | Department of Engineering Design |
| GFRP | Glass fiber reinforced polymer |
| CFRP | Carbon fiber reinforced polymer |
| SFRP | Steel fiber reinforced polymer |
| UD | Unidirectional |
| ASTM | American Society for Testing and Materials |
| HSE | Health safety and environment |
| FE | Finite Element |

### Standards

| | |
|---|---|
| ASTM D3878 | Standard Terminology for Composite Materials |
| ASTM D3171 | Standard Test Methods for Constituent Content of Composite Materials |
| ASTM D2734 | Standard Test Methods for Void Content of Reinforced Plastics |
| ASTM D2996 | Standard Specification for Filament-Wound "Fiberglass" (Glass-Fiber-Reinforced Thermosetting-Resin) Pipe |
| ASTM D2924 | Standard Test Method for External Pressure Resistance of "Fiberglass" (Glass-Fiber-Reinforced Thermosetting-Resin) Pipe |
| ASTM D2343 | Standard Test Method for Tensile Properties of Glass Fiber Strands, Yarns, and Rovings Used in Reinforced Plastics |
| ASTM E2954 | Standard Test Method for Axial Compression Test of Reinforced Plastic and Polymer Matrix Composite Vertical Members |
| DNV-OS-C501 | Composite Components - OFFSHORE STANDARD |
| DNV-RP-C205 | ENVIRONMENTAL CONDITIONS AND ENVIRONMENTAL LOADS |

# 1 General Introduction

Traditionally, offshore structures have been fabricated with moderate strength steels with yield strengths up to 350 MPa. However, there has been a significant growth over the years in the use of advanced composites in the offshore engineering industry, primarily driven by a desire to save weight and cost. However, the high cost of carbon fiber has limited their widespread use in the offshore industry. Especially with today's ongoing global oil and economic crisis, the need for newer and cheaper yet reliable materials has become more vital as cost efficiency has become a major success factor for whether a company will hold or buckle [2, 3, 4]. Nevertheless, change in the industry is needed, and this is the perfect opportunity to think creatively and head into a different direction.

Steel itself is not a new reinforcing material and typically used in tires and conveyor belts in the form of continuous wires to reinforce rubber and in the form of cords and filaments for reinforcement of concrete. In these applications, steel wires or filaments with a diameter of about 150 $\mu m$ or higher are commonly made of high carbon steel that has a high strength but limited ductility in the as-drawn state. The steel is utilized in these applications to increase the stiffness and strength of the base material (e.g. steel wires in rubber or concrete), rather than ductility. Ultra thin unidirectional steel fibers have for a long time not been industrially attractive to mass manufacture because of extensive research and development cost. The main challenges of producing thin steel fibers have been their low fracture strength and strain at fracture, as they were weak and brittle. However, until recently, a new class of stainless steel fibers of continuous unidirectional metallic fibers has been developed and become available for use in polymer composites. They exhibit high temperature and corrosion resistant with excellent thermal and electric conductivity. These steel fibers combine the flexibility of traditional fibers together with high stiffness and strength.

Pipes are major components used in the offshore and processing industry, and in the present work, UD steel fibers with a diameter of 8 $\mu m$ has been used to make a steel fiber reinforced polymer composite pipe to investigate if they can be suitable for offshore applications. The small diameter of these stainless steel fibers is in itself an impressive technological feat seen in the light that the average diameter of a human hair is about 80 $\mu m$. It is important to explore new application areas of these new type of fibers because they can become useful in the not just for the offshore industry, but for other industries as well.

## 1.1 Problem Statement

Many authors have investigated the mechanical behavior of GFRP and CFRP composite cylinders, but the scientific literature that describes the use of steel fibers as a reinforcing

material in polymer composites is very limited. However, the literature on steel fibers grows fast, which indicates the need for cheaper and tougher materials.

So far, research on unidirectional (UD) continuous stainless steel fibers has not used steel fiber reinforcement with a diameter less than 30 $\mu m$ in polymer composites. Also, the majority of published work on stainless steel fiber polymer composites up to now have dealt only with UD cross-ply composites, and steel fiber mats, but not for curved structures such as filament-wound cylindrical composite pipes. A characterization of the mechanical properties and strength parameters for filament wound component compared to flat laminated samples is of particular interest in understanding the material's behavior when subjected to loading modes such as compressive and external pressure during its service life.

Currently, stainless steel fibers are not yet commercially used as reinforcement in polymer composites and is limited to other applications. They are, for instance, employed in heat-resistant textiles, electrically conductive textiles, gas burner membranes or tubes, conductive plastics or for EMI-shielding (electromagnetic interference shielding), heating elements, and electrostatic discharge (ESD) applications [1]. But is it plausible to use stainless steel fibers to filament wind a cylindrical polymer composite pipe? If so, can they be utilized for offshore pipes in the future?

## 1.2 Literature Review

This section includes a literature review on fibers and the current state of research for stainless steel fibers in polymer composites.

### 1.2.1 Traditional Fibers and Stainless Steel Fibers

The typical reinforcing fibers such as glass fibers and carbon fibers have a limited strain-to-failure (only 2%), which can result in sudden material disintegration and collapse and is very unpredictable. The toughness of polymer composites reinforced with these fibers is intrinsically limited due to the fibers. Hence, for traditional composites the focus has rested on enhancing the toughness through the use of ductile matrices and adhesion improvements [5]. The composites ductility can be improved give a pseudo-ductile behavior by choosing a reinforcing fiber with a higher strain-to-failure. Other fibers like polymeric and natural fibers such as silk can offer higher strain-to-failure (15–30%) but exhibit much lower stiffness (less than 30 GPa), which limits their use in structural applications. Fibers which simultaneously combine a high stiffness with a high failure strain are difficult to find. Table 1.1 shows that a trade-off exists between the stiffness and the failure strain.

Throughout this thesis, the toughness for a single fiber or composite is defined as the area underneath the stress-strain curve. The toughness represents the energy dissipated

per volume during deformation and fracture of a single fiber or composite due to matrix cracks, fiber/matrix interphase debonding or growth of delaminations.

Stainless steel fiber has no equal when both high stiffness and high ductility is the goal. Steel holds a unique characteristic that its strain-to-failure can be altered by annealing (heat treatment) them without affecting its stiffness. Annealing can increase their strain-to-failure by up to 20%, which is 10 times higher than the strain-to-failure of carbon fiber. The stiffness of stainless steel fiber is around 193 GPa, which is close to the stiffness of carbon fiber (230 GPa). Thus, a whole range of ductile steel fibers can be created, which combines both high stiffness (193 GPa) and high strain-to-failure (20%). Due to extensive research and development cost, steel fibers have for a long time not been industrially attractive to mass manufacture as the main challenges of producing steel fibers have been their low fracture strength and strain at fracture, as they were weak and brittle.

**Table 1.1:** Table representing fiber types with their advantages and disadvantages.

| | Stiffness | Elongation | Toughness | Density | Cost |
|---|---|---|---|---|---|
| Steel fiber | ✓ | ✓ | ✓ | ✗ | ✓ |
| Carbon fiber | ✓ | ✗ | ✗ | ✓ | ✗ |
| Glass fiber | ✗ | ✗ | ✗ | ✓ | ✓ |

Raw steel is a relatively cheap material (1 $\$/kg$) compared to carbon fibers (10 $\$/kg$). However, expensive alloying elements must be added to achieve stainless steel, thus bringing the price up to par with carbon fiber. But recently novel processing methods has made it possible to substitute the more expensive alloying elements with cheaper ones to reduce cost down to about one-fourth the price of carbon fiber (2.5 $\$/kg$).

The steel fibers used in this thesis have a diameter of 8 $\mu m$ and consists of non-annealed 316L stainless steel alloy with the composition expressed in mass fraction reported in Table 1.2. The steel fibers are made by pulling multiple steel wires through drawing dies typically made of diamond or carbide called a bundled drawing process. Each wire can be drawn multiple times until it becomes a thin fiber of the desired size. Annealing (heat treatment) between two drawing steps can make the steel wires easier to pull through the drawing dies. A higher strain-to-failure can be accomplished by annealing the fibers at $\geq$ 800°C, but at the expense of lower yield strength. The stainless steel fiber filaments produced with the bundle drawing process can have a diameter between 5 to 100 $\mu$m.

**Table 1.2:** Chemical composition ($wt\%$) of the non-annealed steel fibers [1].

| Composition | The alloying elements provides the following advantages |
|---|---|
| $C \leq 0.05\%$ | The carbon content is lower than 0.05% to increase the ductility by reducing martensite transformation. |
| $Mn \leq 5\%$ | The manganese content is lower than 5% to obtain deformable sulfide inclusions. |
| $Si \leq 2\%$ | The silicon content is lower than 2% to improve cold work hardening and increased strength. |
| $8 \leq Ni \leq 12\%$ | The nickel content is between 8 and 12% to give an austenitic crystal structure during drawing and after annealing treatments. |
| $15 \leq Cr \leq 20\%$ | The chromium content is between 15 to 20% to obtain excellent corrosion resistance. |
| $Mo \leq 3\%$ | The molybdenum content is lower than 3% to improve the corrosion resistance. |
| $Cu \leq 4\%$ | The copper content is limited to 4% to avoid wire rod rolling difficulties. |
| $N \leq 0.05\%$ | The nitrogen content is limited to 0.05% to avoid brittleness. |
| $S \leq 0.03\%$ | The sulfur content is lower than 0.03% to avoid brittleness and fractures. |
| $P \leq 0.05\%$ | The phosphorus content is limited to 0.05% to avoid wire rod rolling defects. |

The stainless steel wires are enveloped in an envelope material, such as iron or copper, to separate the individual wires from one another. Once the bundle of enveloped wires, is drawn to the desired diameter, the envelope material is removed by leaching. The metal envelope material has a lower chemical resistance and allows the stainless steel fibers to be freed from the envelope material in a leaching process quite efficiently. Using an alloy as described in Table 1.2 above makes it possible to draw the wire without fracture.

All the steel wires or filaments are produced simultaneously from a single drawing process and bundled together to form a *tow*. The tow is then wound directly into a spool with the required numbers of filaments. The fibers are commonly packaged in 3 K to 36 K tows. The term *tow* is commonly used with fibers and is usually expressed as a count, or K-number, which represents the number of steel wires or filaments in a steel fiber tow in thousands.

The fibers sustain considerable damage during processing as they rub against each other and the equipment. Therefore, a substance called *sizing* are coated on the fibers to protect them from wear. The sizing serves as a lubricant and antistatic agent, but also help to

make it possible to handle the steel fiber without losing its integrity. Furthermore, the sizing incorporates a coupling agent to promote bonding with the matrix in the composite, thus allowing for transferring of shear loads from the steel fibers to the matrix material. Without proper bonding, the fibers can slip in the matrix, causing localized failure. The sizing also prevents moisture attack and chemical degradation during storage or service life of the composite.

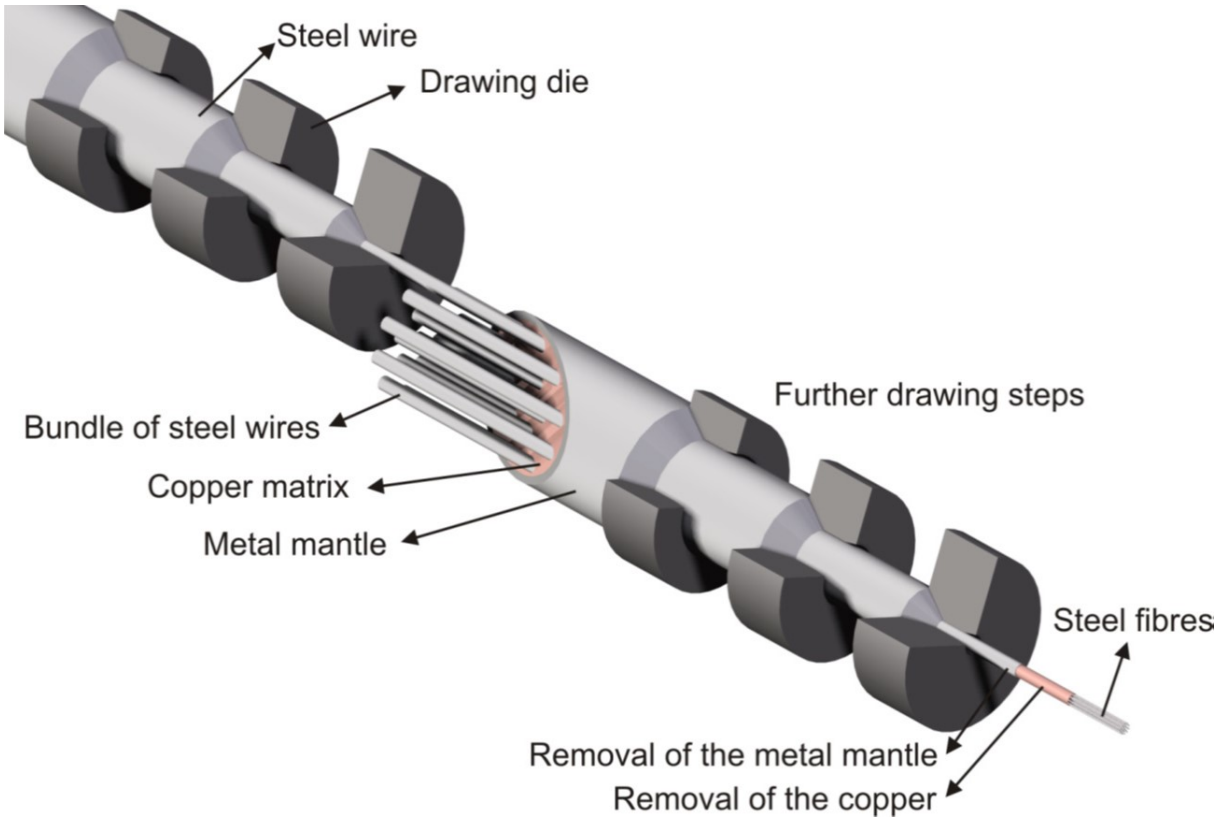


**Figure 1.1:** Illustration of the bundle drawing process to produce fine steel fibers [6].

Table 1.3 reports the mechanical properties of a single steel fiber, along with a representative tensile stress-strain curve shown in Figure 1.2.

**Table 1.3:** Mechanical properties of the non-annealed stainless steel fibers [1].

| Property | 8 $\mu m$ stainless steel fiber |
|---|---|
| Young's modulus, E | $\pm$ 193 $GPa$ |
| Strength, $\sigma_{UTS}$ | 660 $\pm$ 4 $MPa$ |
| Strain-to-failure, $\epsilon_{UTS}$ | $\pm$ 20% |
| Yield strength (0.2%), $\sigma_{yield}$ | $\pm$ 365 $MPa$ |

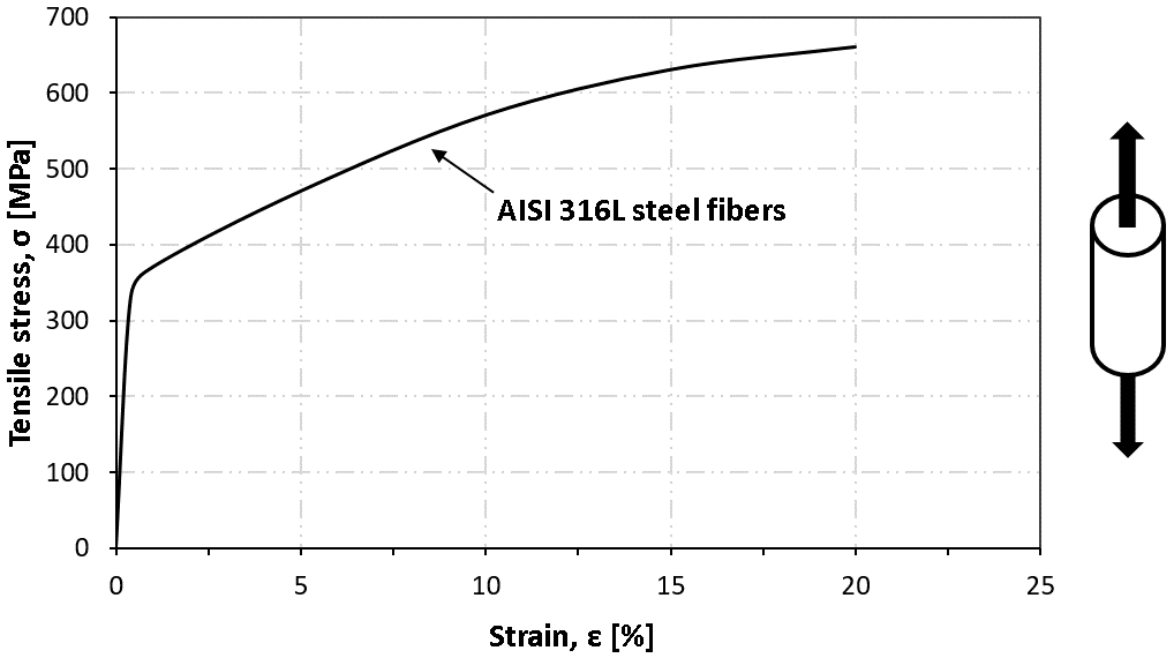


**Figure 1.2:** Representative engineering stress-strain curve of a single steel fiber found by fiber tensile testing.

### 1.2.2 Toughness in Composites

The structural advantages of advanced composites, such as carbon fiber/epoxy composites, is because of their high stiffness and strength including low weight. Hence, these materials have found broad applications in the aerospace, maritime, automobile and sports industries.

In compressive loading, the primary failure mechanisms that could occur is matrix cracking, delamination, fiber/matrix debonding, fiber fracture and kink band formation. The first three failure mechanisms are dominated by the matrix and the fiber/matrix interphase, while the last two is dominated by the fibers [8, 9].

A composite is composed of reinforcing fiber and matrix from different materials creating an interface between the two. The properties of these interfaces influence the mechanical properties of the composite. The definition of an interface in fiber composites is a surface formed by a common boundary of reinforcing fiber and matrix that is in contact with and maintains the bond in between for the transfer of loads. It has physical and mechanical properties that are unique from those of the fiber or the matrix [7].

The fiber/matrix interphase plays a significant role in controlling the mechanical behavior of composites. The optimal properties of the interphase are dependent on the fiber and matrix combination and the required mechanical behavior. Typically a compromise is needed to ensure a combination of a high crack initiation load, a high strength and high

fracture toughness. If the matrix is more brittle than the fibers, it can strongly influence the mechanical behavior of composites in the fiber direction. A higher adhesion may hinder the development of matrix cracks and lead to greater strength and strain-to-failure of the composite. In the case of a too high adhesion, however, the cracks may result in localization and magnification of the strain, which is likely to cause earlier failure of the fibers. Thus, an optimal level of adhesion is sought.

In more traditional composites such as glass, carbon or natural fiber composites, a higher adhesion can increase crack initiation loads and strength, but can decrease the energy needed for crack propagation. Damage initiation and propagation in traditional fiber composites have been studied extensively, but the damage behavior of steel polymer composites is still unknown due to the ductile nature of the stainless steel fibers.

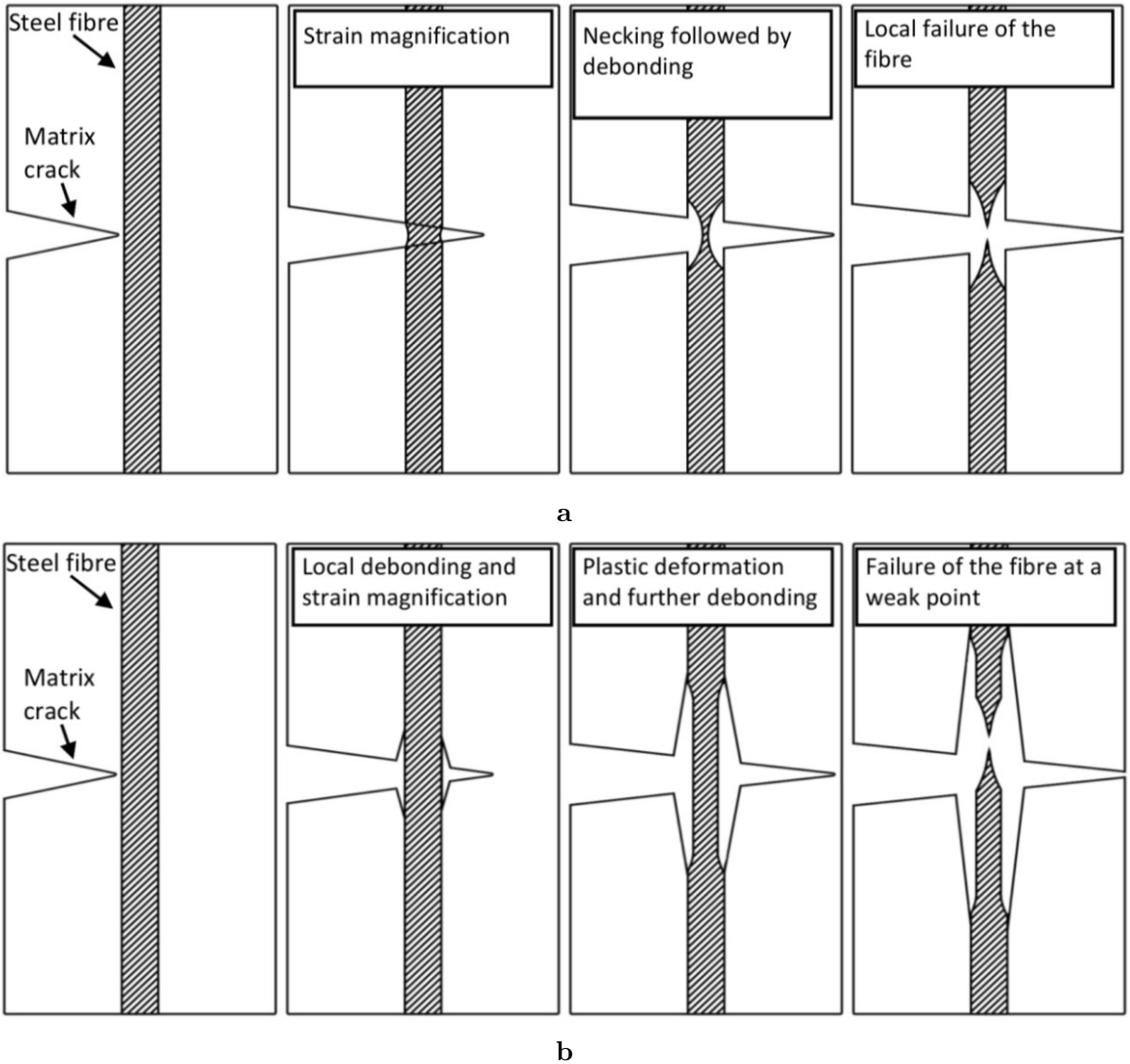


**Figure 1.3:** Hypotheses for failure mechanisms in a composite with ductile fibers and a brittle matrix [6]: (a) Hypothesis 1: Local strain magnification, necking of the fiber followed by debonding. (b) Hypothesis 2: Debonding of the fiber, strain magnification, necking at a local weak point.

Callens et al. [8] studied the effects of matrix ductility and proposed two hypothesis for the failure of a single steel fiber, in the case of brittle and ductile matrix. Figure 1.3a shows two possible explanations for the failure of a single fiber in a steel fiber composite with a brittle matrix (i.e. the matrix fails earlier than the fiber). The first hypothesis is because the interface is sufficiently strong to hinder debonding of the fiber. When a matrix crack approaches a fiber the externally applied strain is locally magnified resulting in plastic deformation of the steel fiber. Due to the Poisson contraction and plastic necking, the fiber debonds from the matrix. Further necking results in failure of the steel fiber. The second hypothesis (Figure 1.3b) implies that the interface is less strong, and when a matrix crack reaches a fiber, the fiber locally debonds from the matrix. Upon further loading, this locally debonded fiber propagate along the fiber/matrix interface, the area of local strain magnification increases and fiber is allowed to deform plastically. Then, final failure of the fiber occurs at its weakest point (most likely at a defect).

### 1.2.3 Previous Studies

Previous research has reported that composites reinforced with steel fibers possess a high stiffness combined with exceptional ductility and tensile failure strains well beyond 10% [9]. Callens et al. [8] [10] conducted an experiment where they found that the ductility and toughness of the composite were enhanced by choosing fibers that had a higher strain-to-failure. They incorporated woven quasi-UD steel fibers in an epoxy matrix and observed that the ductile steel fibers delivered composites with a high stiffness and a high strain-to-failure ratio up almost 20%, which is much greater than the typical composite. In another study, Callens [5] investigated the effect of weave architecture on the tensile and impact behavior of ductile stainless steel fiber/polyamide 6 composites. They tested and compared composites with three different weave architectures: a quasi-unidirectional weave, a basket weave, and a satin weave. Callens found that all weave architectures showed the same composite strain-to-failure. The composite with basket weave had lower stiffness and yield stress in comparison with the other two composites, which contributed to significant out-of-plane deformations observed during the tensile test. The impact penetration results showed that the high ductility of stainless steel fiber composites in tensile tests led into excellent impact performance. In another study [6], he used different silane coupling agents to modify the adhesion and found that it was possible to improve the adhesion strength. The higher adhesion increased the strength and strain-to-failure in tensile tests of UD and cross-ply composites with both brittle and ductile matrices

Allaer et al. [11] made steel fiber composite laminates by Vacuum Assisted Transfer Molding technique. Their objective was to report on the mechanical properties and failure modes of these stainless steel fiber composite laminates impregnated with a ductile epoxy resin system (EPIKOTE™ Resin MGS RIM 135 combined with EPIKURE™ Curing Agent MGS RIM H 137). They observed that under tension, steel fiber reinforced epoxy

exhibits similar ductile deformation behavior to that of the dry continuous steel fiber filaments, i.e., an initial elastic response, a definite yield point and consecutive plastic and strain hardening behavior up to 19.5% failure strain. They reported a difference in tensile and compressive behavior of the unidirectional steel fiber composite.

The studies mentioned above have reported on steel reinforcing materials in composites, using continuous annealed steel wires with diameters ranging from 30 mm to 100 mm, yielding relatively low fiber volume fractions.

## 1.3 Layer and Ply Definitions

The notation used to describe laminates in this thesis is based on the hand lay-up process. The laminate is built starting at the table surface, or bottom of the laminate, stacking layers on top of each other as the process progresses. Therefore, the laminate is given as a stacking sequence numbered starting at the bottom, and the angles are given from the bottom up. For layups using only a single material, and all the layers have the same thickness the layup is described by the orientation angles $[\pm\theta^\circ]$ forming an angle-ply layup with one $\theta$ oriented ply and one $-\theta$ oriented ply or $[\theta/-\theta]$. A subscript $n$ is used to indicate the number of layers that repeats and will be represented by the notation $[\pm\theta^\circ]_n$ or material used i.e. $\text{CFRP}_n$ for a carbon laminate with $n$ repeating layers. The same abbreviations will be used throughout this thesis and are as follows: glass fiber composite ($\text{GFRP}_n$), carbon fiber composite ($\text{CFRP}_n$) and steel fiber composite ($\text{SFRP}_n$).

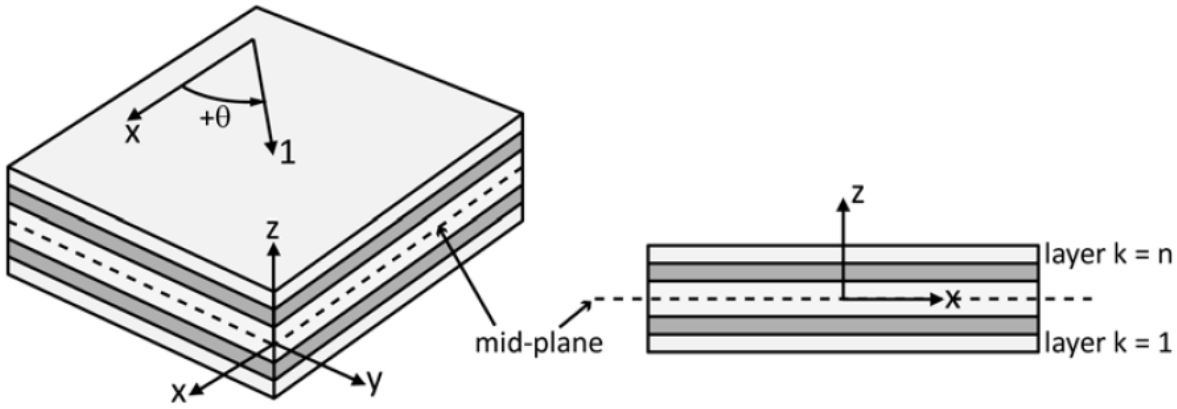


**Figure 1.4:** Laminate is showing mid-plane and definition of the positive orientation angle of a layer [7].

## 1.4 Objective and Outline

This thesis shall investigate the potential of a novel fiber type, stainless steel fiber, for application in filament wound composite pipes. The current study is an extension of earlier work and shall investigate the mechanical properties of ductile stainless steel fibers

in polymer composites. Stainless steel fibers are a novel reinforcement fiber for polymer composites, which combine a high stiffness and a high failure strain. Polymer composites made with these fibers could thus combine a high stiffness and high toughness, which is rare for traditional polymer composites. The in-plane mechanical behavior shall be investigated by quasi-static compression tests in both axial and ring material directions to understand their mechanical behavior and damage development. Also, the buckling properties shall be investigated using external pressure test to understand their buckling behavior. The performance of the produced stainless steel fiber composite samples will be evaluated to see if it is feasible to use them for offshore applications in the future.

The objectives of this thesis are:

- To filament wind a stainless steel fiber reinforced polymer composite pipe.
- To determine the material properties of stainless steel fiber composite pipes under compressive loading in axial and ring direction of the material.
- To understand their mechanical behavior (stiffness and damage development).
- To understand their buckling behavior under external pressure loading.
- To compare their mechanical and buckling properties with more traditional reinforcing fibers such as carbon fiber.

Following this introduction section is a section which is dedicated to explaining the design approach, all constituent materials used to produce the samples, and production method. Section 3 describes the use of simple theoretical micromechanical models to estimate the stiffness of steel fiber composites. Section 4 presents the experimental method which has been conducted to understand the mechanical behavior and damage development of stainless steel fiber composites. Section 5 presents the theoretical and experimental results and a comparison of the estimated stiffness of steel fiber composites to stiffness among other structural materials. Section 6 discusses the theoretical and experimental results. Section 7 presents the conclusions and recommendations for further work.

# 2 Composite Production Method

The following sections describe a natural progression of producing the pipes from design to production phase. The production method was developed regarding simple design, fast production speed, and the materials available. The design of the pipes was based on standards and guidelines of ASTM D2996 [12] and DNV [13, 14].

Many preliminary carbon prototype pipes were produced to ensure that the production method is consistent enough to produce the steel fiber pipes reliably. The principal steps of making an SFRP composite pipe should practically be analogous to that of the CFRP pipe so that as little as possible modifications to the filament winding machine is required. A description of all the data inputs is included so that the pipes can be reproduced without having to learn everything from scratch.

## 2.1 Filament Winding

The composite pipes with the epoxy matrix are produced using a filament winding method by the numerical-controlled winding machine MAW LS20 4/1 at IPM [15]. The machine has 4 degrees of freedom; mandrel rotation, delivery eye rotation, horizontal carriage movement along the mandrel and horizontal carriage movement normal to the mandrel. The machine consists of two units, a filament winding unit and a tensioning unit (METS-8). The filament winding unit controlled by the software *Winding Commander* imports the fiber paths generated by the software *Winding Expert*. The fiber spools are mounted in the tensioning unit on creel racks or tape racks and feed the fiber at a preset tension while the filament winding unit winds it onto the mandrel. The fiber goes through a resin bath where it gets impregnated before applying it to the mandrel. The wound component is cured in an electric oven before it is removed from the mandrel.

The filament winding production method is selected because it is a well-known method to produce cylindrical composite pipes in a semi-continuous process at low cost. The significant limitations of filament winding are size restrictions, geometric possibilities, the orientation of the fibers, and the surface finish of the final product. The winding angle is limited between 10 to 15° for low winding angle and 89° for a high winding angle. Unlike other methods such as vacuum infusion under pressure, the volume fraction of fiber is lower for filament wound components.

The *winding angle*, $\alpha$, as shown in Figure 2.1 is defined as the angle between the fiber and an imaginary X-axis going in the axial direction on the outer surface of the filament wound pipe. Hence, an orientation equal to zero means that the direction is parallel to the x-axis of the cylindrical pipe.

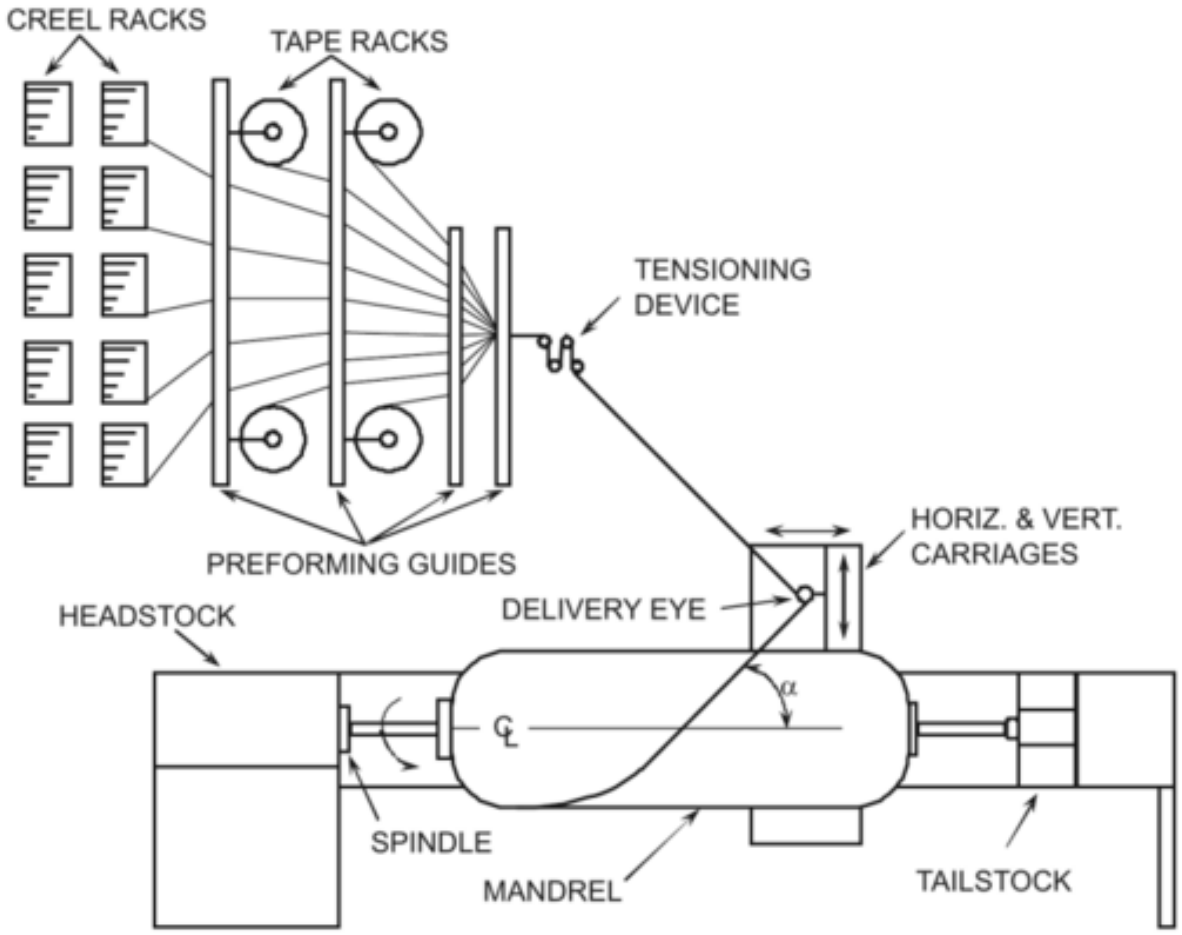


**Figure 2.1:** Illustration of the filament winding method to produce pipes [16].

## 2.2 Materials

NV Bekaert SV supplied the non-annealed AISI 316L stainless steel continuous fibers with a filament diameter of 8 $\mu m$ and an average density of 8.0 $g/cm^3$. These steel fibers consisted of 12 K untwisted filaments. The UD T700SC carbon fibers with a filament diameter of 7 $\mu m$ and an average density of 1.8 $g/cm^3$ were readily available at IPM. These carbon fibers consisted of 12 K untwisted filaments. The ductile epoxy resin system EPIKOTE$^{TM}$ Resin MGS RIMR 135 (diglycidyl ether of bisphenol A or DGEBA) was mixed with a liquid diamine hardener, EPIKOTE$^{TM}$ Curing Agent MGS RIMH 137. The mixing ratio of epoxy and hardener were 100:30, respectively [17]. Table 2.1 reports the mechanical properties of the constituent materials in the composite pipes.

A hollow steel pipe with 2000 $mm$ in length was used to wind the pipes. The mandrel has an outer diameter of 32 mm that limits the inner diameter $D_i$ of the pipes to 32 mm. The mandrel was readily available in the lab and chosen to save time and avoid the expense of making a new mandrel. To facilitate extraction of the pipe cut tool bore oil spray from WÜRTH was used.

**Table 2.1:** Mechanical properties of the constituent materials.

| Constituent materials | E $(GPa)$ | $\nu$ $(-)$ | $\sigma_{UTS}$ $(MPa)$ | $\epsilon_{failure}$ (%) | $\delta$ $(g/cm^3)$ |
|---|---|---|---|---|---|
| 316L stainless steel fibers[b] ($d = 8\ \mu m$) | 193 | 0.30 | 1700 | 19.0 | 8.0 |
| T700SC Carbon fiber[c] ($d = 7\ \mu m$) | 230 | 0.30 | 4900 | 1.2 | 1.8 |
| EPIKOTE MGS RIMR 135 epoxy resin[a] | 3.2 | 0.35 | 65 | 12 | 1.2 |

[a] Data obtained from technical data sheet [17]. [b] Annealed 316L stainless steel fibers data obtained from NV Bekaert SA [1]. [c] Data obtained from technical data sheet [18].

## 2.3 Design, Layup and Limitations

### 2.3.1 Design

As preparation for working on the master's thesis, a pressure vessel was filament wound in autumn of 2015 [19]. A preliminary production of a CFRP-pressure vessel with a $[89^{\circ}_2/\pm 12.5^{\circ}/89^{\circ}_2]$ layup was filament wound and tested for internal hydrostatic pressure. The pressure test revealed that the CFRP-pressure vessel was not water-tight, scrapping the designed solution. The scope of this master's thesis was revised to winding cylindrical pipes instead for testing under external pressure, as the primary objective was to make a filament wound SFRP composite to prove the concept.

From a production viewpoint, winding pipes are much simpler compared to pressure vessels because of the geometry. For pipes, there are no end-domes to take into consideration, which reduces the time required to setup the machine. For a cylindrical pipe almost any high-angle winding (between 20 to 90°) can be selected, which is a significant advantage over pressure vessel.

The limitations of the filament winding machine are the ability to wind long pipe sections due to the size the machine. Also, there is a limit for low-angle winding because there is no dome for the fibers to hold on to during transition of helical winding, which causes the fiber to slip off on the mandrel. A pin-wall clamped around the mandrel at each end could be used to give the fibers something to hold on during the transition period.

Production rates for filament winding vary widely because the size of the part and the mandrel type dictate the amount of time needed to setup and remove the part from the winding machine and mandrel. The fiber feed rate at dictates the production rate if setup and removal time are not considered. The fiber feed rates vary according to the strength of the fiber used, typically 10 - 35 m/min.

### 2.3.2 Layup

The layup (described by stacking sequence) of the individual layers and ply orientation angle has significant effects on the overall behavior and strength of the filament-wound components, and its mechanical properties. Therefore, a long while was spent on selecting the layup for the pipes.

The $[90°/0°/90°]_n$ cross-ply layup and $[\pm 55°]_n$ angle-ply layup were chosen for comparison in this study. The $[\pm 55°]_n$ angle-ply layup is an optimized version of the $[90°/0°/90°]_n$ cross-ply layup. The optimum winding angle can be found by netting analysis [20] with a 2:1 hoop-to-longitudinal strength ratio. The primary assumption in the netting analysis is that all the fibers carry the load neglecting the stiffness of the matrix [21].

The fiber orientation of the $[\pm 55°]_n$ layup enables all the fibers to be loaded evenly without shear. Several experimental tests and FE studies have confirmed that the $[\pm 55°]_n$ layup offers the best resistance to internal pressure but is not optimal for buckling under external loading, which is the primary load for immersed deep sea structures such as offshore oil and gas pipe lines [22].

Messager et al. [23] used optimization methods to select the best orientation to avoid buckling under external pressure. They found that wound pipes including 90° oriented plies about the tube axis show higher buckling stability than tubes with only ±55° layers for the same thickness. The fundamental idea for the cross-ply layup, $[90°/0°/90°]_2$, is that the 90° plies will give additional stability for the 0° and keep them in place during loading [23]. In reality, the manufacturing of cross-ply layups is not always as straightforward as the angle-ply layups.

While the $[90°/0°/90°]_n$ cross-ply layup is a simple layup for hand-layed laminates, it is challenging to wind in practice due to the small winding angles causing the fiber slip on the mandrel. As mentioned earlier, there is a limitation to the winding angle that used to filament wind the pipes. The lowest winding angle that is possible without fiber slippage is approximately 12.5°, while the highest winding possible is 89°. The resulting layups is therefore not a cross-ply $[90°/0°/90°]_n$, but instead a layup that is $[89_n°/\pm 12.5^{\circ}_n/89_n°]$, which is a symmetric quasi-isotropic laminate. The angle deviates about 1% and won't have much effect on the overall behavior of the laminate and will be considered to behave like a cross-ply laminate.

The $[\pm 55°]_n$ angle-ply layup has some advantages over the$[90°/0°/90°]_n$ cross-ply layup, due to how the helical and hoop winding works. The angle-ply layup has a shorter production time and requires less material to cover the mandrel, which is a significant advantage over the cross-ply layup. Winding with a small angle is avoided to remove any additional production steps and parts, to reduce costs and production time. Therefore, the angle-ply $[\pm 55°]_n$ layup was chosen over the $[90°/0°/90°]_n$ cross-ply layup.

The ±55° layers will require a transition area as the fibers are wrapped back and forth on the mandrel. The transition area at the pipe ends will be cut off as waste, and therefore, it is more beneficial to produce as long pipes as possible to reduce waste material.

### 2.3.3 Calculation of Fiber Length and Fiber Cross-sectional Area

It was critical to calculate exactly how much steel fiber that was available in the spool due to a limited supply of steel fiber. The fiber length was calculated by Eq. (2.1) since the fiber length per unit weight (YIELD $[km/g]$) is inversely proportional TEX $[g/km]$

$$TEX\left[g/km\right] = \frac{\pi d_f^2}{4}\rho_f K \tag{2.1}$$

Where TEX is the weight per unit length in $[g/km]$, K in thousands, $\rho_f$ is the density of fibers in $[g/cm^3]$, and $d_f$ is the diameter of the filaments in microns $[\mu m]$.

The supplied spool weighed 1 $kg$ with a density of the steel fibers being 8 $g/cm^3$ and the diameter of the filaments is 8 $\mu m$. The fiber length in the fiber spool was calculated to be approximately 220 $m$. After calculating the required fiber length for various combinations of thickness and lengths, a decision was made to wind a three and six layered composite pipe with a length of 400 mm. The three and six layered pipes would require approximately 65 m and 130 m of fiber, respectively. In total, the required fiber length to wind the two pipes is 195 m. Also, considerations for the need for extra fiber length to fasten the fiber to the mandrel, production errors, and additional fiber length for the tension system was taken into account. An additional 15 m of fiber length was, therefore, added to account for any production errors. Which in total requires 210 m of fiber to produce both pipes leaving only 10 m of fiber left on the spool. In addition to the calculations, the calculated fiber length was verified by cutting open a dry wound CFRP-prototype pipe and measuring the length of the fiber that was required to wind the pipes. This process was done three times to make sure that the numbers added up.

$$A_f[cm^2] = \frac{TEX\left[g/km\right]}{\rho_f\left[g/cm^3\right]} \tag{2.2}$$

Winding expert requires information about the cross-sectional area occupied by the fibers to be able to calculate the necessary number of cycles to cover the entire mandrel. The cross-sectional area occupied by the fibers when applied to the mandrel was calculated to be 5 mm using Eq. (2.2).

### 2.3.4 Concluding Remarks

Based on the materials available, assessment of design and production limitations the selected thickness and pipe length for the layup was an antisymmetric angle-ply layup $[\pm 55°]_3$ and $[\pm 55°]_6$ with a pipe length of 400 mm and an internal diameter of 32 mm. To save time on making several pipes it was decided to wind two pipes simultaneously on the same mandrel with different thickness now referred to as Pipe A and Pipe B. Table 2.2 summarizes the design specifications for the pipe. The analysis of winding angles requires several samples with varying degree to be included and has received much less attention.

**Table 2.2:** Design specifications for the pipes.

| What | Value |
|---|---|
| Winding angle | 55° |
| Layup | $[\pm 55°]_3$ , $[\pm 55°]_6$ |
| Internal diameter, $D_i$ | 32 $mm$ |
| Pipe length | 400 $mm$ |
| Reinforcement | Steel fiber |
| | Carbon fiber |

## 2.4 Method

The method section shall show natural progress of how to make the stainless steel fiber pipes, though describing only the most relevant and significant production procedures. The main steps in the producing the pipes are:

1. Preparing the winding machine.
2. Preparing the materials.
3. Winding the pipes.
4. Curing and extracting the pipes.

### 2.4.1 Winding Machine Programming

The fiber paths were generated according to the layup found in section 2.3 with the computer software Winding Expert made by Microsam (Appendix A). The software automatically calculates the fiber path coordinates for the mandrel based on the fiber band width, winding angle and pattern that was selected.

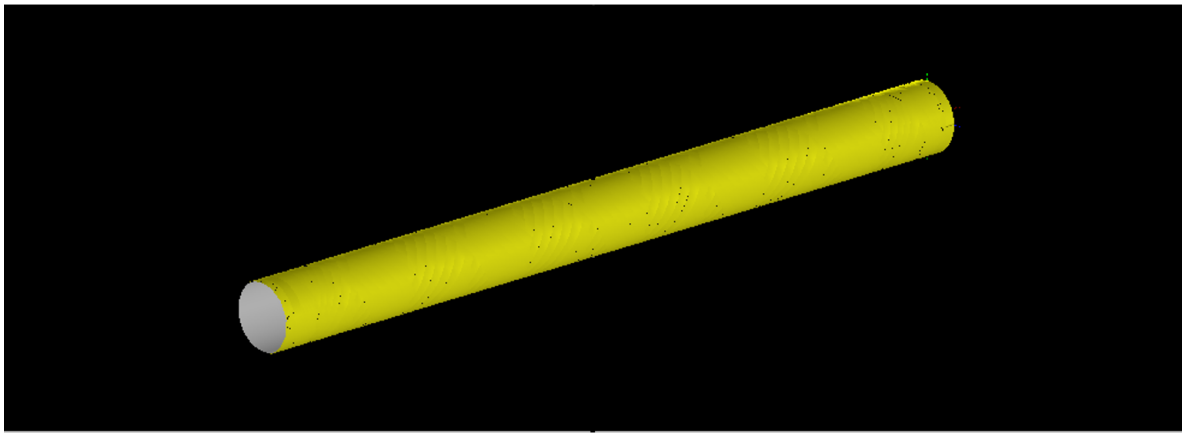

**Figure 2.2:** The picture is showing the virtual mandrel in Winding Expert.

The first step in Winding Expert was to create or import a virtual mandrel to the project; that represented the real mandrel. In this case, a new virtual mandrel was generated, as shown in Figure 2.2. Winding Expert only needs the diameter y (in mm) at any given position x-coordinate to define the whole mandrel. The mandrel definition file created in Winding Expert for this project is shown in Table 2.3. For a simple cylindrical pipe geometry, the starting frame (nr. 1) is set to length x = 0 with the diameter y set to 32 mm, and the ending frame (nr. 2) is set to length x = 400 mm with the diameter y set to 32 mm.

**Table 2.3:** Key points of the DXF file.

| Frame (nr.) | Length x (mm) | Diameter, y (mm) |
|---|---|---|
| 1 | 0 | 32 |
| 2 | 400 | 32 |

Figure 2.5 shows the reference system for the winding head and mandrel. For the winding head reference system is defined by its movement in the horizontal axes Y and Z, including rotation about an axis X. The mandrel reference system is only defined by the axes x and y-coordinates since the mandrel is cylindrical and symmetric about its x-axis along the longitudinal direction.

The second step was to set the winding parameters. A minimal distance Z was set to 35 mm to avoid collision of the winding eye with the mandrel. To wind the two pipes A and B on the same mandrel the Position length Y was utilized to move the virtual mandrel (400 mm long and 32 mm in diameter) along the longitudinal axis of the real mandrel. Since the actual mandrel is 2000 mm long with a 32 mm in diameter, there is a large area that can be used to move the virtual mandrel along the real mandrel. For Pipe A the Position length Y was set to 345 mm from the reference point, which becomes its starting

point A when winding the pipe. Similarly, for Pipe B the Position length Y was set 895 mm from the reference point, which becomes its starting B when winding the pipe.

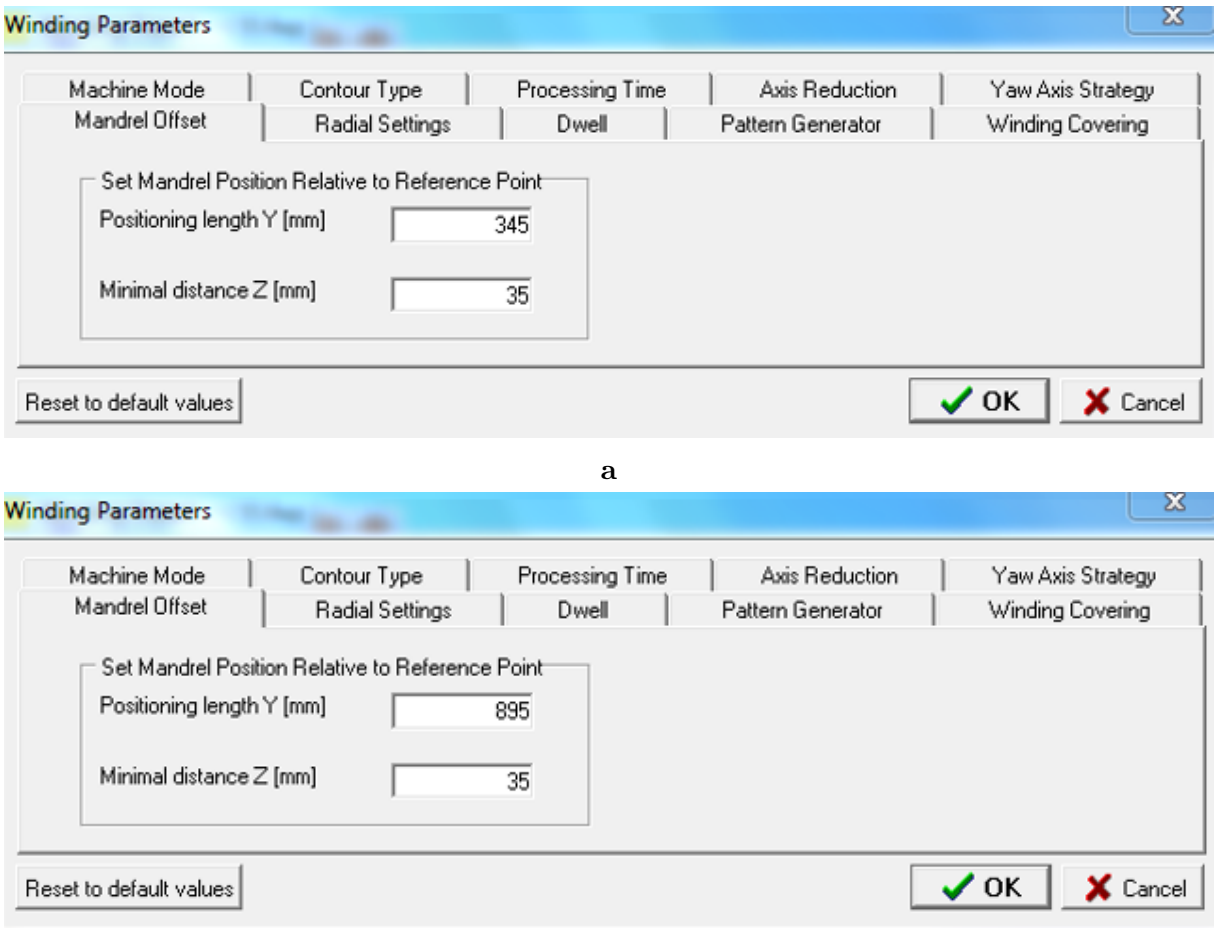


**Figure 2.3:** Winding parameters: (a) Winding parameters for Pipe A. (b) Winding parameters for Pipe B.

It is recommended to define these parameters first because the segments that are created later with Winding Expert is based on these parameters. Clicking on the segments and changing the minimal distance and Y-position after its creation will not change anything.

The third step is to build the layup in Winding Expert. The layup is built up off segments in the software, where each segment is defined by parameters such as fiber speed, winding angle, and band width, as shown in Figure 2.4. The winding angle was set to 55°, and the band width set to 5 mm. The band width was calculated from Eq. (2.2) above. The transition area was set to 50 mm for helical winding to avoid fiber slippage during production. Usually, an option for optimizing the pattern (consisting of segments) is available, but for unknown reasons, the program would freeze when attempting to optimize the pattern. Therefore, no optimization has been performed on the segments. An optimized pattern gives more accurate fiber placement during winding, which reduces fiber slippage, but for a simple pipe geometry, this shouldn't cause any problems. It was decided to wind only

one layer at a time to give full control over the process in case any machine errors occur, which reduces the risk of starting the entire process all over. Therefore, only one segment is needed to be defined. The winding input for Winding Expert is summarized in Table 2.4.

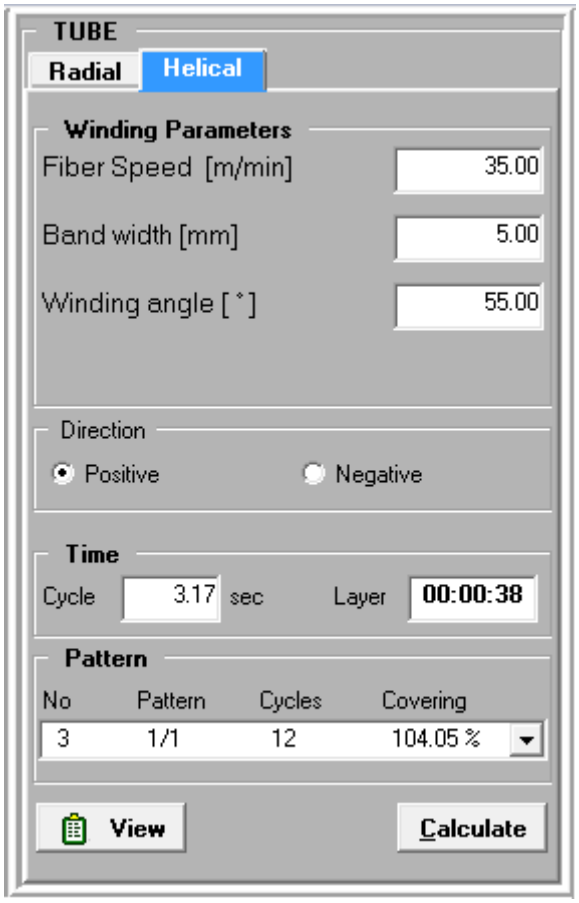


**Figure 2.4:** Winding parameters for the segment in Winding Expert.

Winding Expert calculated that it would take 12 cycles (successive returns of the winding eye starting from the starting point) to cover the entire mandrel surface, forming one layer consisting of two angled plies of $+55^{\circ}$ and $-55^{\circ}$. A test run was performed without any fiber before wet winding to ensure that the machine was correctly set up. The dry winding process is the same as wet winding without applying any resin to the reinforcement during winding. The dry winding verified the calculated required fiber length for winding, which was in good agreement with the calculated length found by Eq. (2.1).

Lastly, the segments in the project file are then imported into the program Winding Commander 8.0 where it is loaded and made ready for winding.

**Comments**

Many hours was spent on properly setting up the winding machine so that it would wind the helical layers correctly. During winding, there were periods where the machine would stop for unknown reasons and troubleshooting was time-consuming. For future winding,

a list of errors and how to troubleshoot them was made. The list saved a lot of time and was very helpful when the errors occurred. The troubleshooting list can be found in Appendix A.

**Table 2.4:** Summary of Winding Expert parameters.

| What | Value |
|---|---|
| Winding angle | 55° |
| Y-position (Pipe A) | 345 (mm) |
| Y-position (Pipe B) | 895 (mm) |
| Minimal distance, Z | 35 (mm) |
| Fiber speed | 35 (m/min) |
| Coverage | 104.05 (%) |
| Cycles | 12 |
| Band width | 5 (mm) |
| Pattern | 1/1 |
| Fiber tension | 80* (N) |

*The winding tension had to be lowered to 35 N during winding of the SFRP composite due to fiber breakage.

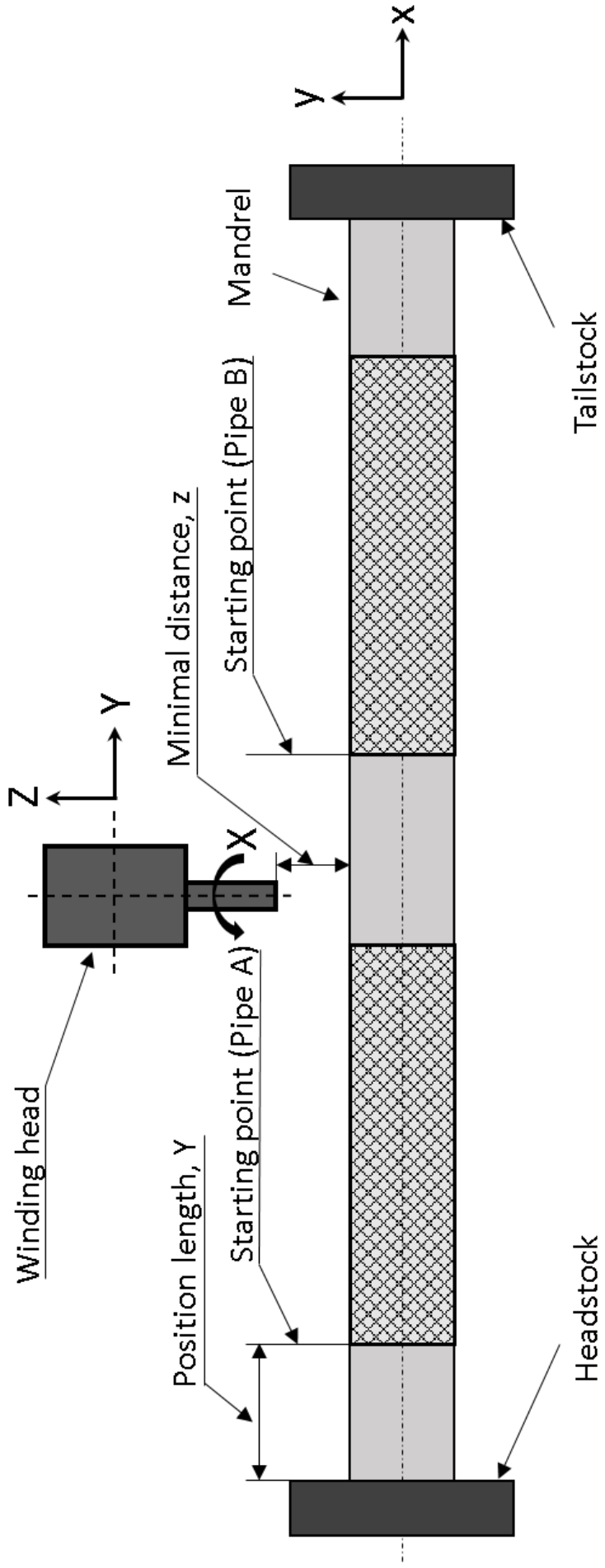


**Figure 2.5:** A picture illustrating the mandrel together with minimal distance, position length and, starting points A and B.

### 2.4.2 Fiber Spool and Tension System

Figure 2.6 shows the fiber spool mounted properly onto the creel rack inside the METS-8 tensioning unit and no modifications to the tensioning unit were required.

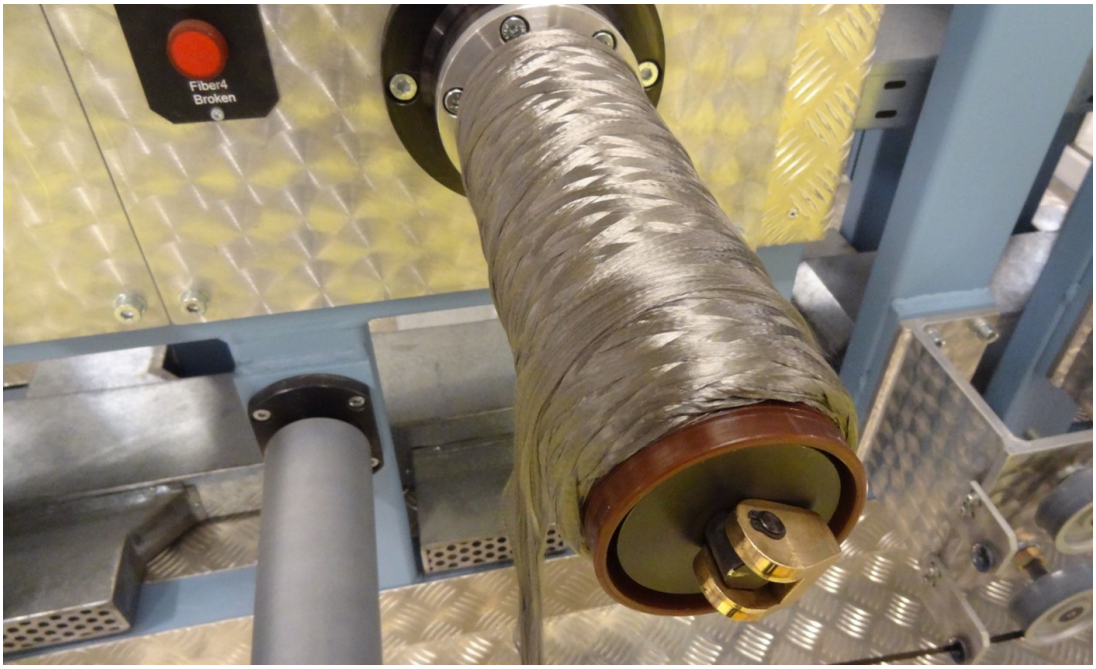


**Figure 2.6:** Steel fiber bobbin fitted into the METS-8 tension system.

Before pulling the fiber through the different rollers, as shown in Fig 2.11, the insert fiber button was activated. The fiber was fed through the resin carriage and winding head before tieing the fiber to the delivery eye, illustrated in Figure 2.8.

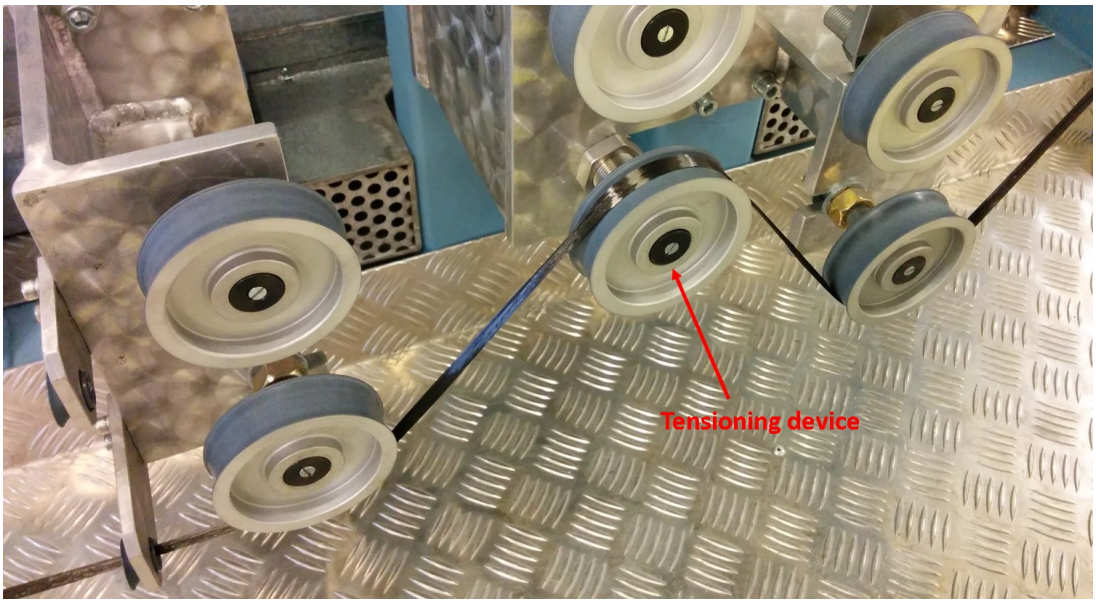


**Figure 2.7:** Picture showing the tensioning device with the fiber pulled through it.

The winding tension is set to 80 N to maximize the compression of the plies to remove entrapped air bubbles and excess resin when winding. The tensioning motors must be enabled, and the insert fiber button deactivated before the tension system can operate. Pulling lightly on the fiber will activate the tensioning device shown in Figure 2.7.

### 2.4.3 Mandrel Preparation and Resin Mixing

The mandrel is thoroughly cleaned with acetone to remove dirt and particles on the mandrel surface. To facilitate extraction of the mandrel from the wound pipes, a layer of cut tool bore grease spray from WÜRTH was applied to mandrel before covering it with plastic wrapping, as shown in Figure 2.10.

The epoxy resin was slowly and thoroughly mixed for three minutes before pouring it into the resin bath, shown in Figure 2.9. The hardener has a dye added to aid in seeing how well the material is mixed. The resin may not cure properly if the resin system is not fully mixed. Because the heat flow from the mixing container is very low, small quantities of resin were mixed at a time to avoid heat build-up from the exothermic reaction. The exothermic reaction can result in temperatures of more than 200°C in the mixing container, which may cause smoke-intensive burning of the resin mass[17].

**Figure 2.8:** Steel fiber tied to the delivery by a simple double knot.

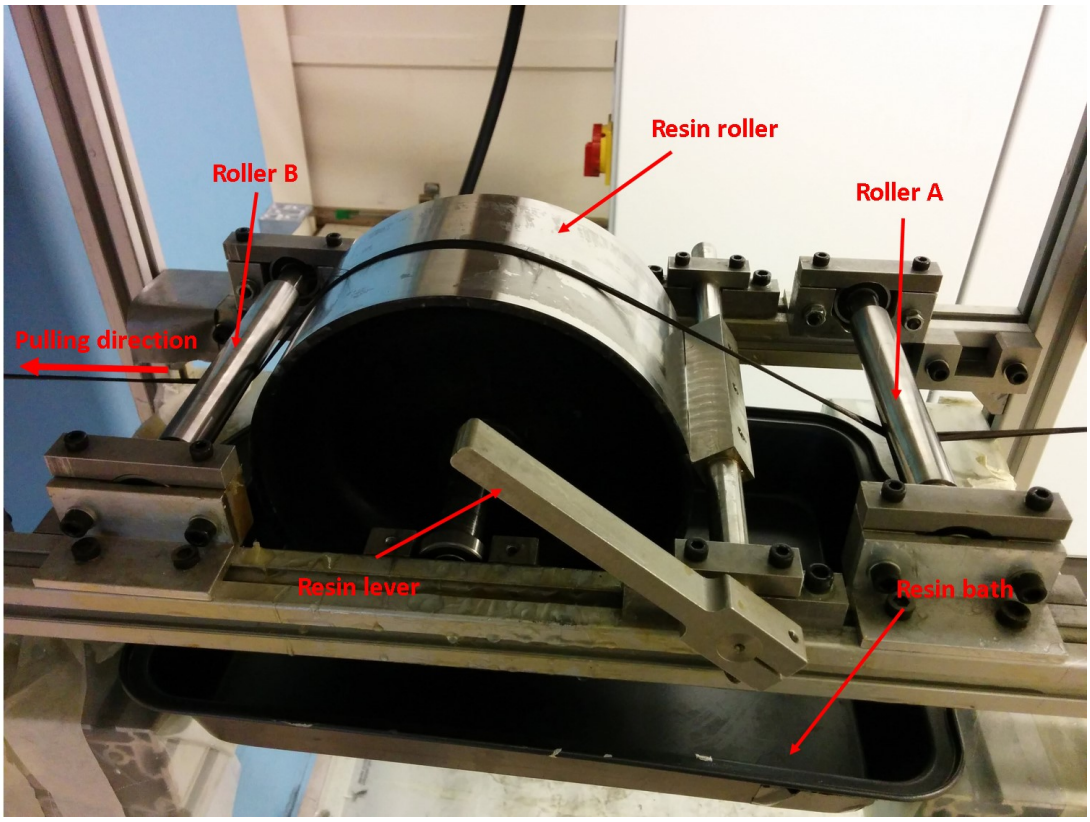


**Figure 2.9:** A picture of the resin carriage with fiber fed through it.

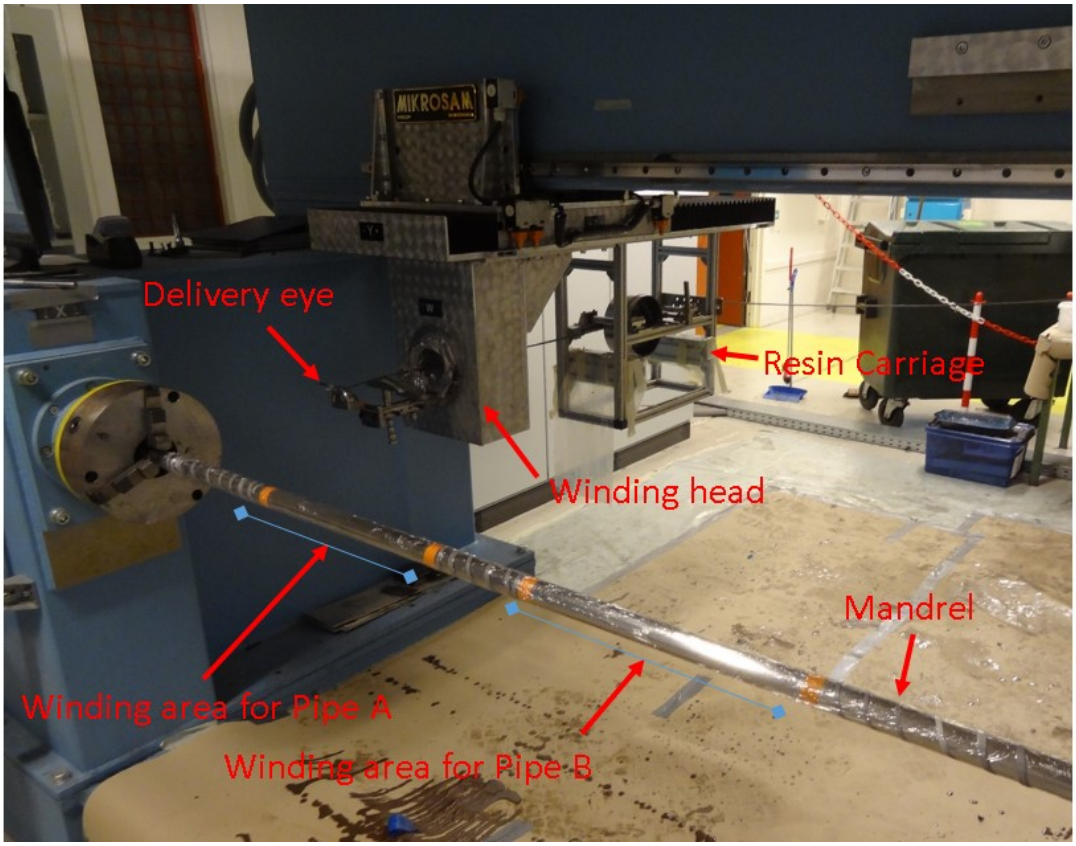


**Figure 2.10:** The machine correctly set-up and ready to wind the pipes.

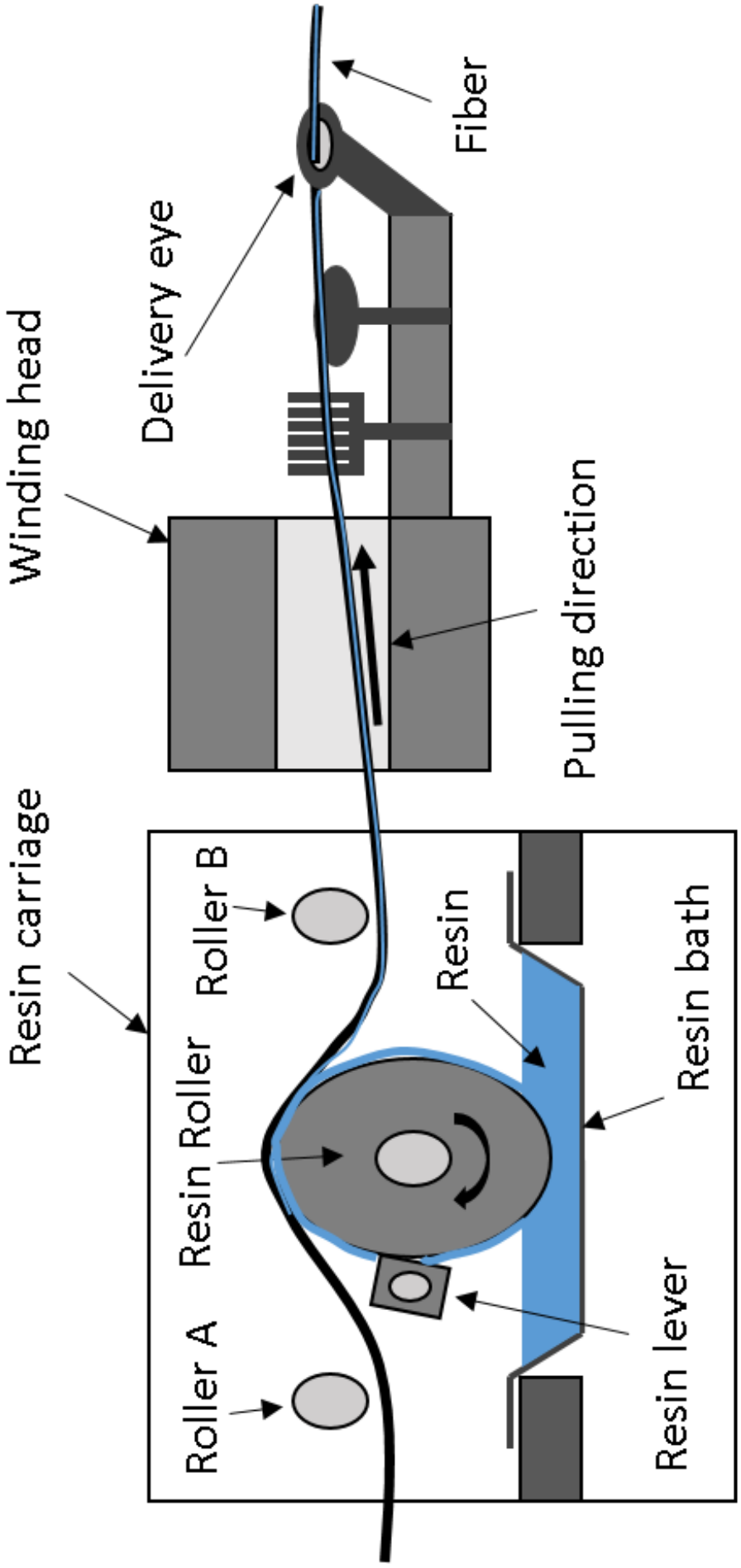


**Figure 2.11:** The picture illustrates how the fiber passes through the system.

### 2.4.4 Winding Procedure

Next, the segments were loaded into Winding Commander ready for winding. Pipe A or the three layered carbon fiber (CFRP3) pipe was wound first, and as such the winding head was moved to its starting position A, by pushing the start button once. Fiber tension was deactivated, and the fiber fastened to the mandrel by a piece of tape, before activating the tension system again. The winding process was then launched by pushing the start button once more. Figure 2.12 shows the steel fiber pipes being wound onto the mandrel. Figure 2.12a shows the first cycle for layer number one being wound and Figure 2.12b shows the mandrel after 8 completed cycles.

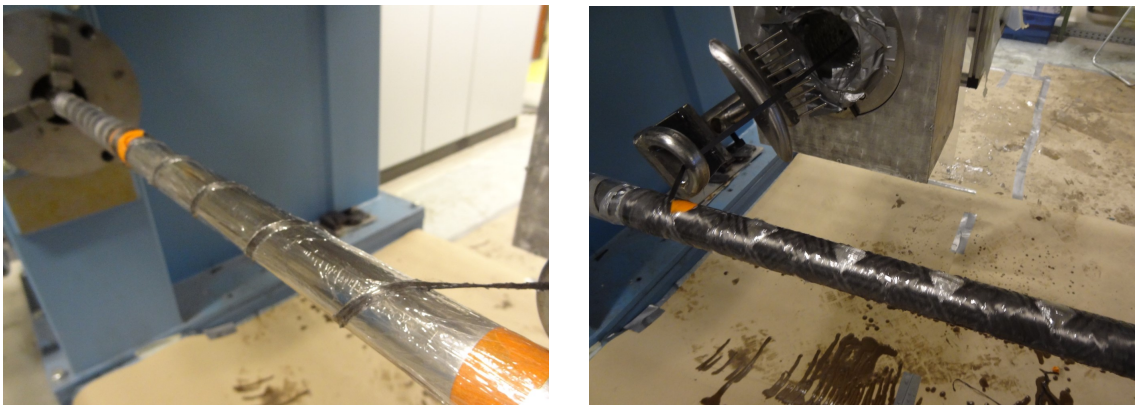

**a** **b**

**Figure 2.12:** The picture illustrating the winding progress: (a) The first winding cycle. (b) Winding after 8 completed cycles.

During winding the winding head moves back and forth completing the number of cycles that is required for the layer. The override speed can be varied between 0 and 200% to speed up or down the process when needed. An override speed of 25% was used

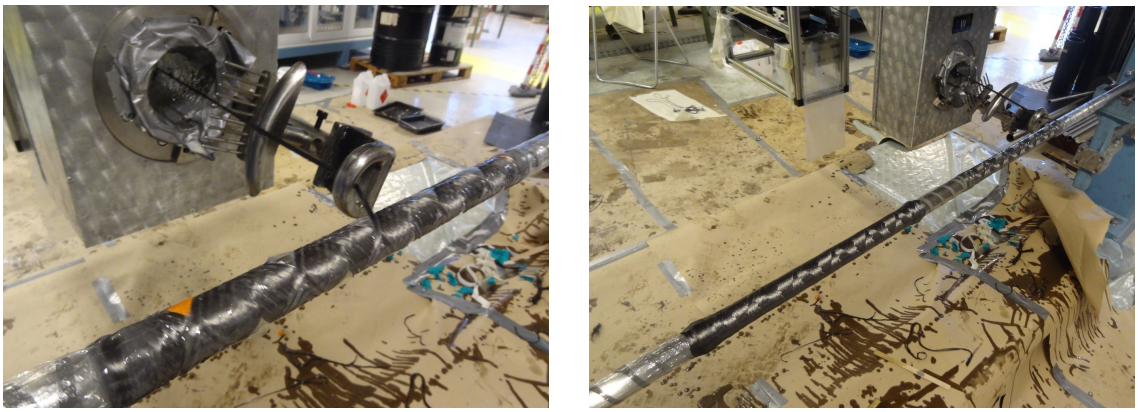

**a** **b**

**Figure 2.13:** The picture shows both Pipe A and Pipe B being wound on the mandrel: (a) Pipe A just before completion. (b) Pipe B after 2 completed layers.

for the first two cycles and then accelerated up to 50% when the process was sufficiently

under control. The machine automatically moved back to the starting position; once all the cycles were completed for the layer. Pushing the start button once more continues the process all over. The process was repeated layer by layer until the pipe consisted of three layers. In between completing the layers, the tension was activated at all times to prevent the fiber from splitting and to ensure that the fiber would not be dragged out of its position when the machine switches to the starting point of the new layer.

Figure 2.13a shows the Pipe A just before its was complete. After finishing Pipe A, the fiber was cut and tied to the delivery eye, before moving the winding head to its new starting position B. The second Pipe B has the same method used to wind Pipe A. Except for this pipe, the number of layers is six. Figure 2.13b shows the Pipe B after 2 completed layers. Each cycle took approximately 13 seconds to wind, which gives a total of 1 minute and 30 seconds for each layer to wind. The total time to wind $[\pm 55°]_3$ and $[\pm 55°]_6$ took approximately 5 and 10 minutes, respectively. When the preceding helical layers are wound over the previous layer, a wake of resin is formed in front of the fiber. A paintbrush was used during winding to remove excess resin. After completing both Pipe A and Pipe B, the pipes were pre-cured by continuously rotating them for 24 hours (at room temperature) before the mandrel was transferred to an electric oven for curing. This last step is important to maintain uniformity of resin content around the circumference of the pipe.

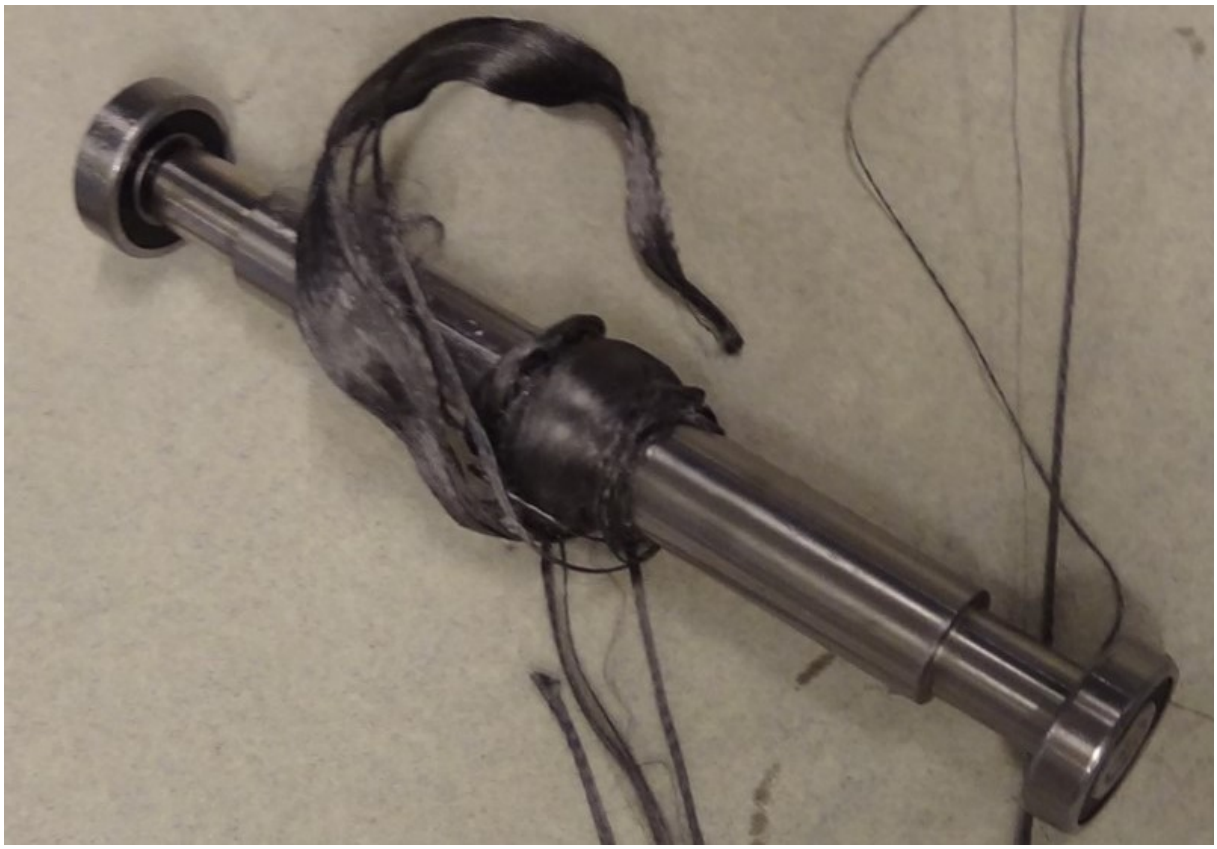

**Figure 2.14:** The broken fiber splits up and tangles around Roller A in the resin carriage.

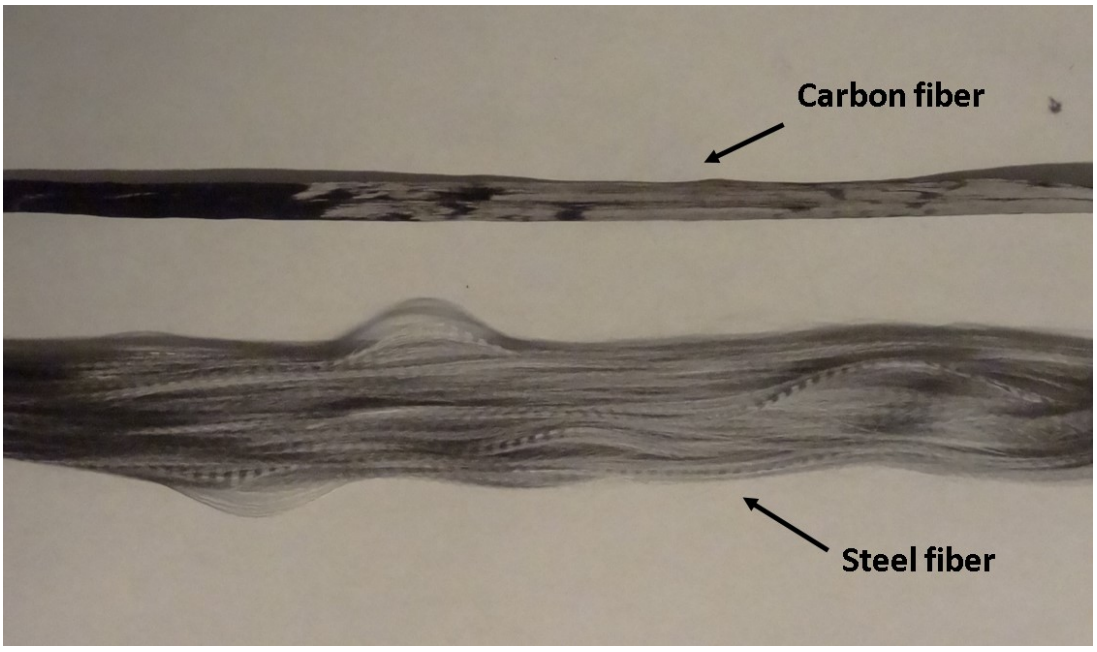


**Figure 2.15:** Comparison of steel fiber and carbon fiber. The picture shows that the steel fiber loses its shape when there is no tension. The carbon fiber is shown for reference.

The winding procedure for the SFRP pipe was identical to the CFRP pipe. With the exception that the fiber broke on two occasions when winding the first Pipe A. The winding process was continued and monitored until it was observed that Roller A in the resin carriage had sharp uncured resin on its surface.

The sharp uncured resin cut through the individual fibers and caused it to splinter up. As the fiber was pulled with high winding tension the over Roller A, it started to tangle up and coil around Roller A, until in the end causing the fiber to break, as shown in Figure 2.14. Therefore, the winding tension was reduced to 35 N instead and Roller A in the resin carriage was removed. Removing Roller A had no practical implications on the winding process and no fiber breakage occurred after that. The rest of the layers of Pipe A and Pipe B were wound in a straight forward process with a tension of 35 N and an override speed of 25%.

**Figure 2.16:** The picture shows that the broken fiber splits and tangles very easily.

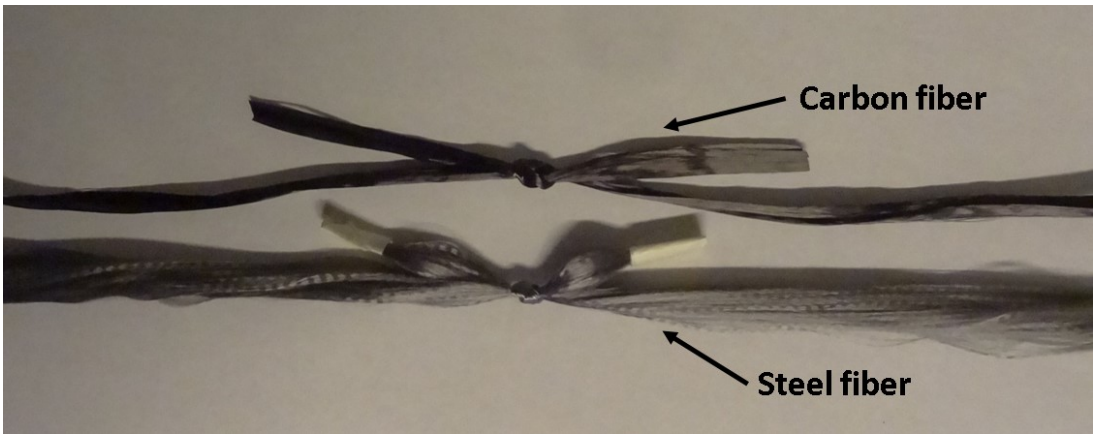


**Figure 2.17:** Picture show the square knot used to splice the fibers. The carbon fiber is shown for reference.

Figure 2.15 shows that without tension on, the steel fiber splits easily. When the fiber broke during winding, the fiber lost tension and started to split up, as shown in Figure 2.16. The challenge was to bundle split fibers nicely together again, but about 3 meters of the tangled steel fiber had to be cut because of this. Despite this, splicing two broken fiber ends together again were no problem. Just a simple square knot, as shown in Figure 2.17, was used to splice the fibers together, and the winding procedure could be continued. Figure 2.18 shows a close up picture of the double knot.

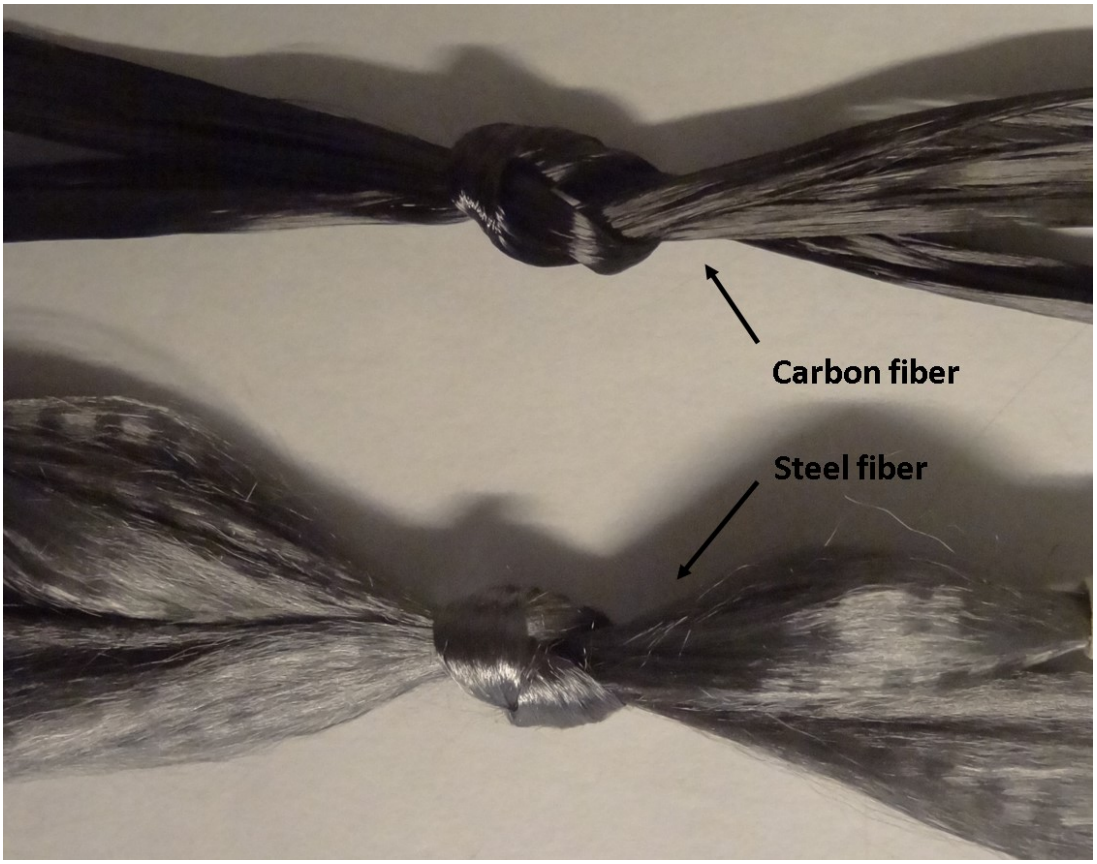


**Figure 2.18:** A close up picture showing the square knot used to splice the fibers. The carbon fiber is shown for reference.

### 2.4.5 Curing and Pipe Extraction

The wound pipes were pre-cured by rotating them in the filament winding machine in manual mode for 24 hours to prevent resin migration, as shown in Figure 2.19. After pre-curing, the pipes were then transferred to an electrical oven shown in Figure 2.20 and post-cured without pressure at 80°C for 15 hours. The pipes are rotated during the curing process to ensure that uniform heat distribution on the pipes. Typical curing processes recommend 15 hours at 50°C, 8 to 10 hours at 60°C or 6 to 8 hours at 80°C. The temperature and time for the curing process depend on the size of the component. But a curing temperature at 80° C for 15 hours was selected to ensure proper curing before extracting the pipes.

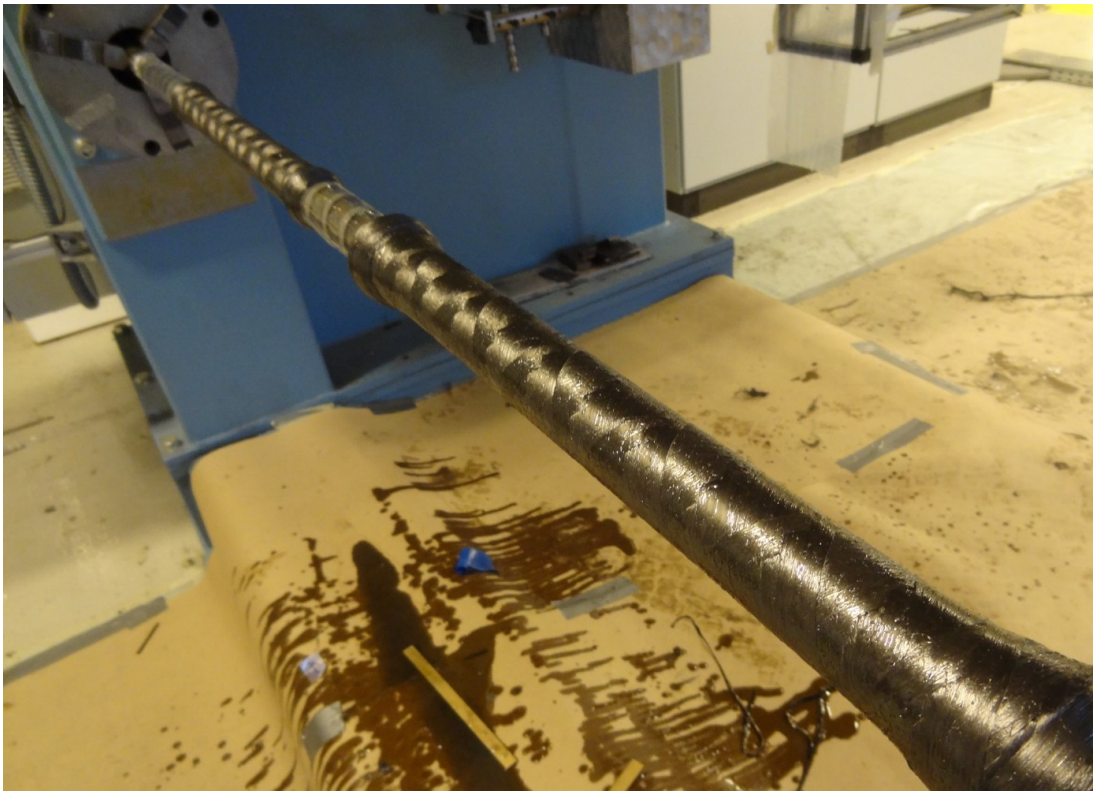

**Figure 2.19:** Mandrel rotating in winding machine for 24 hours to prevent resin migration after winding procedure is finished.

The mandrel was removed from the pipes, by connecting a lever chain hoist to a nut welded inside the mandrel ends, shown in Figure 2.21. By pulling the lever chain hoist, the pipe is extracted from the mandrel, thus freeing it to wind another pipe. The extraction arrangement is shown in Fig 2.22. Figure 2.23 shows that there were not enough grease on the surface to allow the pipes to slip off easily causing the mandrel to bend. Figure 2.24 shows the pipes extracted from the mandrel. Since the mandrel and pipe are under high tension when extracting them; A glass shielding was used as a safety precaution just in case the connection between the lever chain hoist and mandrel snapped.

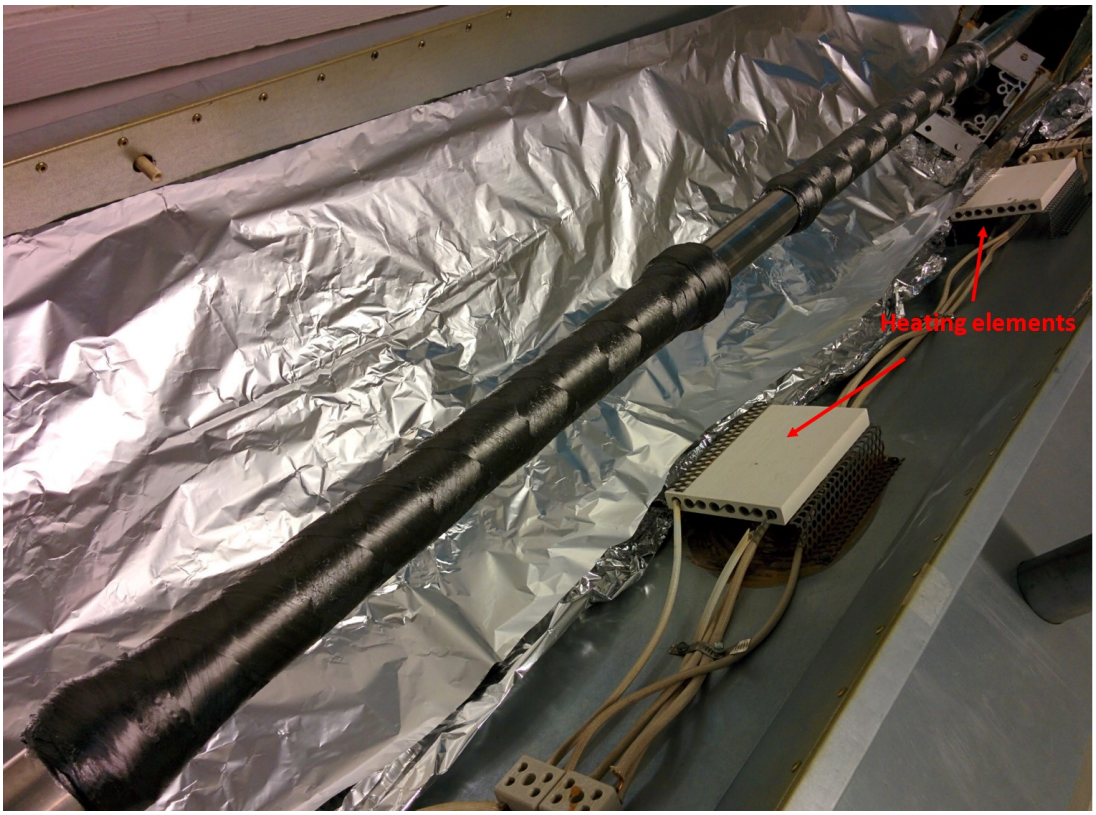


**Figure 2.20:** The SFRP3 and SFRP6 pipe in the electrical oven just before post-curing.

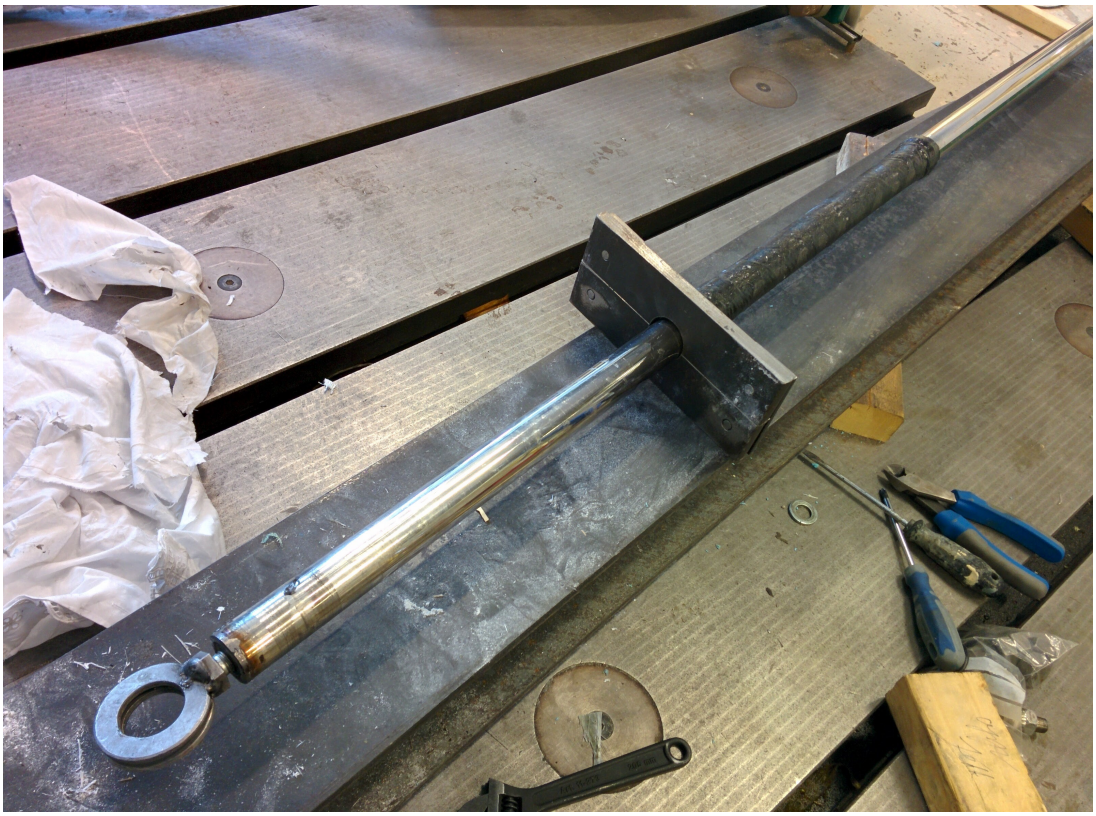

**Figure 2.21:** A picture showing the connection point for the lever chain hoist to the mandrel.


**Figure 2.22:** The picture shows the arrangement used to extract the pipes.

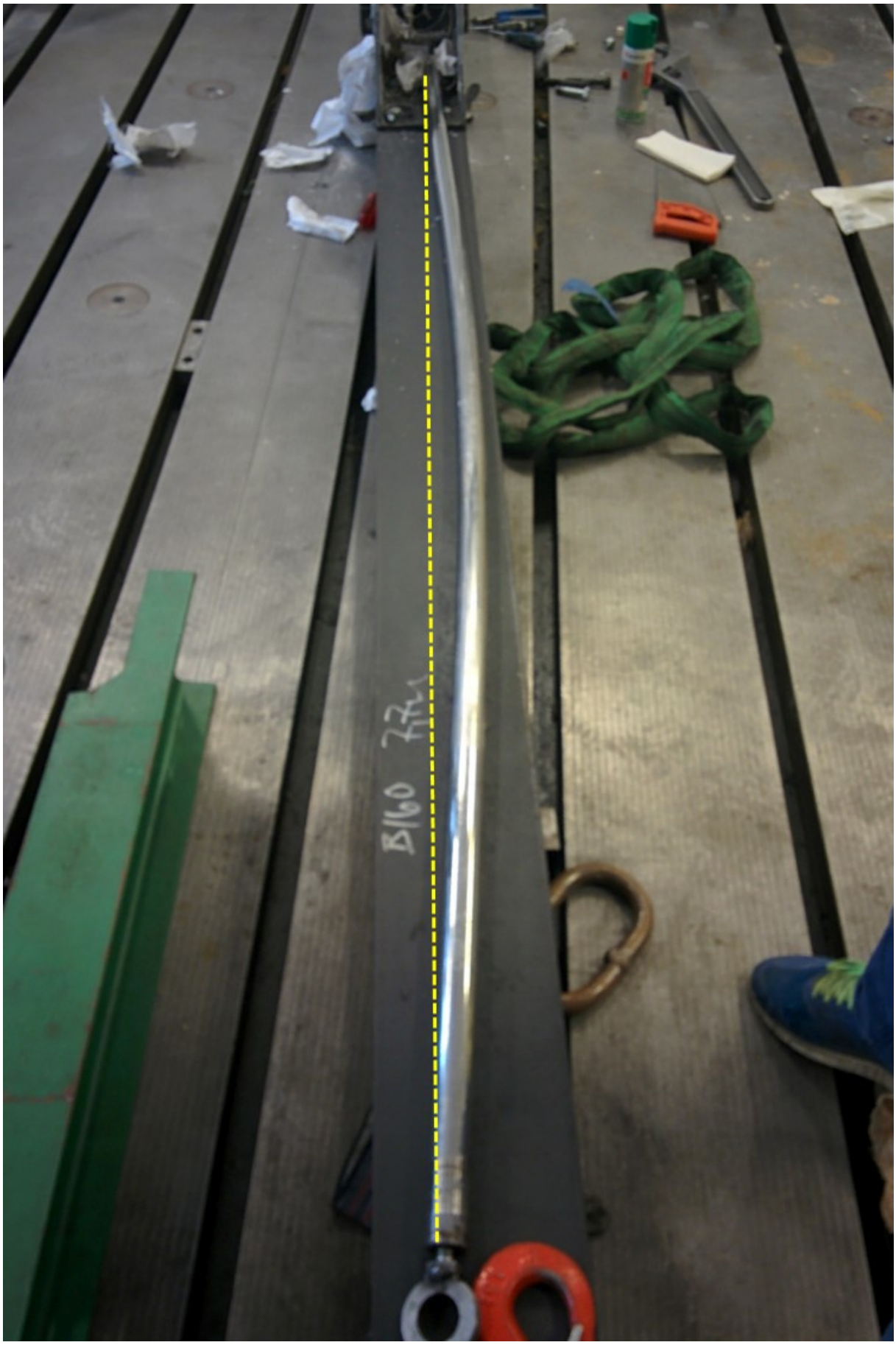

**Figure 2.23:** The picture shows that too much friction caused the steel mandrel to bend during extraction. The yellow line indicates the mandrel shape before extraction.

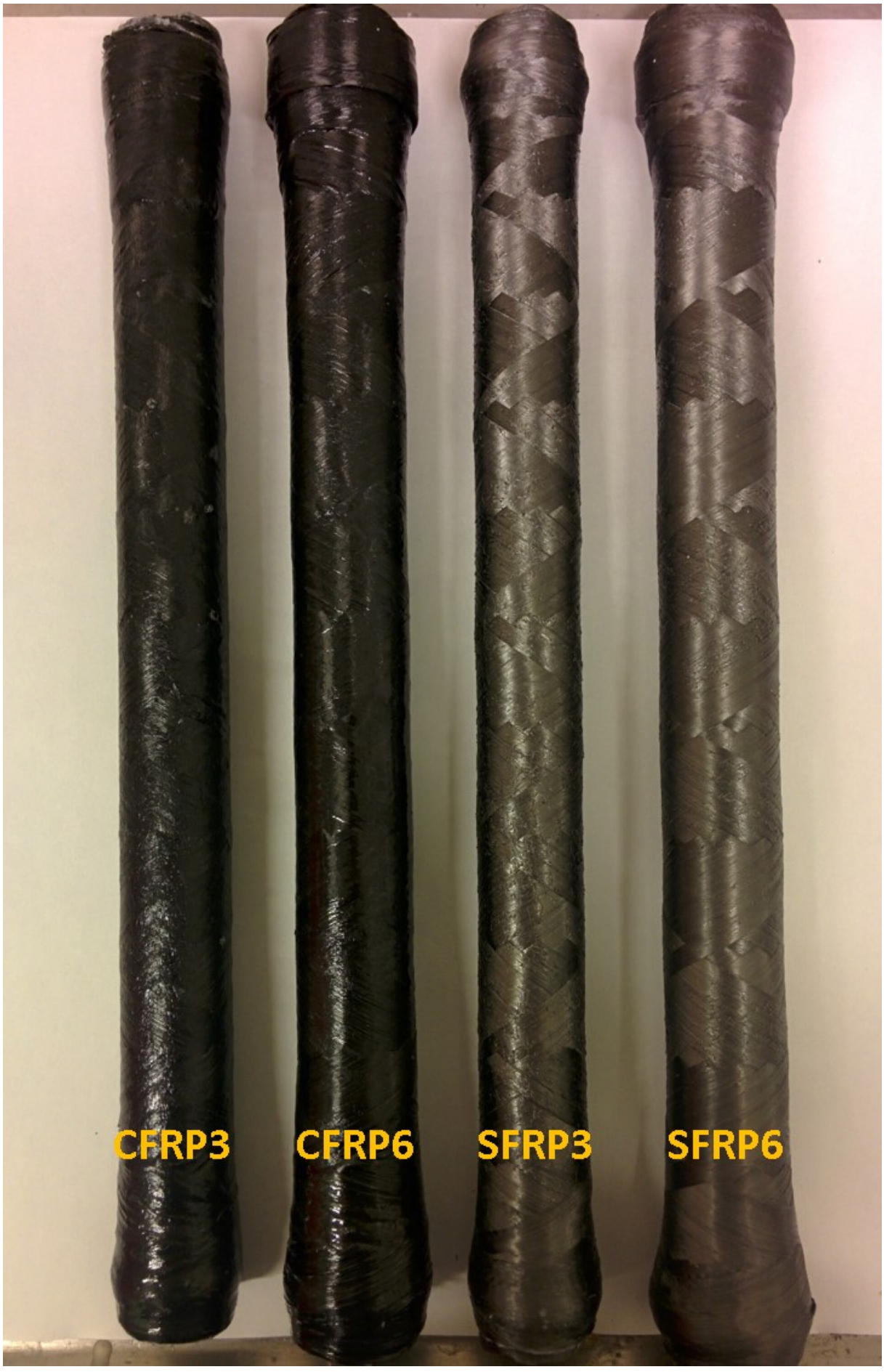


**Figure 2.24:** The picture shows the extracted pipes.

# 3 Theoretical Method

This section describes the theoretical models used to determine the composite properties and critical buckling pressures of cylindrical pipes under external pressure.

## 3.1 Determination of Composite Properties

Laminate theory together with various analytical micromechanical models has been used to calculate the composite elastic properties. These models are based on the elastic properties of the constituent materials and the morphology of the composite, such as fiber volume fraction. Vedvik [7] gives the full explanation of the laminate theory and micromechanical models in his textbook. Using simple rules of mixture (ROM) formula the elastic properties of the unidirectional lamina were calculated using the set of Eqs. (3.1) – (3.6). The expressions for the longitudinal modulus and Poisson's ratio reduce to the same form as the rule of mixture equations. Indices $f$ and $m$ are referring to fiber and matrix, respectively.

The stiffness in the longitudinal direction $E_1$ of the composite was determined using the following equation:

$$E_1 = E_{1f}V_f + E_m(1 - V_f) \tag{3.1}$$

where $E_{1f}$ and $E_m$ are the stiffness of fiber along its length and the matrix (Table 2.1). $V_f$ is volume fraction of fiber.

The stiffness in the transverse direction $E_2$ of the composite is estimated using the inverse ROM formula by the following equation:

$$\frac{1}{E_2} = \frac{V_f}{E_{1f}} + \frac{(1 - V_f)}{E_m} \tag{3.2}$$

The transverse modulus, $E_2$, is a matrix-dominated property since the fibers do not contribute to the stiffness in the transverse direction (unless $V_f$ is very high).

The density of the composite was calculated as follows:

$$\delta_{composite} = \delta_f V_f + \delta_m(1 - V_f) \tag{3.3}$$

where $\delta_f$ and $\delta_m$ are the density of the fiber and matrix (Table 2.1).

The in-plane Poisson's ratio in the 12 directions of the composite $\nu_{12}$ can be found by the following:

$$\nu_{12} = \nu_f V_f + \nu_m(1 - V_f) \tag{3.4}$$

where $\nu_f$ and $\nu_m$ are the Poisson's ratio fo the fiber and matrix (Table 2.1).

Assuming that the matrix and fibers are isotropic, the shear modulus $G_f$ and $G_m$ of the fiber and matrix was then found by the following:

$$G_m = \frac{E_1}{2(1+\nu_m)} \qquad G_f = \frac{E_1}{2(1+\nu_f)} \tag{3.5}$$

where $G_m$ and $G_f$ are the shear modulus of the fiber and matrix (Table 2.1).

The in-plane shear modulus in the 12 directions of the composite $G_{12}$ was found by the following:

$$\frac{1}{G_{12}} = \frac{V_f}{G_f} + \frac{(1-V_f)}{G_m} \tag{3.6}$$

where $G_{12}$ is the in-plane shear modulus in 12 direction (Table 2.1).

## 3.2 Determining Critical Buckling Pressure of Cylindrical Pipes

Under uniform external pressure, a cylinder pipe can fail by non-symmetric bifurcation buckling or shell buckling at a much smaller pressure than that required to cause axisymmetric yield or material failure [24]. A long thin circular cylindrical pipe will fail in a flattening or ovalling mode, but the shorter circular cylindrical pipe will fail by bifurcation buckling or shell buckling.

The critical buckling pressure ($P_{cr}$) for elastic buckling of infinitely long thin-walled circular cylinders was calculated with the formula proposed by Bryan [25]. For shorter cylinders, this formula is replaced by the von Mises formula, which has simply supported ends [26]. The von Mises formula states that the buckling pressure varies with a given number of circumferential lobes or waves, namely "n" as shown below:

$$P_{cr} = \left\{ \frac{E(t/a)}{[n^2 - 1 + 0.5(\pi a/L)^2]} \right\} \times \left\{ \frac{1}{[n^2(L/\pi a)^2 + 1]^2} + \frac{t^2}{12a^2(1-\nu^2)} \left[ n^2 - 1 + (\pi a/L)^2 \right]^2 \right\}, \tag{3.7}$$

where $L$ is the unsupported length of the cylinder, a is the mean radius of circular cylindrical shell, E the Young's modulus, $t$ the material thickness and $\nu$ the Poisson's ratio. The number of lobes has to be changed until the lowest buckling pressure, $P_{cr}$, is found.

Windenburg and Trilling simplified this formula in a way that the critical buckling pressure is given by a single calculation known as the David Taylor Model Basin (DTMB) formula [27], as follows:

$$P_{cr} = \frac{2.42E(t/2a)^{\frac{5}{2}}}{(1-\nu^2)^{0.75}[(L/2a) - 0.45(t/2a)^{\frac{1}{2}}]} \tag{3.8}$$

With this simplified formula, it was possible to predict the critical buckling pressure without the need for determining the respective number of lobes, corresponding to the mode with the lowest buckling pressure.

# 4 Experimental Method

The primary aim of the experimental investigation was to determine the compressive properties and buckling properties of the produced samples to evaluate the performance of the SFRP composite. The analysis of the produced SFRP samples performance started its investigation by first looking into the physical properties (thickness, fiber volume fraction, weight and void content). The quality of the produced samples was investigated using optical microscopy to check the for presence of voids or defects. Additionally, the fiber volume fraction was measured using a matrix burn-off test to compare with the calculation based on image analysis of the composite cross-section, to analyze local fiber volume fractions.

After the quality check, the investigation was carried on to study the mechanical properties (buckling strength, compressive strength, elastic modulus and Poisson's ratio). The compressive properties of steel fiber composites were found using quasi-static compression testing (loaded in axial and radially to the hoop direction), followed by an external pressure test to observe the buckling behavior. The samples used for testing were made by filament winding method with different thickness (thick and thin-walled), as described in section 2.

The composite pipes investigated are intended for marine applications and can suffer catastrophic collapse under external pressure in the deep sea. Their principal function is to resist hydrostatic pressure during immersion in the deep sea. Tests have been performed at IPM using an autoclave pressure chamber to simulate the external pressure. The autoclave has a maximum pressure capacity of 50 MPa, corresponding to roughly 5000 m below sea level.

## 4.1 Sample Preparation and Instrumentation

Figure 2.24 shows the finished pipes after extraction, which consists of composite pipes made of CFRP3, CFRP6, SFRP3, and SFRP6. Approximately 50 mm of the produced pipes were cut off at each end to remove the transition area necessary for helical winding. The pipes were then cut into the required dimensions for the external pressure test and compression test, see Figure 4.1a and Figure 4.1b, respectively. Their main dimensions are given in Table 4.1. The unsupported length was the actual length $L_0$ of the specimen minus the depths of the shoulders of the end caps. The samples were cut using a water-cooled diamond saw to avoid melting of the matrix during cutting. Due to the ductile fibers, the sample edges of all samples were thoroughly sanded to remove any unwanted damage introduced during the cutting procedure.

**Table 4.1:** Dimensions of the samples for testing. Nominal specimen dimensions, in mm.

| Sample | Overall length, $L_0$ | Unsupported length, $L$ | Diameter, $D$ | Thickness, $t$ | D/t ratio |
|---|---|---|---|---|---|
| *External pressure* | | | | | |
| CFRP3 | 203.3 | 193.3 | 36.4 | 2.20 | 16.5 |
| CFRP6 | 199.7 | 189.7 | 40.4 | 4.20 | 9.6 |
| SFRP3 | 201.2 | 191.2 | 36.8 | 2.39 | 15.4 |
| SFRP6 | 198.1 | 188.1 | 40.9 | 4.46 | 9.2 |
| *Axial compression* | | | | | |
| CFRP3 | 39.8 | - | 36.5 | 2.25 | 16.2 |
| CFRP6 | 41.2 | - | 40.7 | 4.36 | 9.3 |
| SFRP3 | 40.4 | - | 37.0 | 2.50 | 14.8 |
| SFRP6 | 43.6 | - | 41.3 | 4.67 | 8.8 |
| *Hoop compression* | | | | | |
| CFRP3 | 13.6 | - | 36.4 | 2.18 | 16.7 |
| CFRP6 | 14.2 | - | 40.4 | 4.20 | 9.6 |
| SFRP3 | 14.4 | - | 36.8 | 2.41 | 15.3 |
| SFRP6 | 13.9 | - | 41.3 | 4.65 | 8.9 |

The wall thickness and diameter of the samples were measured at several points around the circumference (angle increments of 10°) using a micrometer. The measured wall thickness of the samples is shown in Table 4.1. In this case, the three layered pipes is a thin-walled pipe because the diameter to thickness ratio is bigger than 10 ($\frac{D}{t} \geq 10$), and the six-layered pipes is a thick-walled pipe because the diameter to thickness ratio is smaller than 10 ($\frac{D}{t} \leq 10$).

After cutting and measuring the composite pipes, a quality control, and microstructural analysis were performed on the test samples. Optical microscopy is used to analyze the volume fraction of fiber and the presence of voids or defects for all produced samples. The volume fraction of fiber for the samples was calculated based on microscopy of the composite cross section and image analysis (section 4.2.1). Additionally, a matrix burn-off test in a muffle furnace (section 4.2.2) based on ASTM D3171 [28] was performed, to compare to the volume fraction of fiber found by image analysis. The void fraction of the produced specimens was measured based on ASTM D2734 standard [29].


**a**

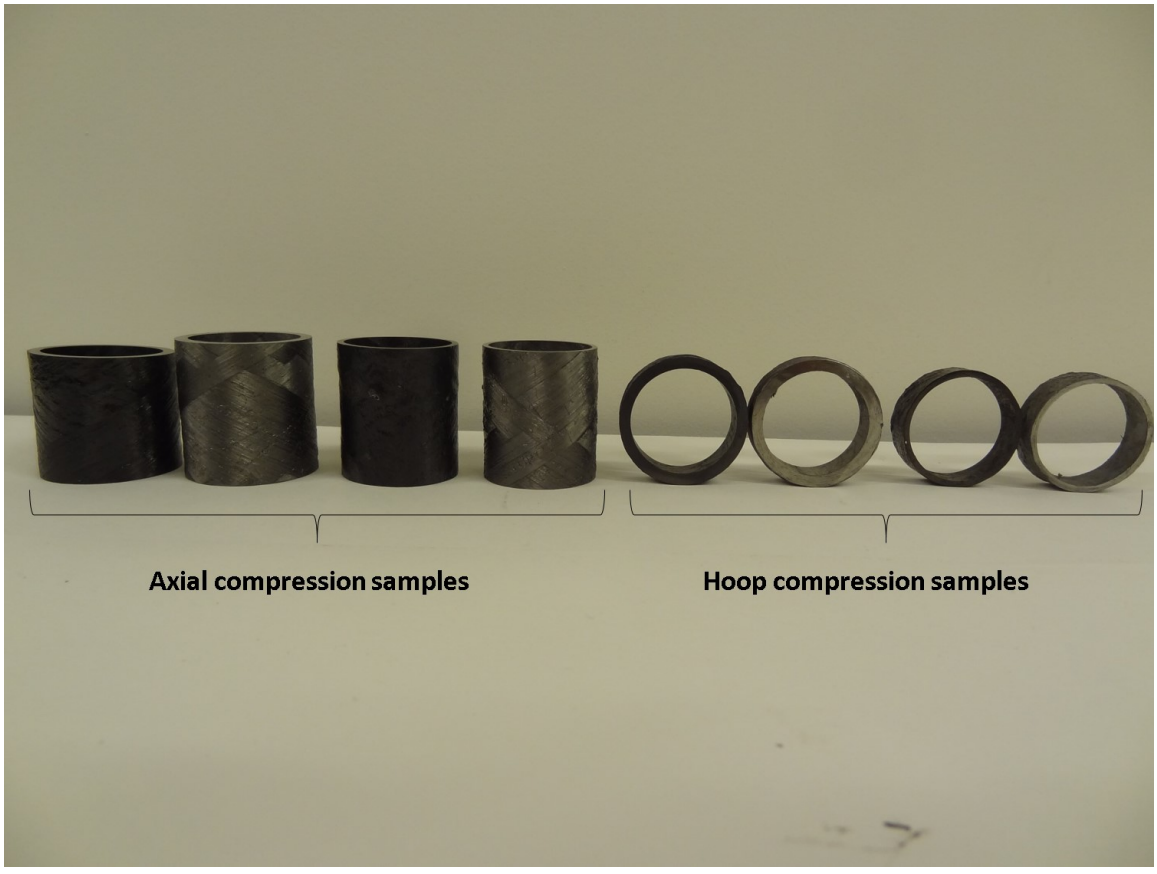


**b**

**Figure 4.1:** Specimens for testing: (a) Samples for the external pressure test. (b) Axial compression samples to the left and hoop compression specimens to the right.

For the compression test specimens, the samples were instrumented with strain gauges on the sample surface to monitor the axial and hoop strain during the compression test. The strain gauge rosette with a vertical and horizontal grid is aligned in axial and hoop direction of the sample. The strain gauges are bonded to the specimen surface by a cyanoacrylate adhesive at 55° angle to principal material direction. The strain gauges connect to a data logger in a half bridge configuration. Proper surface preparations are important to ensure sufficient bonding of strain gauges to the specimen surface. The sample surface is therefore lightly sanded to give a rough surface for better bonding of strain gauges. In the case of debonding the strain gauge will give zero measurements.

The samples for the external pressure test required specially designed end caps to prevent premature damage to the pipe ends due to high-stress concentrations, and to seal the two ends of each specimen under external pressure. These end caps were machined out of mild steel according to the schematics given in Fig 4.2, and designed for push fit connections into the cylindrical pipe ends. For the external pressure test, it was not possible to measure strains with strain gauges due to the pressure rating of the electrical passage through the autoclave would be too high and cause a leakage.

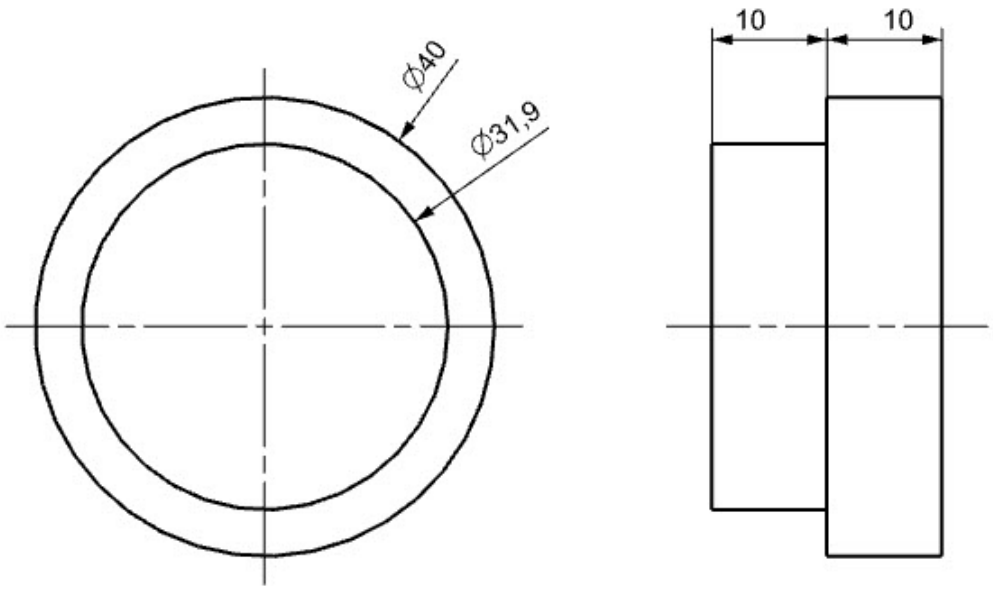


**Figure 4.2:** Schematics of end caps.

The steel rod was readily available in the lab and therefore chosen to save time and money on new material. Fig 4.3 shows the finished end caps. The end caps edges were rounded off at the edges to prevent them from damaging the pipe ends when inserting them. A watertight sealing was achieved by adding a layer of vacuum bag sealant tape between the pipe ends and end caps before assembling the test specimen. Fig 4.4 shows the assembled sample with the end caps fitted to together with vacuum bag sealant tape.

**Figure 4.3:** End-caps as produced for testing.


**Figure 4.4:** Assembled samples ready for buckling test with the end caps fitted into it with vacuum bag sealant tape.

## 4.2 Quality Control of the Produced Samples

### 4.2.1 Microscopy

The layer composition was photographed using a microscope, with magnified pictures of the polished surface perpendicular to the rotational axis of each sample. For microstructure characterization, an image analysis program was used to determine the global and local volume fractions of fiber. The program accurately identifies the edges of the steel fibers using the gray scale histogram and then converts the image to a black and white image to accurately determine the average fiber volume fraction.

Images were recorded by the Leica MeF4 microscope [30] and then analyzed with image analysis application iSolution [31]. The specimens are sanded with P120, P800, P2400 and P4000 SiC grit paper using standard metallographic procedures before microscopy. The test samples were not cast in epoxy as they would be tested in compression later. Ethanol was used to clean the specimen surface instead of water to avoid evaporation marks on the surface to be analyzed. The specimens are cross-sectioned perpendicular to the pipe longitudinal axis. The cross-section is viewed at an appropriate magnification (typically 50-200X). The red lines on the microscopy pictures indicate where the borders between the plies were considered to be, and these lines were in turn used to determine the relative thickness of each ply. The absolute thickness of each ply is found by scaling the relative thickness with the thickness of the pipe as reported in Table 5.1.

The volume fraction of fiber of these smaller regions can be used to analyze the distribution of the fiber volume fraction and to calculate an average value for the entire image. At least three different images of various cross-sections were used for each sample to calculate an overall average distribution and overall average volume fraction of fiber.

### 4.2.2 Burn-off Test

The burn-off test is used to find the volume fraction of fiber and void fraction of the composite samples produced. The burn-off test was carried out by heating small samples of the pipe put in a ceramic cup at $500°C$ for 300 minutes in a muffle furnace. The high temperature burns the resin away leaving the fiber bed behind. The burn off temperature should be below the temperature at which samples will spontaneously ignite and the maximum time for burn-off should be six hours. The matrix is considered combusted if no matrix/reinforcement block exists. The only visible items should be ash and reinforcement. The average fiber volume fraction for each produced pipe can be calculated by knowing the weight of each section before and after the burnout procedure, and the densities of the constituents. Table 5.1 shows the fiber volume fraction obtained from the burn-off test.

The volume fraction of fiber can be determined by using Eq. (4.1) and Eq. (4.2) [7]:

$$V_f = \frac{\frac{W_f}{\rho_f}}{\frac{W_c}{\rho_c}} \tag{4.1}$$

$$W_f = \frac{m_f}{m_c} \times 100 \tag{4.2}$$

where, $W_f$ is the fiber weight fraction, $m_f$ is the mass of fibers, $m_c$ is the mass of composite, $\rho_f$ is the fiber density, $W_c$ is the composite weight, and $\rho_c$ is the composite density, and $V_f$ is the fiber volume fraction. Potential sources of errors in the measure measurements of the volume fraction are the void fraction. The loss of fiber during burn-off test and accumulation of error from the density measurements.

The void fraction was found by Eq. (4.3):

$$V_v = \frac{\rho_{ct} - \rho_{ce}}{\rho_{ct}} \times 100 \tag{4.3}$$

where, $V_v$ is the void fraction, $\rho_{ct}$ is the theoretical density of composite, $\rho_{ce}$ is the experimental density of composite. The theoretical and experimental densities of the composites with the corresponding void fraction are presented in Table 5.2.

**Figure 4.5:** Samples in muffle oven ready for burn-off test.

## 4.3 In-plane Compression Test

Two types of compression tests were performed to determine the Young's moduli in the axial and hoop direction. A uniaxial loading was carried out to obtain the Young's modulus in the axial direction, as shown in Figure 4.6a, and then a hoop (O-ring shaped) sample was loaded radially to determine the Young's modulus in the hoop direction, as shown in Figure 4.6b. The compression tests are performed at room temperature on an Instron 4505 machine based on ASTM E2954 [32]. In-plane shear properties could also be determined using the specimens under uniaxial loading. The in-plane shear stress in the material coordinate system was directly calculated from the applied axial load. The related shear strain was deduced from the axial and hoop normal strain data measured by the strain gauges.

In the test set-up shown in Figure 4.6a and Figure 4.6b the compressive load is applied to the test samples through flat steel end plates. Due to the high compression loads exerted on the test specimens, this configuration requires that the samples are properly aligned with the plates to avoid crushing of the material, or uneven loading may cause the sample to shoot out in any direction.

The quasi-static compression tests were displacement-controlled with a crosshead speed of 3 mm/min. The load and displacement were recorded using a 100 kN load cell, the data are given by the Spider 8 digital controller, were sampled on the same time basis. Data signals from the strain gauge measurements were acquired synchronously with force–displacement data throughout the test using catman AP data acquisition software. The specimens were tested to destruction and a sudden drop of the applied load indicated failure. The yield stress was calculated based on the composite stiffness and a specified offset of 0.2%. In the case of a progressively failing sample in compression, the strain-to-failure is determined as the strain at which the stress drops below 50 MPa.

## 4.4 Fiber Tensile Test

A quasi-static tensile test of a single fiber was carried out on the rest of the fiber from the pipe production to find the tensile properties. The fibers were just clamped in the load cell and loaded until failure of the steel fiber. The mechanical properties and composition of a single steel fiber are reported in Table 1.2 and Table 1.3, respectively, along with a representative tensile stress-strain curve (Figure 1.2). Failure strain of a single fiber was measured without an extensometer or strain gauges and hence is only an indicative value.

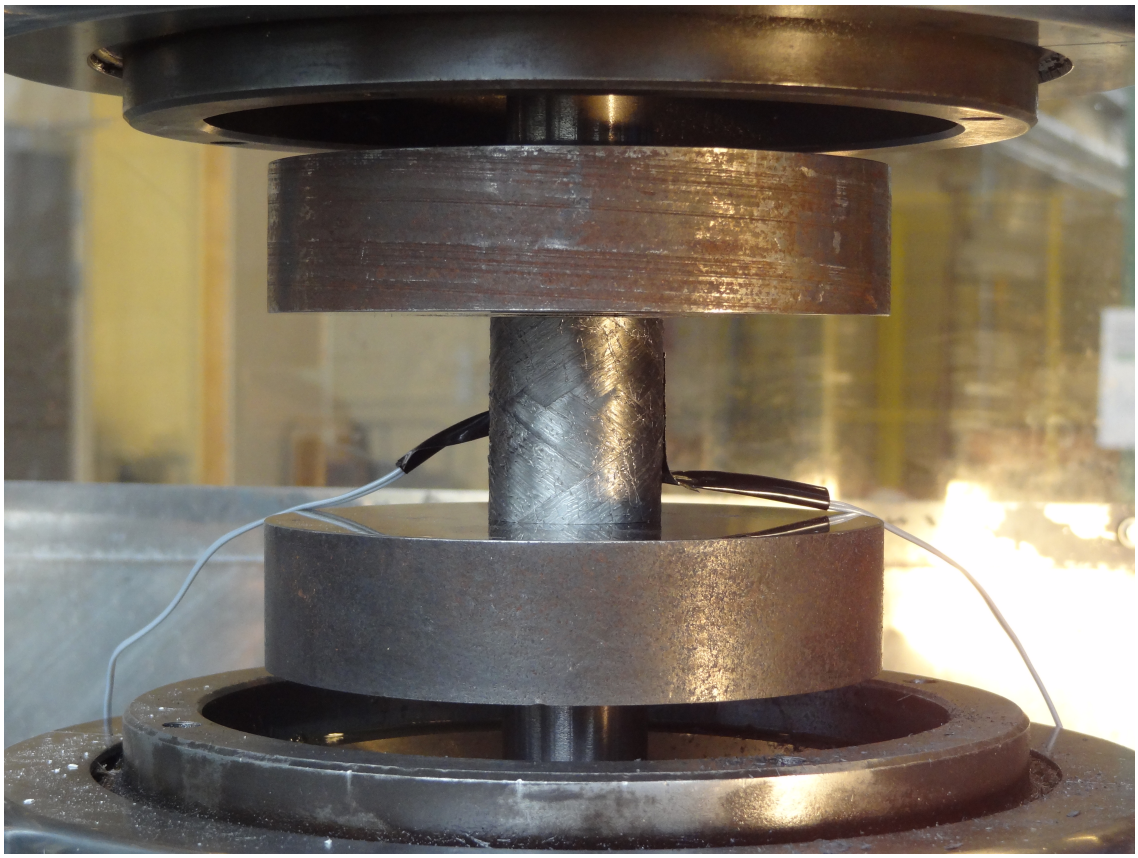

**a**

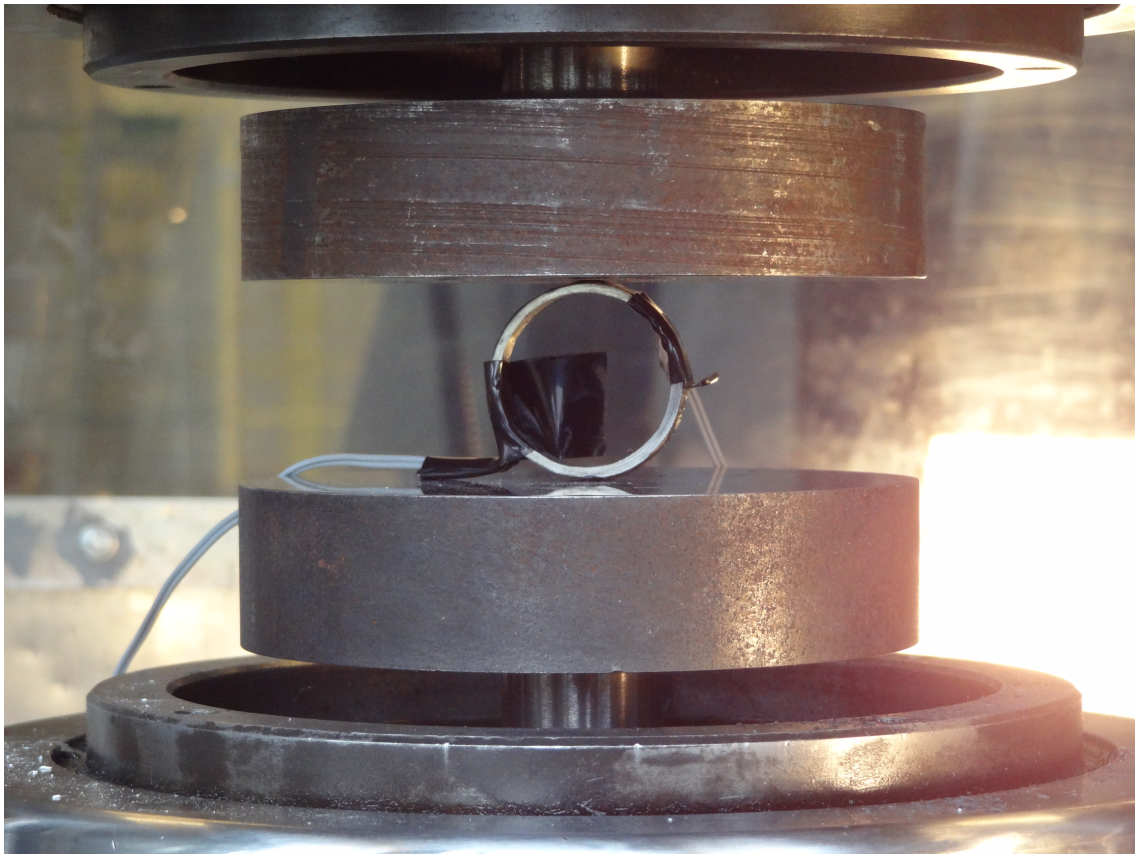

**b**

**Figure 4.6:** Experimental set-up for compression test: (a) Compressive loading in the axial direction of the composite sample. (b) Compressive radial loading in hoop direction of the composite sample.

## 4.5 External Pressure Test

The external pressure test procedure was performed based on ASTM D2924 [33]. The experimental set-up for the external pressure test is as shown in Figure 4.7.

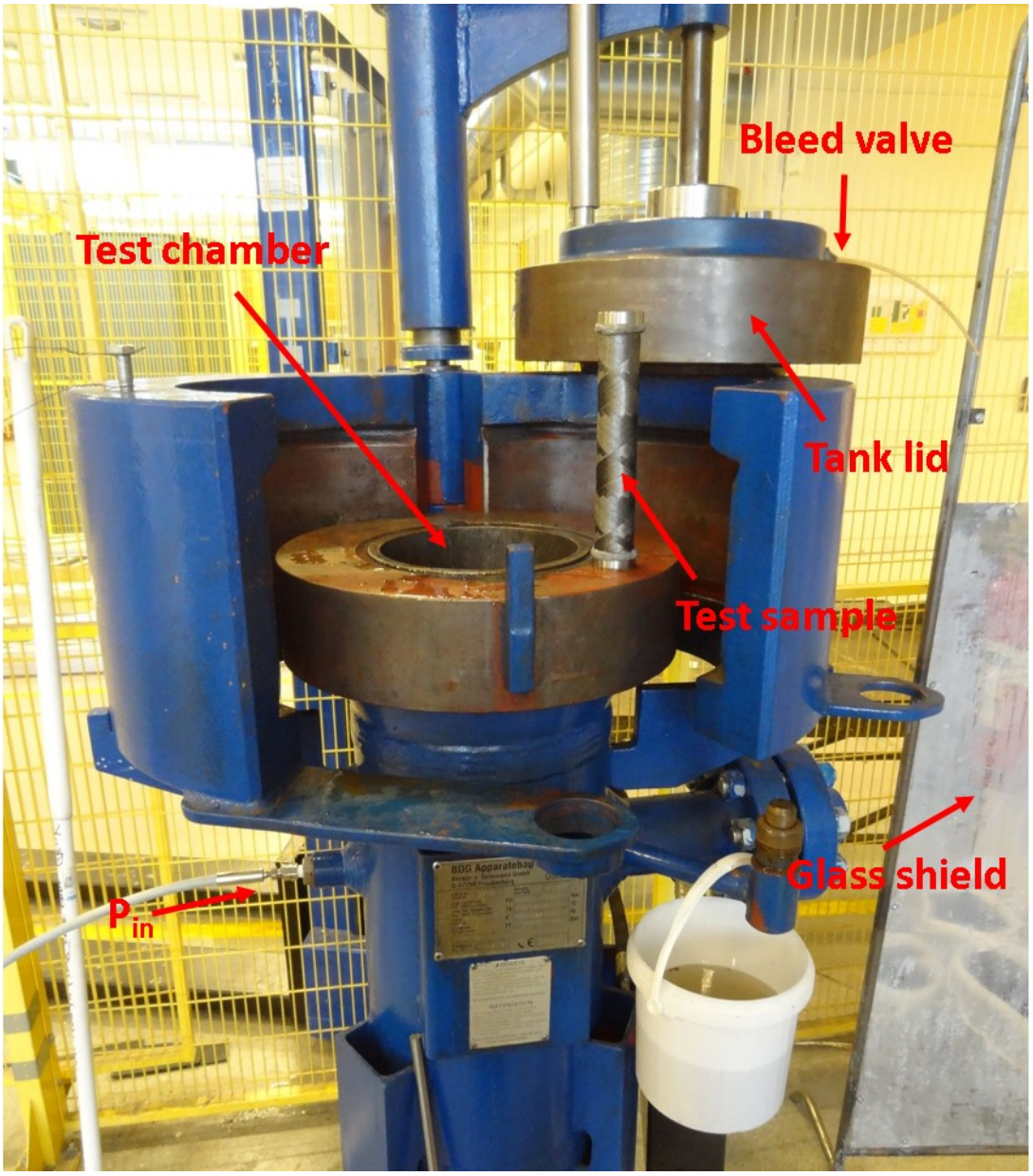


**Figure 4.7:** Experimental set-up for the external pressure test and pipe just before introduction into the chamber for the test.

The external pressure is created in a high-pressure autoclave chamber from BDG with a nominal internal diameter of 200 mm, depth of 800 mm, and volume of 24 liters. The autoclave can handle a temperature range of -10 to +70 and a maximum allowable pressure of 50 MPa, which equals to a depth of roughly 5000 m below sea level. A mixture of regular water and cooling fluid was used to fill the autoclave chamber. An air powered compressor that could exert a maximum pressure of 100 MPa was used to pressurize the autoclave.

The ambient temperature during testing was approximate 21°$C$ and a glass shielding was placed next to the autoclave to provide containment in the event of a rupture.

As the powered compressor was hand operated, any line losses were negligible. An LEO 3 manometer from Keller AG was used to log the applied pressure, ambient pressure, ambient temperature, and time throughout testing. The manometer has a laptop connected via a USB interface with the software Control Center Series 30 (CCS 30) supplied by Keller AG. The pressure tank was capable of sustaining a pressure of 50 MPa, which equals to a depth of roughly 5000 m below sea level. The ambient temperature during testing was approximate 21°$C$ and a glass shielding was placed next to the autoclave to provide containment in the event of a rupture.

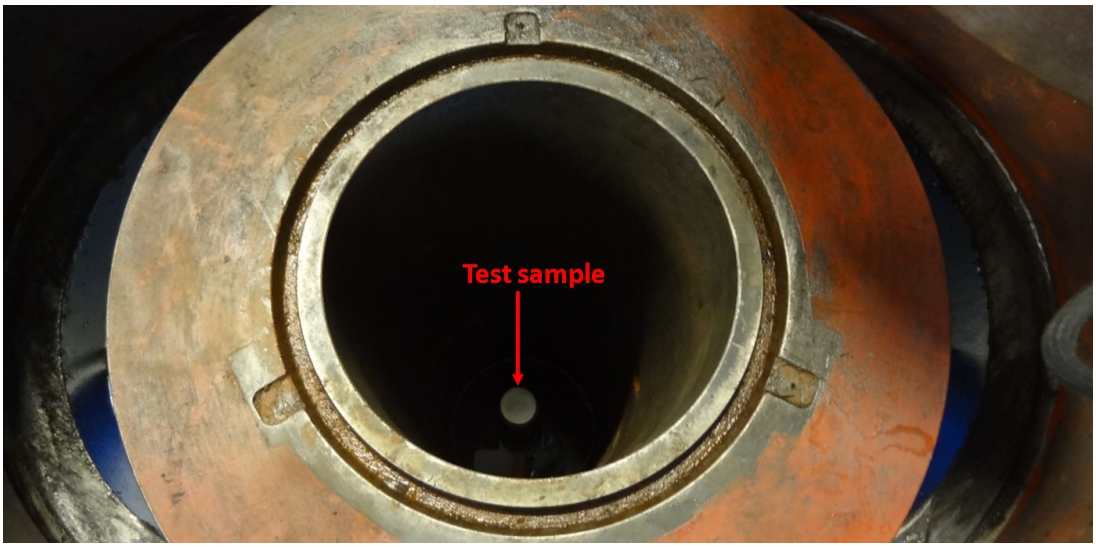


**Figure 4.8:** The test sample is resting at the bottom of the pressure chamber.

A thorough inspection of the samples for damages and cracks were performed before placing them in the autoclave. Figure 4.7 shows the SFRP6 sample just before introduction into the chamber of the external pressure test. The sample rests on the bottom of the pressure tank, as shown in Figure 4.8 and the ends of the sample are free to rotate during the collapse of each specimen. The tank lid was lowered down by a crane and fitted to secure the lid tightly. Any trapped air inside the tank was expelled by loosening the bleed valve at the top of the tank. The bleed valve was shut after the trapped air was expelled, to make the system pressure-tight. The pressure in the tank was increased via a hydraulic pump in small increments until failure. The pressure gauge (LEO3) was carefully monitored until failure occurred. The test would be stopped if at all during testing a sudden loss of pressure was evident. The buckling pressure was recorded, and the pressure drop noted, as well. The hydraulic pressure was released, and then the tank lid was removed to retrieve and examine the tested specimens. A thorough inspection for any deformation or nonconformance due the applied pressure was performed after the test was completed.

# 5 Results

This section presents all the results related to the study regarding composite production, theoretical modeling, and experimental testing. Samples of conventional carbon fiber polymer composites were also produced to compare the performance of the stainless steel fiber composites.

## 5.1 Quality Control of Produced Samples

The volume fraction of the produced samples was found by microscopy analysis and burn-off testing. The fiber volume fraction based on the burn-off test will be used in the rest of this thesis to get a more conservative estimation since the volume fraction of fiber has the biggest impact on the materials overall mechanical behavior. Assuming densities of 8.0 $g/cm^3$ for the steel fiber, and 1.8 $g/cm^3$ for the carbon fiber, and 1.2 $g/cm^3$ the matrix. Table 5.1 shows the volume fraction of fiber obtained from the microscopy and burn-off method.

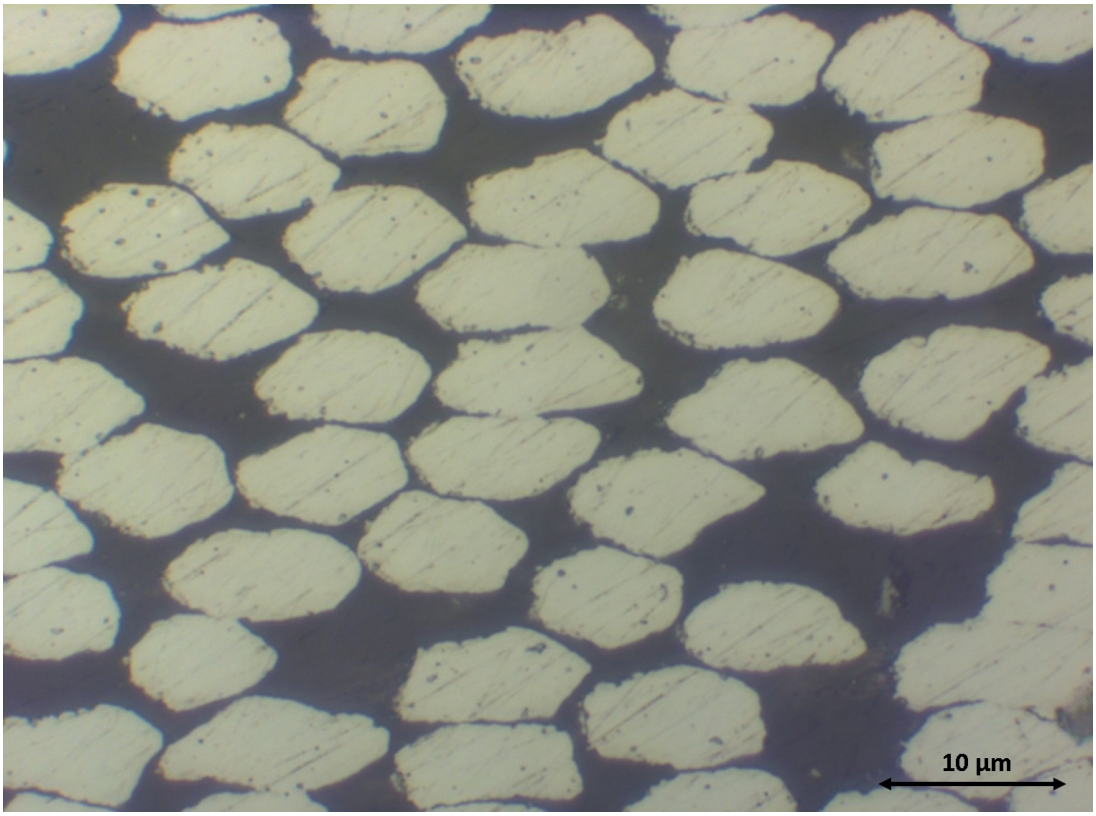


**Figure 5.1:** A microscopy image of the composite cross-section at 1000X showing good impregnation of closely packed fiber bundles in the ±55° layers. The picture also illustrates the irregular cross-section of the fibers due to the bundle drawing.

In parallel to determining the volume fraction of the composite, an investigation on the local volume fraction and thickness of the individual plies was carried out by counting

fibers within control areas on the microscopy pictures. The average volume fraction of fiber measured inside the plies, using the same image analysis method, ranges between 60% and 70%. As shown in Figure 5.1, the fibers have irregular hexagonal cross-sections due to the winding angle of $\pm 55°$ combined with the bundle drawing process. Inside the layers, it could be observed that the fibers are closely packed and well impregnated, but some signs of voids and cracks. The volume fraction of fiber in the individual plies of the SFRP composite pipes was so even that any variation was within the standard deviation. No further investigation of the plies' volume fraction of fiber was carried out. Only microscopy pictures of the SFRP pipes is included in the appendix. Also, the microscopy images indicate that there were little variations in ply thickness, and an average ply thickness is therefore given in Table 5.1.

Analysis of the cross-sections of the sample axis has shown that these microcracks are present through the thickness of the composite. Figure 5.1 indicates that the microstructures in some areas of the SFRP composites have a good resin impregnation of the fibers and little voids can be observed. However, Figure 5.2a and Figure 5.2b shows one of the many microcracks and voids that could be observed in the SFRP3 and SFRP6 samples. The results indicate that the steel fiber composites have more voids and cracks compared to the carbon fiber composites.

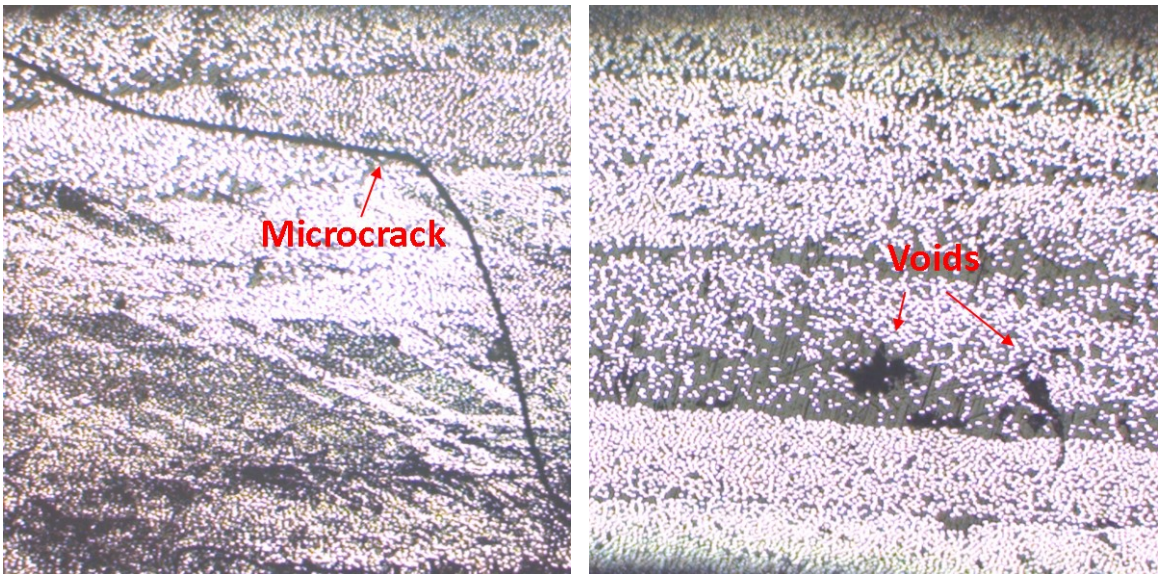


**a** **b**

**Figure 5.2:** Microscopy pictures of the SFRP: (a) Microcrack going through the layers. (b) Presence of voids in the composite.

**Table 5.1:** Wall thickness, ply thickness and volume fraction of fiber of the produced composites using different methods.

| Material | Wall thickness $[mm]$ | Ply thickness $[mm]$ | $V_f$ image analysis [%] | $V_f$ burn-off [%] |
|---|---|---|---|---|
| CFRP3 | 2.20 ± 0.20 | 0.31 ± 0.03 | 53.4 ± 2.7 | 51.9 ± 2.8 |
| SFRP3 | 2.39 ± 0.20 | 0.33 ± 0.04 | 48.3 ± 2.5 | 47.1 ± 2.4 |
| CFRP6 | 4.20 ± 0.34 | 0.33 ± 0.14 | 58.0 ± 2.5 | 57.2 ± 2.6 |
| SFRP6 | 4.46 ± 0.31 | 0.35 ± 0.16 | 47.8 ± 2.9 | 46.5 ± 3.0 |

**Table 5.2:** Theoretical density, experimental density, and void fraction of the produced composite pipes.

| Material | Theoretical density, $\rho_{ct}$ $[g/cm^3]$ | Experimental density, $\rho_{ce}$ $[g/cm^3]$ | Void fraction, $V_v$ [%] |
|---|---|---|---|
| $CFRP_3$ | 1.47 | 1.51 | 2.6 |
| $SFRP_3$ | 4.26 | 4.41 | 3.4 |
| $CFRP_6$ | 1.47 | 1.54 | 4.5 |
| $SFRP_6$ | 4.26 | 4.36 | 2.3 |

Density of steel fiber = 8.0 $g/cm^3$, density of carbon fiber = 1.8 $g/cm^3$, and density of resin = 1.2 $g/cm^3$. A volume fraction of fiber of 45% was assumed to calculate the theoretical density of the composites.

## 5.2 Compressive Test Results

### 5.2.1 Results for CFRP3 and SFRP3 Samples

Figure 5.4a and Figure 5.4b shows the typical stress-strain curves for samples, tested to destruction in axial compression, and radial hoop compression test. When loaded in axial compression (Figure 5.4a), both the CFRP3 and SFRP3 composite exhibits a linear elastic stress–strain relation up to approximately 0.87% strain, after which a transit to a recognizable nonlinear behavior. As the compressive strain reaches a magnitude of 0.87%, a distinct yield region is noticed, further compressive loading ultimately leads to the sample failing by simple crushing and gradually decreasing tangent modulus.

**Figure 5.3:** Failure of SFRP3 hoop sample.

The CFRP3 failed mostly by material crushing, but the SFRP3 sample failed by fractures forming in a ring around the circumference of the sample, as shown in Fig 5.3. The failure had the appearance of axisymmetric shell buckling. From the strain gauges, it could be observed a local strain concentration across the width of the sample. The compressive elastic modulus was calculated as the slope of the elastic portion of the stress–strain curves. Poisson's ratio was calculated as the ratio of the hoop strain to the axial strain. It was observed that under compression, a localized failure zone is noticed, associated with microbuckling or kink-band formation of the fibers (Figure 5.5). It was noticed that the strength determined from the loading curves in the axial direction of the samples

have different values in compression. By contrast with the longitudinal strength, the ring strength of both materials has approximately the same magnitude in compression.

When loaded radially in the hoop direction, the composite material experiences mainly elastic deformation before failure, indicating that hoop failure of the samples is dominated primarily by the matrix properties and state of stress at the fiber/matrix interface. Figure 5.4b shows that both samples exhibit a linear elastic stress–strain relation up till 12.7 and 18.4% strain, respectively, before failure. During loading, microcracks propagating between the layers of the steel fiber sample could be observed. These microcracks propagated perpendicular to the loading direction and initiated fiber/matrix debonding at the interface. Even after cracking and debonding of the matrix and fiber yielding, the laminate continued to carry increasing compressive stresses. Successive damage development and fiber plastic straining ultimately lead to catastrophic failure of the sample (Figure 5.6).

Figure 5.7a shows the relation between the shear stress and the strains, measured from the axial and hoop strain gauges, bonded to the specimens surface at a 55°angle to the principal material directions. From this experimental data, the shear stress–strain curve was determined as shown in Figure 5.7b. The material response is linear up to approximately 0.6% shear strain, followed by nonlinear behavior. As the level of stress is increased, a peak shear stress is reached, followed by a softening process which results in a uniform stress plateau. The onset of nonlinear behavior lies at a relatively higher applied strain for SFRP3 composite compared to the CFRP3 specimens. The elastic shear modulus values were determined were derived from the slopes of the stress/strain curves up to 0.1% strain obtained from the strain gauges. The shear yield stress was calculated based on the applied load before the point of non-linearity, and the obtained experimental values are listed in Table 5.3. The in-plane shear stress were determined from Eq. (5.1), using the applied load F and the samples original cross-sectional area, ($A_o$) [7]:

$$\tau_{12} = \frac{F}{A_o} \tag{5.1}$$

The in-plane shear strain was calculated from the individual strain values using Eq. (5.2), where $\epsilon_{axial}$ and $\epsilon_{hoop}$ are the axial and hoop strain, measured at a 55° offset angle to the principle material coordinate system

$$\gamma_{12} = \epsilon_{axial} - \epsilon_{hoop} \tag{5.2}$$

The in-plane shear modulus was determined by the slope of the least-squares linear regression fit to the elastic region of the shear stress–strain curve. The in-plane mechanical properties of the CFRP3 and SFRP3 composite is summarized in Table 5.3. The pre-

dicted properties was found by Eqs. (3.1) – (3.6). The results of the predicted elastic constants and the experimental results are shown in Table 5.4.

**Table 5.3:** In-plane mechanical properties of CFRP3 and SFRP3 composite samples.

| Compressive properties | CFRP3 | SFRP3 |
|---|---|---|
| Volume fraction of fiber [%] | 51.9 | 47.1 |
| Axial compressive modulus, $E_1$ [GPa] | 103.8 | 83.2 |
| Hoop compressive modulus, $E_2$ [GPa] | 4.8 | 3.5 |
| Axial compressive strength, $X_1$ [MPa] | 109.4 | 74.5 |
| Hoop compressive strength, $Y_2$ [MPa] | 5.6 | 5.8 |
| Axial failure strain, $\epsilon^f_{axial}$ [%] | 4.2 | 6.7 |
| Hoop failure strain, $\epsilon^f_{hoop}$ [%] | 12.7 | 18.4 |
| | | |
| *Shear properties* | | |
| Shear modulus, $G_{12}$ $[GPa]$ | 2.49 | 2.63 |
| Shear strength, $S_{12}$ $[MPa]$ | 54.7 | 37.3 |
| Shear strain at shear strength, $\gamma_{12}$ [%] | 1.4 | 2.6 |

**Table 5.4:** Calculated and experimental in-plane elastic properties for CFRP3 and SFRP3 composite pipe.

| Material | CFRP3 | | SFRP3 | |
|---|---|---|---|---|
| Property | Calculated | Experimental | Calculated | Experimental |
| $E_1$ [GPa] | 120.9 | 103.8 | 92.6 | 83.2 |
| $E_2$ [GPa] | 7.4 | 4.8 | 6.0 | 3.5 |
| $v_{12}$ [ - ] | 0.32 | 0.30 | 0.33 | 0.31 |
| $G_{12}$ [GPa] | 2.42 | 2.49 | 2.57 | 2.63 |

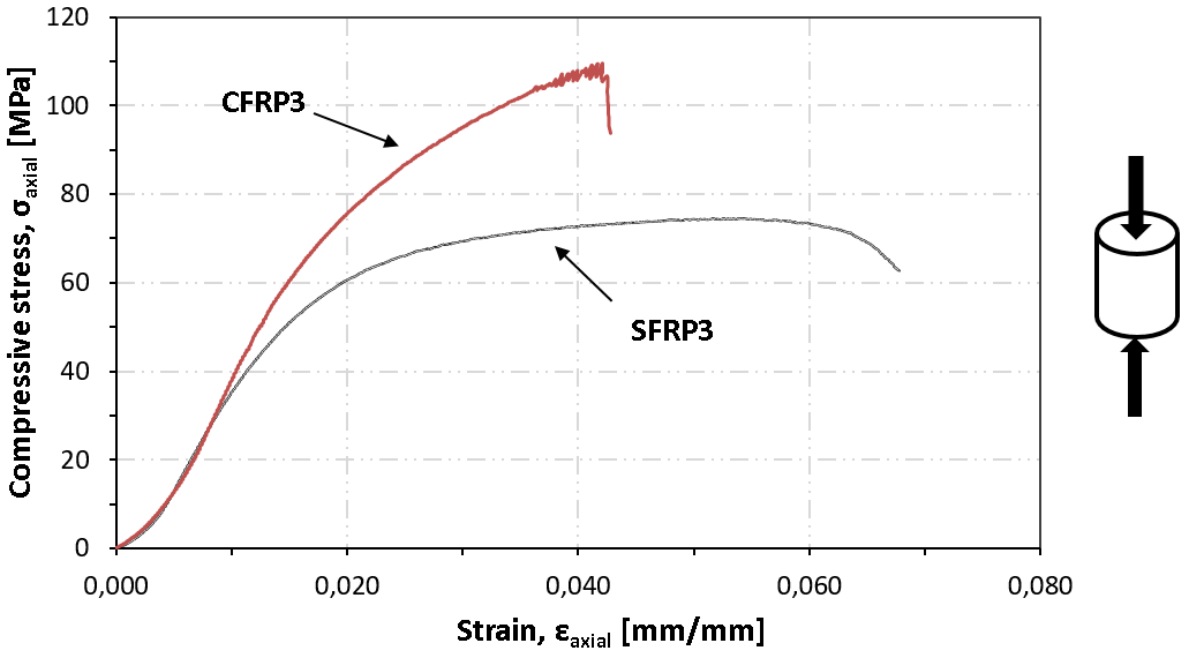


a

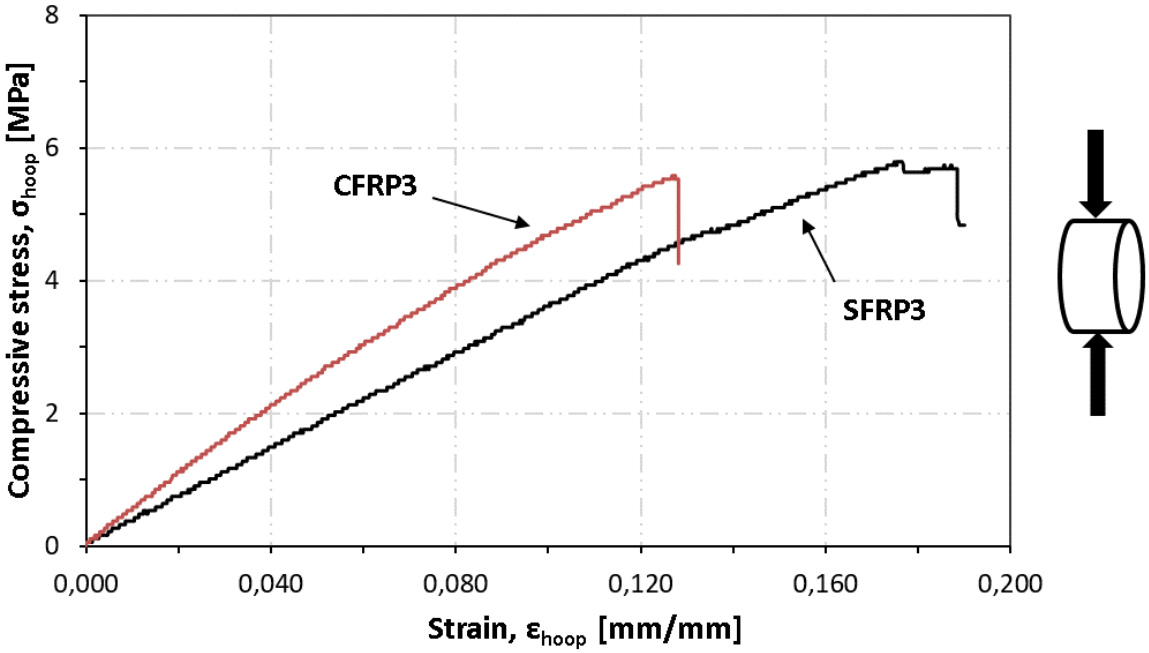


b

**Figure 5.4:** Stress–strain response of UD carbon fiber/epoxy and UD steel fiber/epoxy composite samples: (a) Compressive loading in the axial direction of SFRP3 and CFRP3 composite samples. (b) Compressive loading radially to the hoop direction of SFRP3 and CFRP3 composite samples.

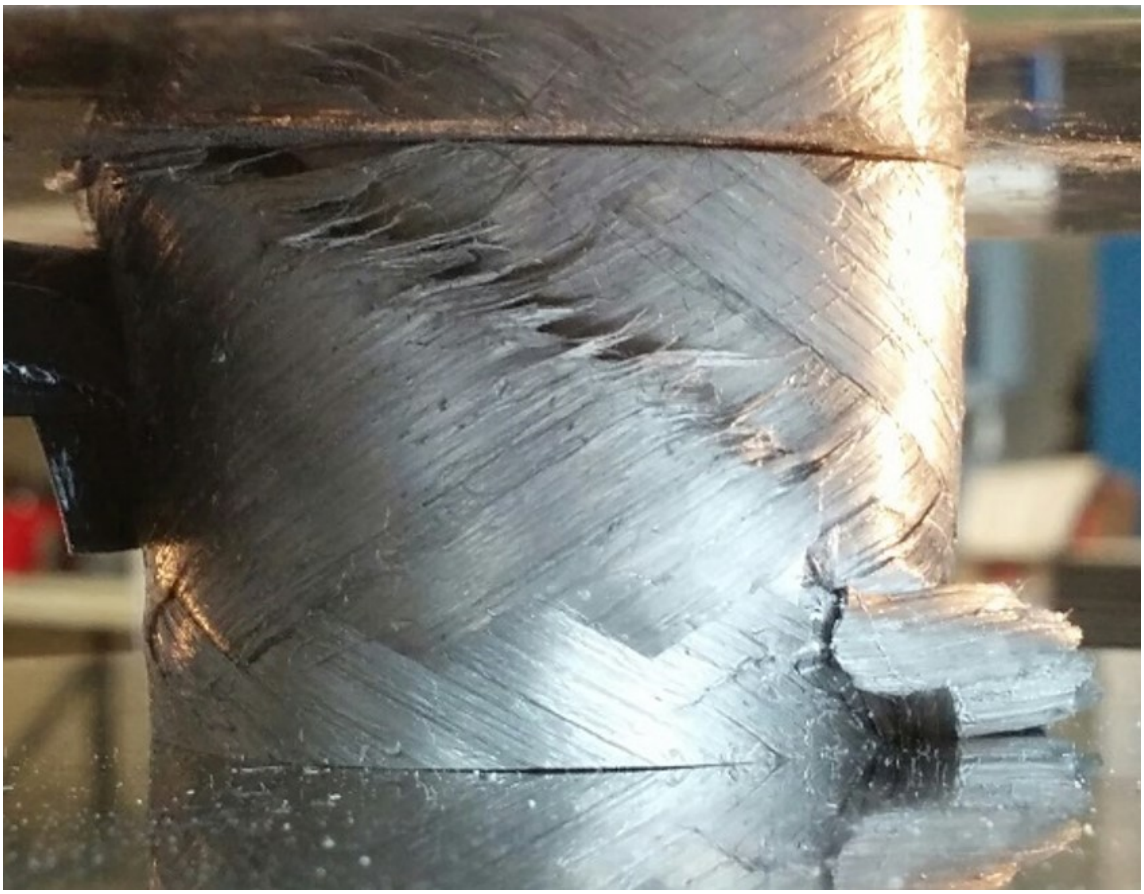

**Figure 5.5:** Failure and kink band formation during axial compressive loading of the SFRP3 sample.

**Figure 5.6:** Failure of SFRP3 hoop sample.

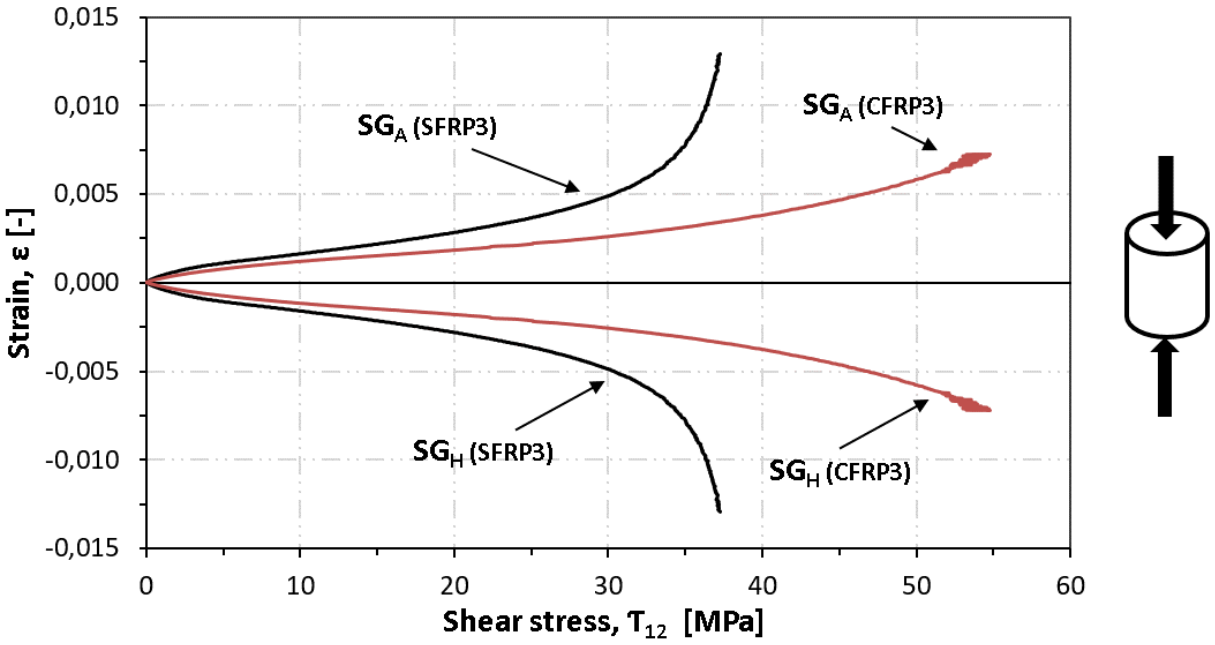


a

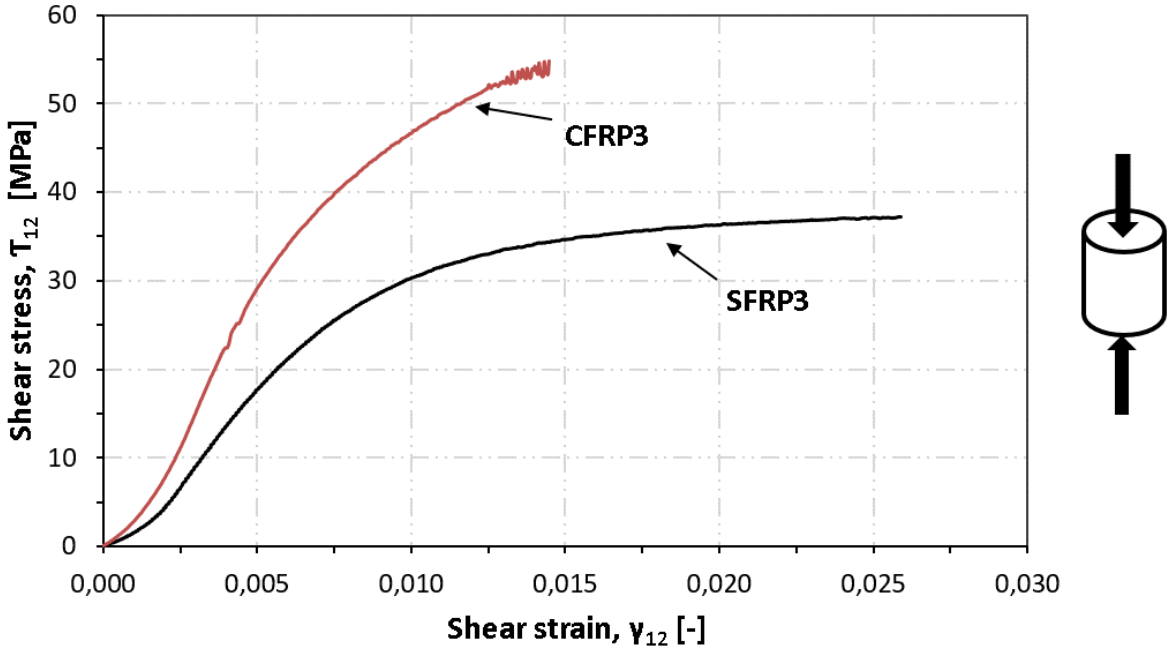


b

**Figure 5.7:** Shear properties of CFRP3 and SFRP3 composite samples: (a) Strain gauge readings ($SG_A$ = axial strain gauge, $SG_H$ = hoop strain gauge). (b) In-plane shear stress–strain behaviour of CFRP3 and SFRP3 composite samples.

### 5.2.2 Results for CFRP6 and SFRP6 Samples

Figure 5.8a and Figure 5.8b shows the typical stress-strain curves for samples, tested to destruction in axial compression, and radial hoop compression test.

Figure 5.8a shows the case of axial compression the SFRP6 sample exhibits a linear elastic stress–strain relation up to approximately 0.87% strain, after which a transit to a recognizable nonlinear behavior. As the compressive strain reaches a magnitude of 2%, a distinct yield region is noticed, further compressive loading ultimately leads to the sample failing by simple crushing at approximately 9% strain. However, the CFRP6 sample only exhibits a linear elastic stress–strain relation up to about 3% strain, after which failure occurs, failing at a much lower compressive strength compared to the SFRP6 sample. In the SFRP6 samples, the failure region was more extensive compared to the CFRP6, and there were pronounced fractures running in directions parallel to the fibers. In a similar way to the CFRP3 and SFRP3, a local strain concentration could be observed across the width of the sample. Hence, microbuckling or kink-band formation of the fibers could be observed on the specimen (Figure 5.9).

Figure 5.8b shows that in the case of hoop compression both the CFRP6 and SFRP6 samples exhibit a linear elastic stress–strain relation up till approximately 10% strain before failing. During loading, microcracks propagating between the layers of the steel fiber sample could be observed. These microcracks propagated perpendicular to the loading direction and initiated fiber/matrix debonding at the interface. Even after cracking and debonding of the matrix and fiber yielding, the laminate continued to carry increasing compressive stresses. Successive damage development and fiber plastic straining ultimately lead to catastrophic failure of the sample (Figure 5.10).

Figure 5.11a shows the relation between the shear stress and the strains, measured from the axial and hoop strain gauges, bonded to the specimens surface at a 55° angle to the principal material directions. From this experimental data, the shear stress–strain curve was determined as illustrated in Figure 5.11b. The material response is linear up to approximately 0.6% shear strain, followed by nonlinear behavior. As the level of stress is increased, a peak shear stress is reached, followed by a softening process which results in a uniform stress plateau, indicating interlaminar shearing between adjacent plies and plastic deformation of the matrix material. The onset of nonlinear behavior lies at a relatively higher applied strain for SFRP6 composite compared to the SFRP3 specimens. The obtained experimental values are listed in Table 5.5. The results of the predicted elastic constants and the experimental results are shown in Table 5.6.

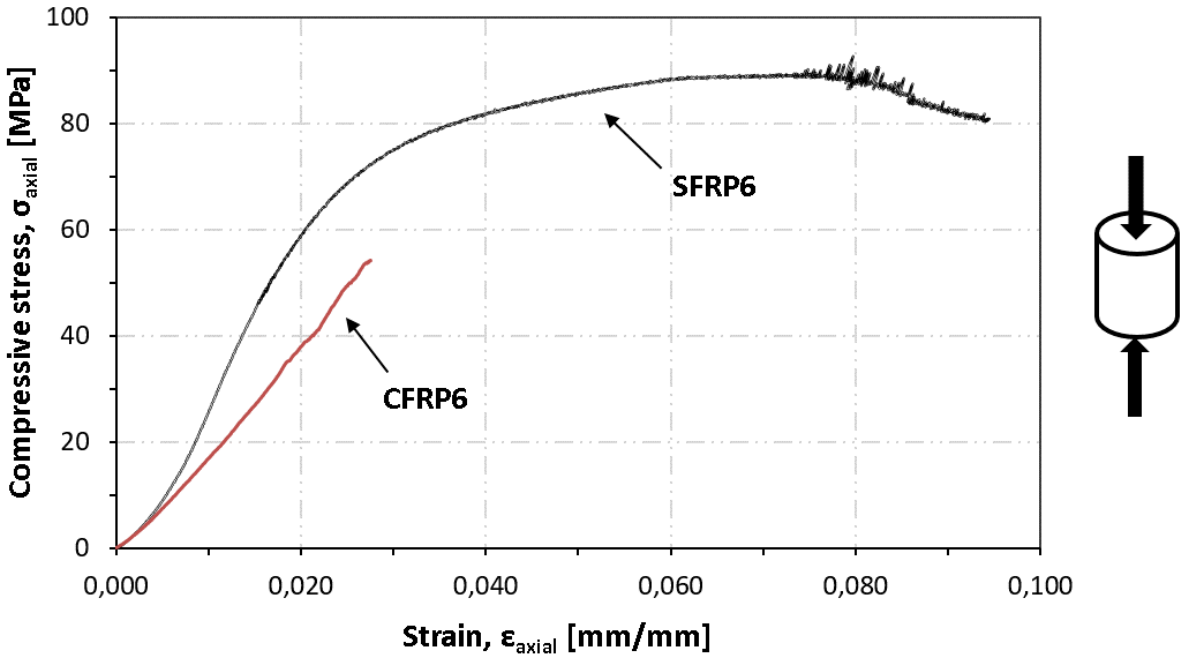


a

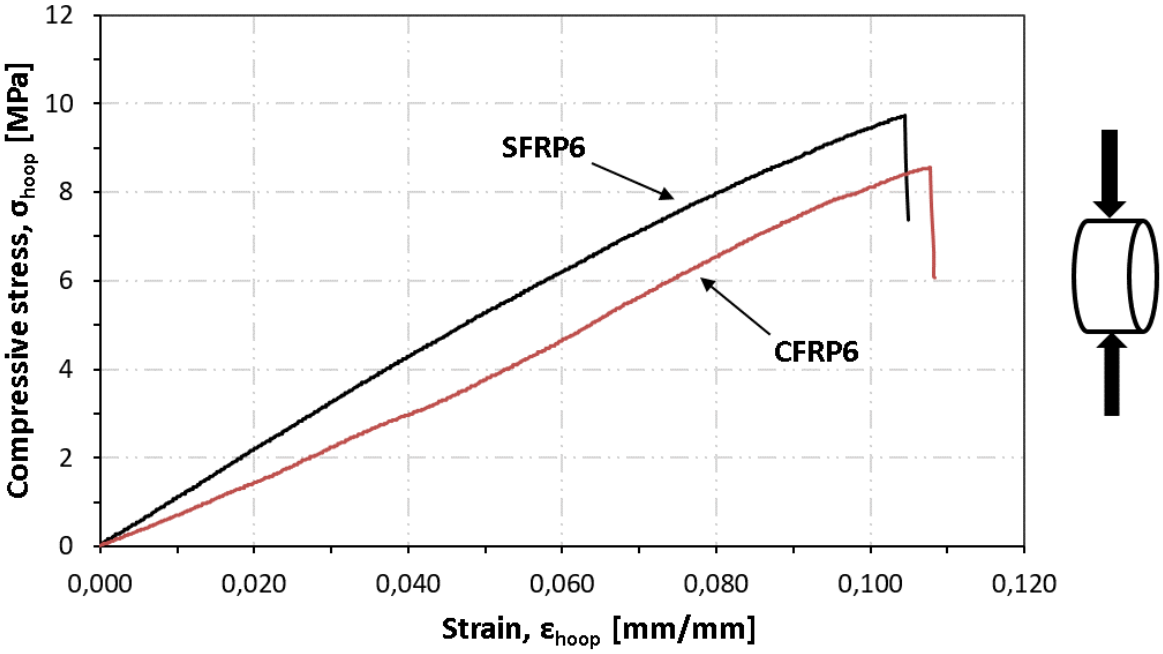


b

**Figure 5.8:** Stress–strain response of UD carbon fiber/epoxy and UD steel fiber/epoxy composite samples: (a) Compressive loading in axial direction of SFRP6 and CFRP6 composite samples. (b) Compressive loading radially to the hoop direction of SFRP6 and CFRP6 composite samples.

**Table 5.5:** In-plane mechanical properties of CFRP6 and SFRP6 composite samples.

| Compressive properties | CFRP6 | SFRP6 |
|---|---|---|
| Volume fraction of fiber [%] | 57.2 | 46.5 |
| Axial compressive modulus, $E_1$ [GPa] | 116.2 | 80.5 |
| Hoop compressive modulus, $E_2$ [GPa] | 7 .1 | 8.7 |
| Axial compressive strength, $X_1$ [MPa] | 54.2 | 92.7 |
| Hoop compressive strength, $Y_2$ [MPa] | 8.6 | 9.7 |
| Axial failure strain, $\epsilon^f_{axial}$ [%] | 2.8 | 9.4 |
| Hoop failure strain, $\epsilon^f_{hoop}$ [%] | 10.8 | 10.4 |
| | | |
| *Shear properties* | | |
| Shear modulus, $G_{12}$ $[GPa]$ | 2.8 | 2.34 |
| Shear strength, $S_{12}$ $[MPa]$ | 27.1 | 46.2 |
| Shear strain at shear strength, $\gamma_{12}$ [%] | 1.6 | 3.2 |

**Table 5.6:** Calculated and experimental in-plane elastic properties of the CFRP6 and SFRP6 composite pipe.

| Material | CFRP6 | | SFRP6 | |
|---|---|---|---|---|
| Property | Calculated | Experimental | Calculated | Experimental |
| $E_1$ [GPa] | 139.2 | 116.2 | 91.5 | 80.5 |
| $E_2$ [GPa] | 7.4 | 7.1 | 6.0 | 8.7 |
| $v_{12}$ [ - ] | 0.32 | 0.31 | 0.33 | 0.32 |
| $G_{12}$ [GPa] | 2.72 | 2.80 | 2.19 | 2.34 |

**Figure 5.9:** Failure of the SFRP6 axial sample.

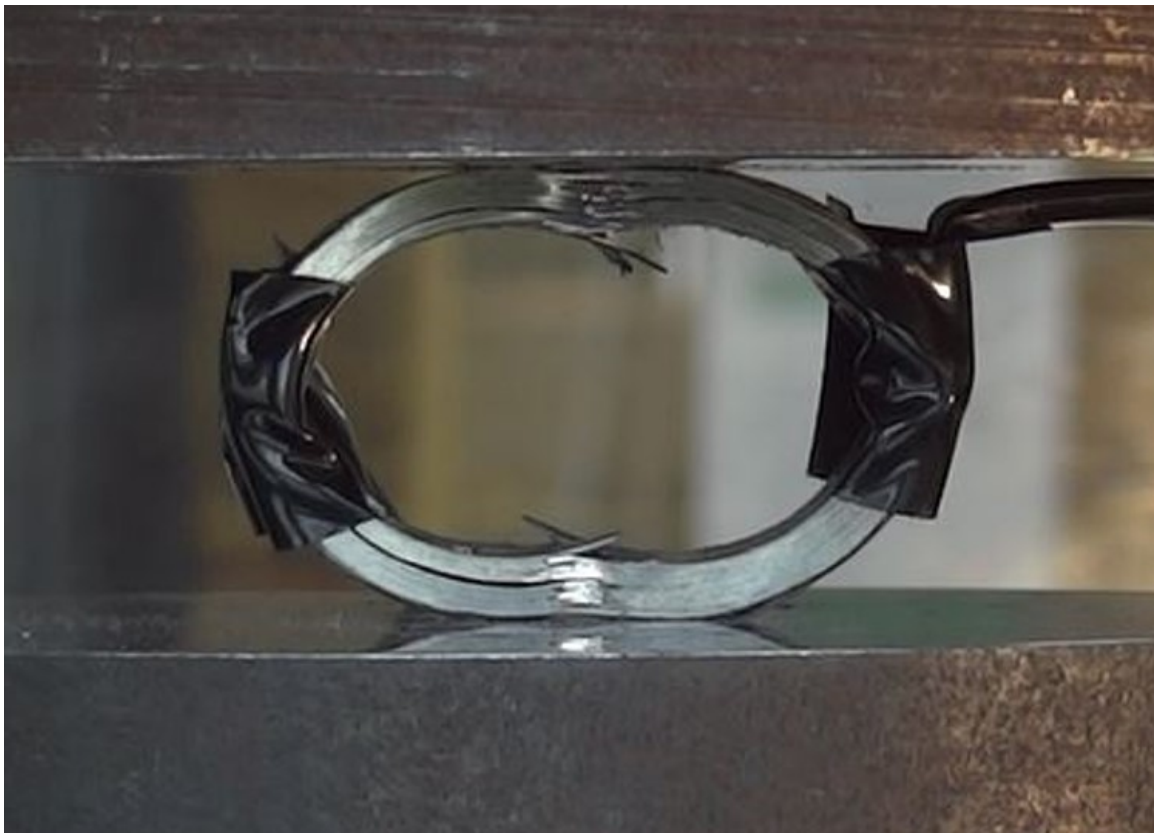

**Figure 5.10:** Failure of the SFRP6 hoop sample.

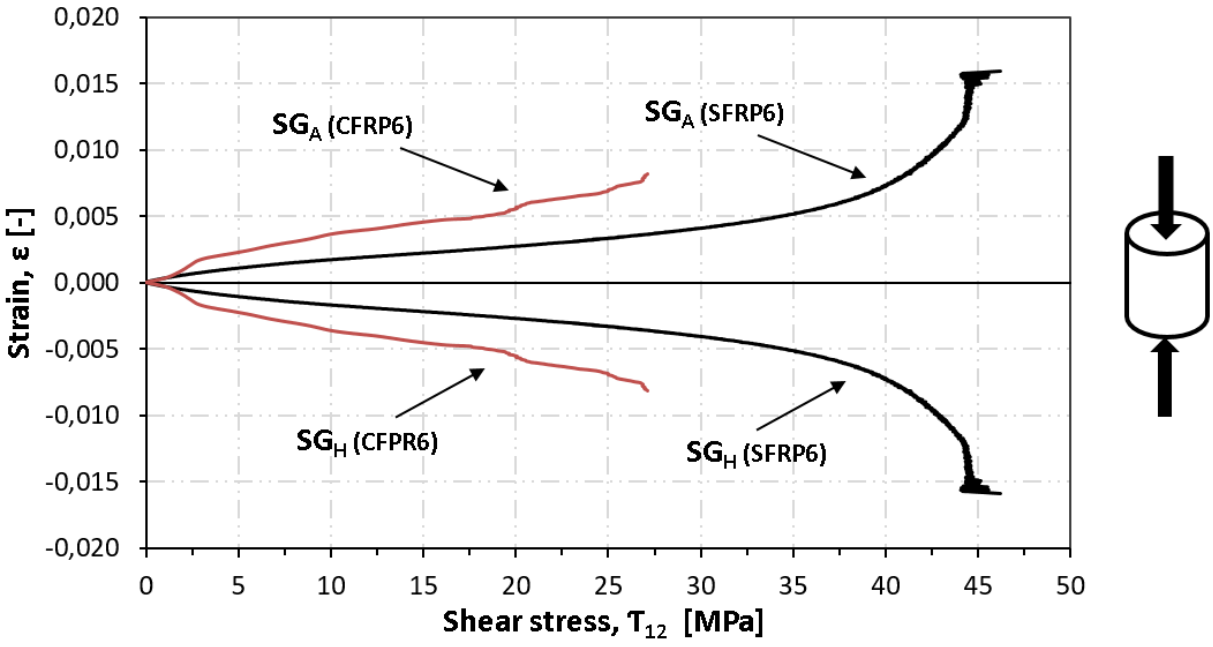


a

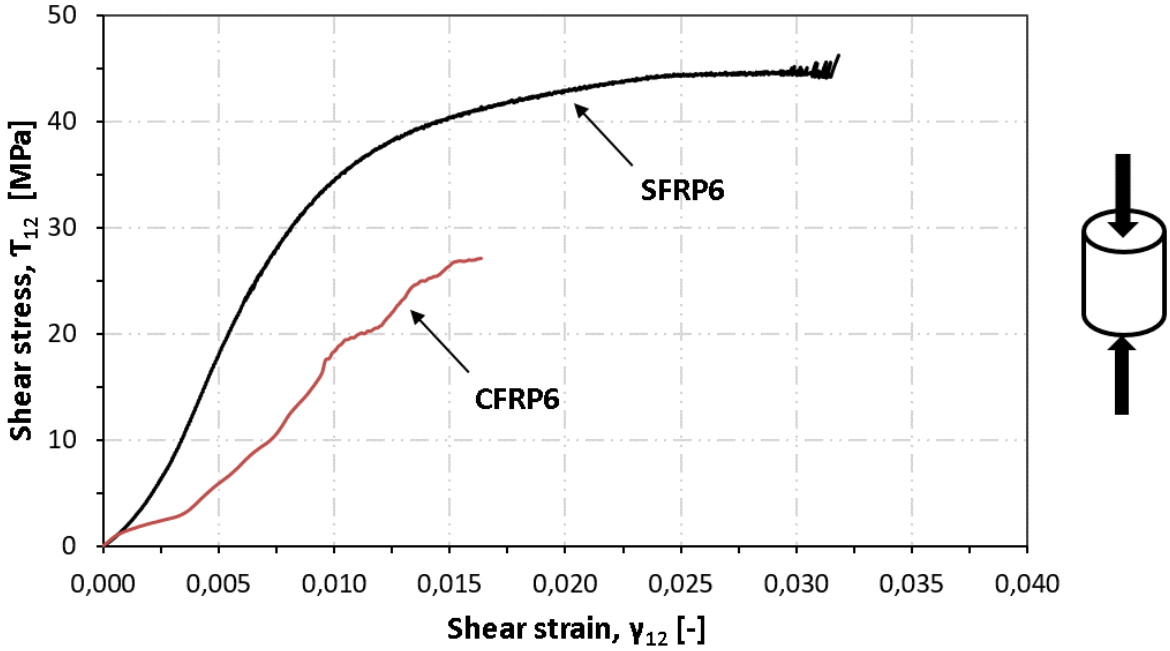


b

**Figure 5.11:** Shear properties of CFRP6 and SFRP6 composite samples: (a) Strain gauge readings ($SG_A$ = axial strain gauge, $SG_H$ = hoop strain gauge). (b) In-plane shear stress–strain behaviour of CFRP6 and SFRP6 composite samples.

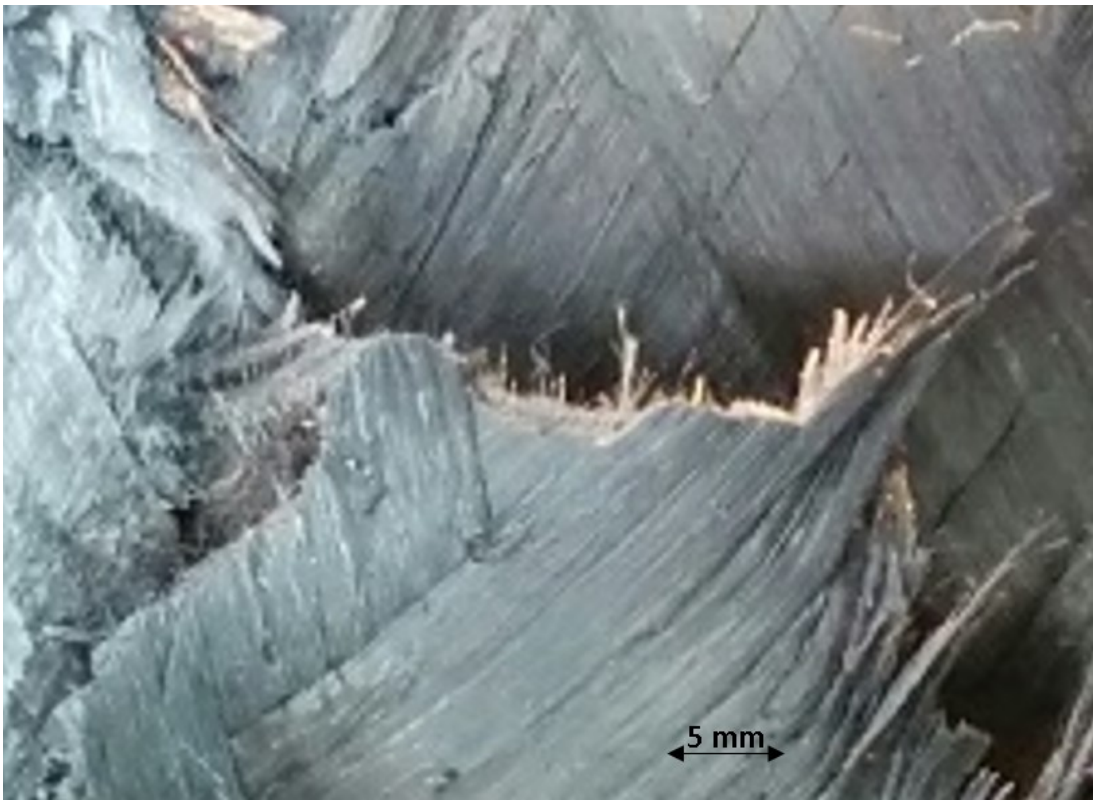


**Figure 5.12:** Shear failure of the SFRP6 hoop sample.

## 5.3 External Pressure Test Results

Figure 5.14 and Figure 5.15 shows that the pressure graph for the CFRP3 and SFRP3, respectively. For both the CFRP3 sample and SFRP3 sample, failure occurred at a critical buckling pressure by a significant drop in pressure, together with a loud bang. A visual inspection of the fractured specimens provided further insights into the mechanisms accompanying structural failure. The results indicate that the deformation before buckling was significant so that the material yielded and buckled inelastically. However, these changes were not measurable with the existing test set-up. Hence, stresses were calculated assuming unchanged specimen dimensions.

**Table 5.7:** Theoretical and experimental buckling results.

| Specimen | $P_{cr}$ DTMB $[MPa]$ | $P_{cr}$ von Mises $[MPa]$ (n-lobes) | $P_{exp}$ $[MPa]$ |
|---|---|---|---|
| $CFRP_3$ | 23.4 | 21.1 (2) | 14.6 |
| $SFRP_3$ | 18.2 | 17.1 (2) | 11.7 |
| $CFRP_6$ | 69.3 | 62.4 (5) | 49.3* |
| $SFRP_6$ | 55.3 | 52.5 (5) | 49.5* |

*No buckling of the test sample.

Figure 5.16 and Figure 5.17 shows that the pressure graph for the CFRP6 and SFRP6, respectively. For the CFRP6 and SFRP6 sample, the experiment had to be stopped because the pressure inside the tank reached the maximum allowable pressure limit of the pressure tank (maximum operating pressure of 50 MPa). A visual inspection of the fractured specimens indicates that the CFRP6 and SFRP6 samples showed no indication of buckling even when the autoclave reached the pressure limit. Figure 5.13 shows the samples after being loaded under external pressure. Table 5.7 contains the analytical and experimental values for the critical pressure for each of the four pipes.

**Figure 5.13:** A picture showing the samples after external pressure test.

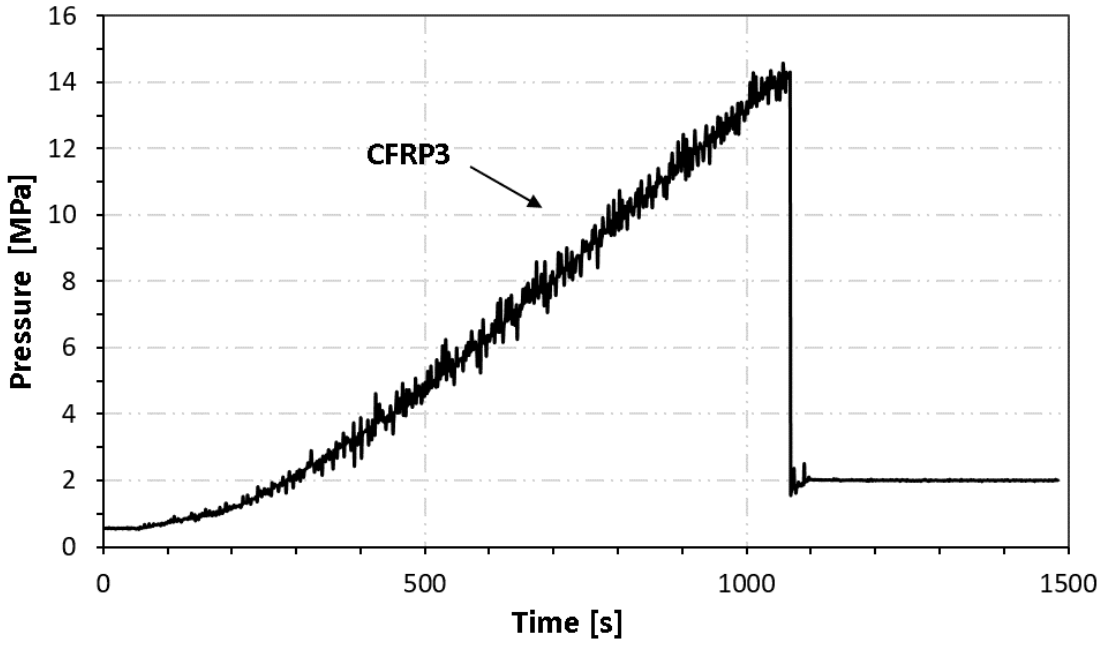


**Figure 5.14:** External pressure test graph for the CFRP3 sample.

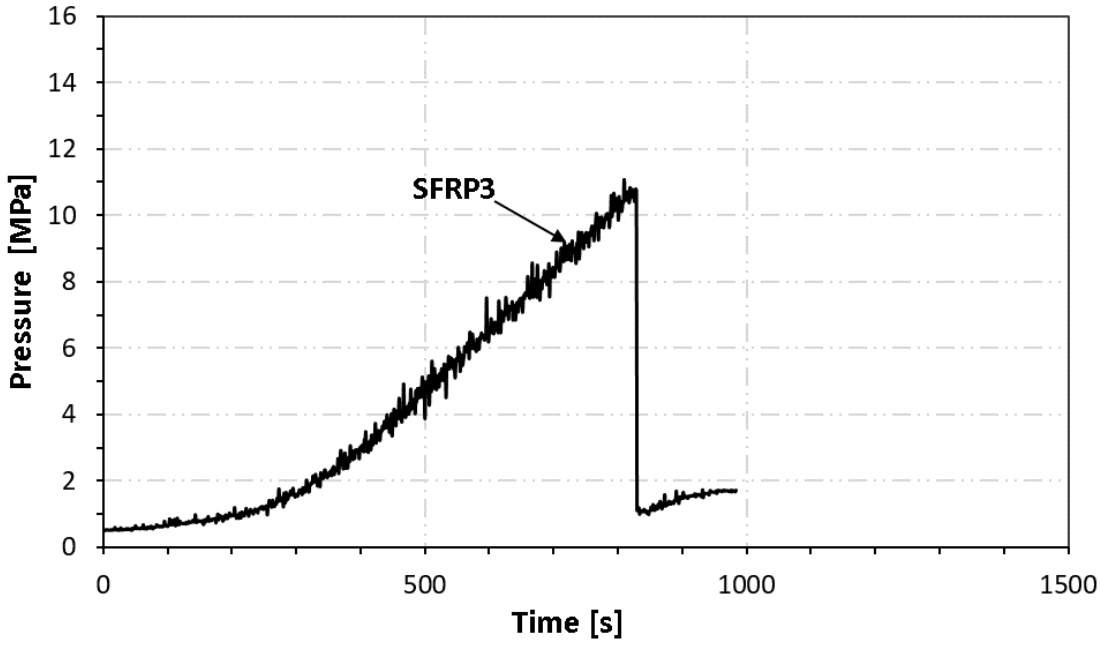


**Figure 5.15:** External pressure test graph for the SFRP3 sample.

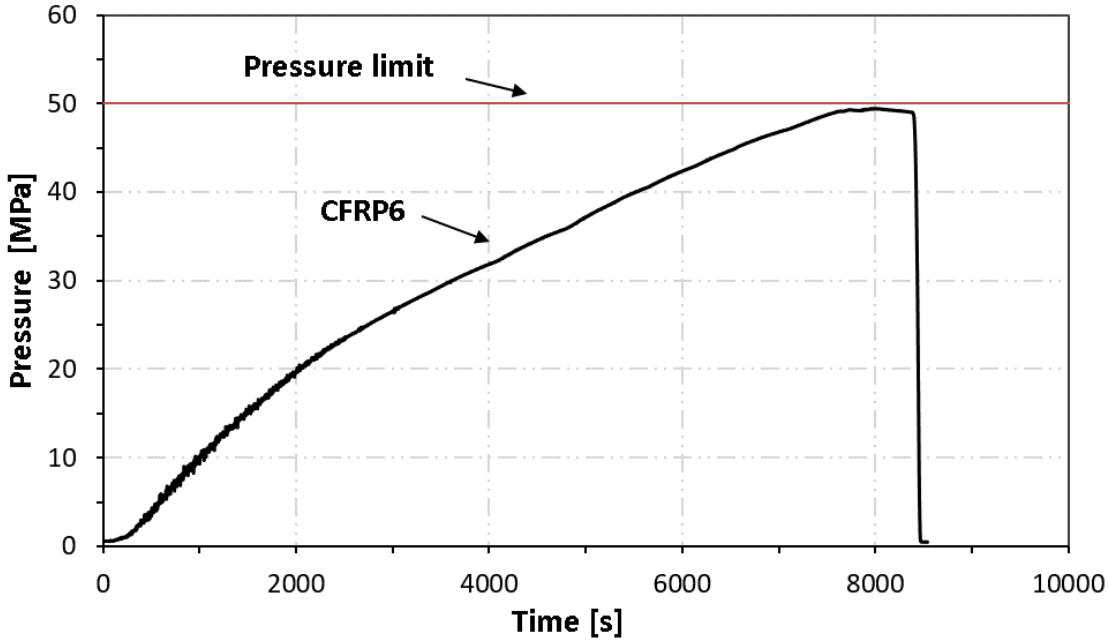


**Figure 5.16:** External pressure test graph for the CFRP6 sample.

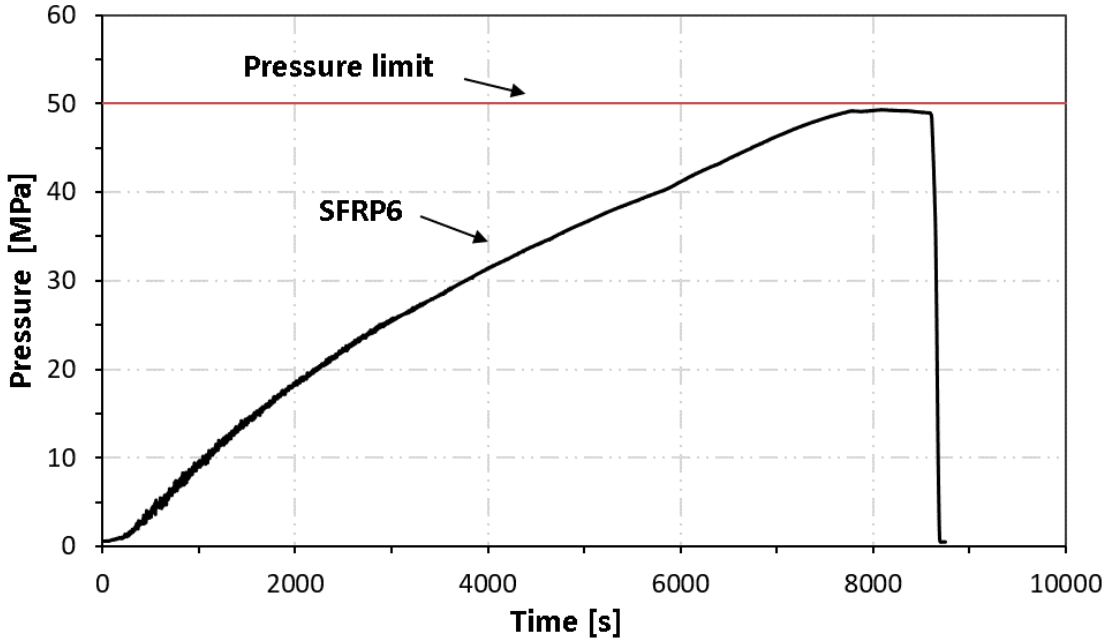


**Figure 5.17:** External pressure test graph for the SFRP6 sample.

## 5.4 Stiffness Comparison of Steel Fiber Composites and Other Materials

This section has utilized simple micromechanical models to predict the stiffness, and density of the steel fiber reinforced polymer composites. Followed by a comparison to typical metals used in the offshore oil and gas industry, and traditional reinforced fiber composites. Table 1.1 showed that steel fibers combine a high stiffness with a high strain-to-failure, but was only a comparison between the different reinforcing fibers themselves, and not the material property for their respective composites. Table 5.8 lists the material properties of metals and the constituent materials used to calculate the composite properties. These simple stiffness models should render adequate predictions, which is much more challenging in the case of strength or toughness models. Hence, only the stiffness of steel fiber composites will be considered.

### 5.4.1 Stiffness and Density Comparison

Figure 5.18 shows the stiffness as a function of volume fraction for UD glass fiber composites (GFRP), UD carbon fiber composites (CFRP) and UD steel fiber composites (SFRP), and stiffness of metals steel (Fe), aluminum (Al) and titanium (Ti).

At a volume fraction of fiber at 50%, the SFRP composite has almost equal stiffness Ti and higher stiffness than Al and GFRP composites. However, the stiffness of the SFRP composite is outperformed by the CFRP composite when at an equal volume fraction of fiber.

**Table 5.8:** Mechanical properties of different materials used for modeling.

| Material | Stiffness $[GPa]$ | Strength $[MPa]$ | Poisson's Ratio | Density $[g/cm^3]$ | Shear stiffness $[GPa]$ | Percent Elongation |
|---|---|---|---|---|---|---|
| Steel [34] | 200 | 500 | 0.30 | 7.9 | 79.3 | 1.5 |
| Titanium [34] | 116 | 1100 | 0.34 | 4.5 | 41.0 | 10 |
| Aluminum [34] | 70 | 124 | 0.33 | 2.7 | 24.0 | 5.7 |
| Steel fiber [1] | 193 | 660 | 0.30 | 8.0 | 74.2 | 20 |
| Glass fiber [34] | 70 | 2400 | 0.30 | 2.6 | 26.2 | 1.6 |
| Carbon fiber [18] | 230 | 4400 | 0.30 | 1.8 | 27.0 | 1.9 |
| Matrix [17] | 3.2 | 65 | 0.35 | 1.0 | 1.1 | 12 |

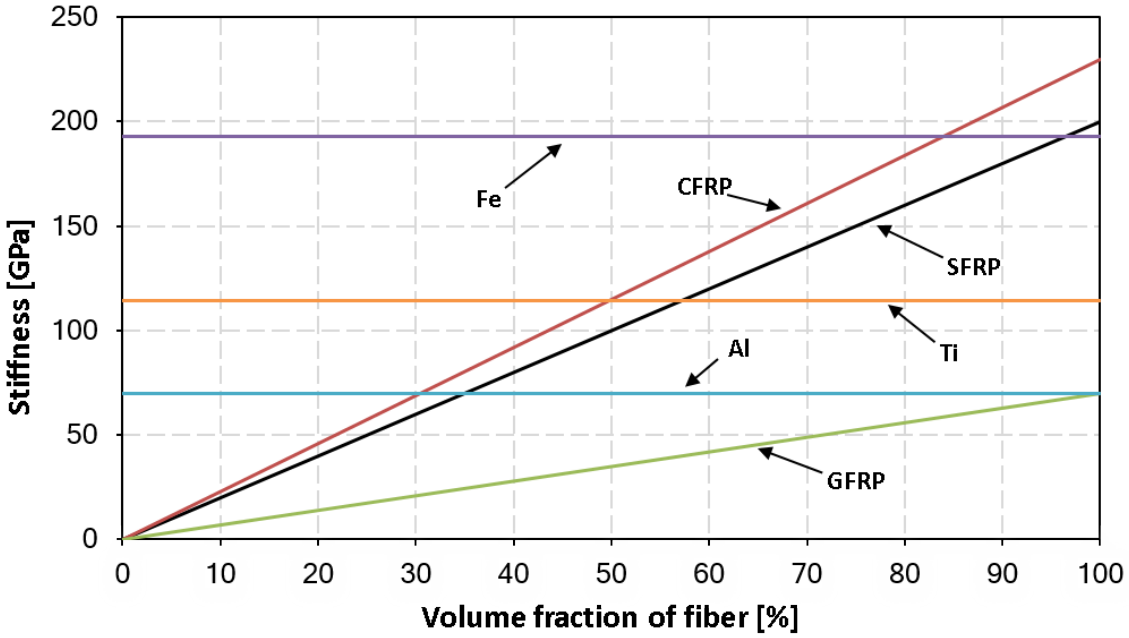


**Figure 5.18:** Modeled stiffness of glass, carbon and steel fiber composites for increasing volume fraction of fiber.

Figure 5.19 presents the density of the different materials. For SFRP composites, the density as a function of the volume fraction of fiber shows a high slope, due to the high density of steel fibers.

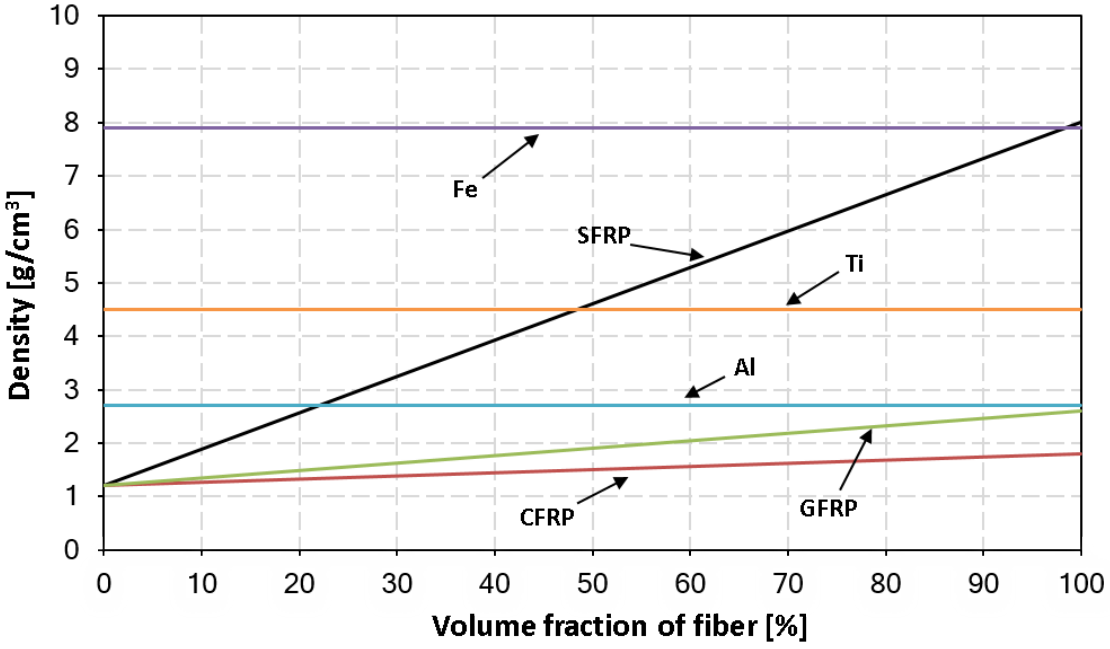


**Figure 5.19:** Modeled density of glass, carbon and steel fiber composites for increasing volume fraction of fiber.

Hence at a fiber volume fraction of 50%, it has a density similar as titanium but is 60% heavier than aluminum, 1.5 times heavier than glass fiber composites and 2 times heavier than carbon fiber composites with the same volume fraction of fiber.

### 5.4.2 Specific Stiffness Comparison

In the case of designing for high stiffness and light-weight applications, the stiffness can just be divided by the density to get the specific density. Figure 5.20 shows the specific stiffness of the different materials. The SFRP composites get outperformed by the CFRP composites, which is not surprising because of their low density. CFRP composites have the highest specific stiffness in all cases, and the SFRP composites show either greater or equal specific stiffness as that of GFRP composites and almost comparable to aluminum or titanium. The specific stiffness of the SFRP composite is lower than of the CFRP because the stiffness of the base materials is similar, but the density is four times higher. As a result of this, the specific stiffness of the SFRP is approximately half of the stiffness of CFRP composites.

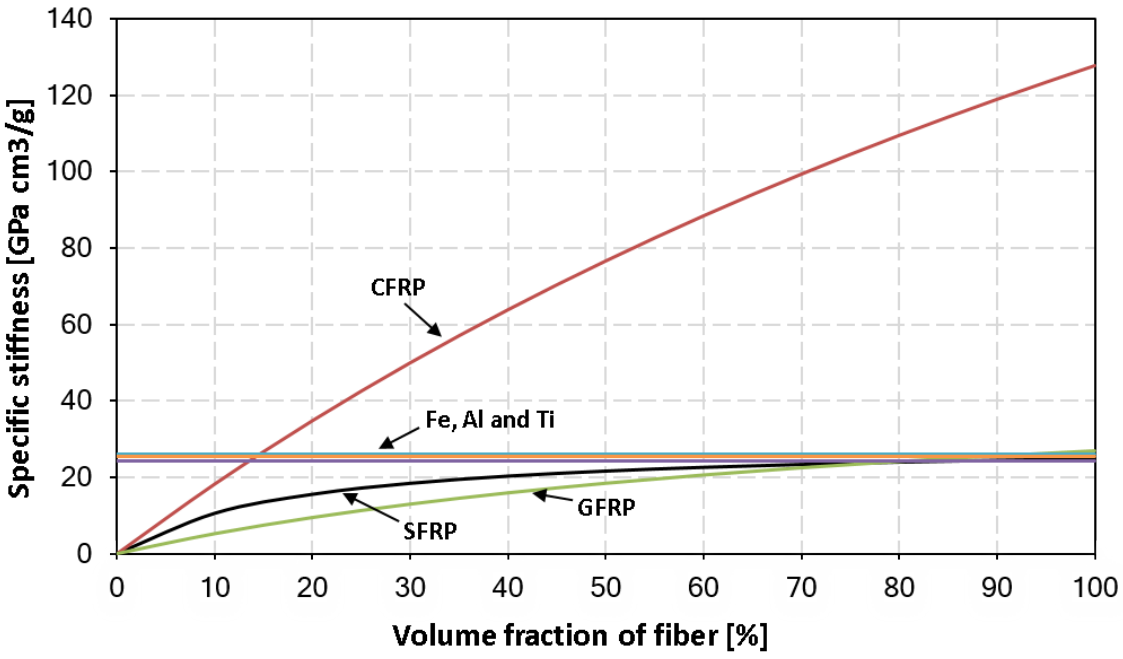


**Figure 5.20:** Modeled specific stiffness of glass, carbon and steel fiber composites for increasing volume fraction of fiber.

# 6 Discussion

## 6.1 Method and Data Acquisition

The primary emphasis of this project has been on a simple approach to avoid selection of a technically elegant solution, which cannot produce pipes consistently or reliably. The size of the samples is small due to a limited supply of steel fiber available for production. Consequently, only one pipe was produced for each layup, thickness, and material. Therefore, the statistical confidence of the results obtained is low. However, even though the statistical confidence is low, the results have been discussed with the assumption that the results are absolute because it's the only results available. Values found or obtained for the material properties, and strength of composites are associated with significant scatter, single point measures, average values and other statistically derived values such as the characteristic values. Therefore, some values are strongly dependent on the quantity and location of measurements and applied method; the results have given an indication of the performance of filament wound SFRP compared to CFRP despite this. Also, the small samples were ideal for testing given the autoclave's dimension (400 mm in diameter and 1 m in length), compared to a pressure vessel solution used in earlier work [19].

The ROM formula is a simple equation to be used for qualitative evaluation of different candidate materials and was good enough for preliminary design purposes and provided a first estimate of the composite properties. The material properties of the composite are based on several assumptions made during this study, and the properties of the constituent materials were partially given by the manufacturer but did not include parameters for other directions than the main parameters. Therefore, the values for the Poisson's ratio and the shear modulus in the other directions were found from textbook and assumed to be the same.

FEA analysis of the buckling behavior could have been useful to obtain data. One of the goals, in the beginning, was to use FEA to model and match the buckling behavior of these SFRP cylindrical pipes under external pressure. But the FEA-analysis proved to be time-consuming, and errors occurred all the time. It was decided to disregard the results obtained from the FEA-analysis to narrow the scope of the thesis. The choice to disregard the FEA results was because of the lack of experience on using FEA tools from the authors' side. To obtain any meaningful FEA results, the investigator must know the principles underlying the finite-element method. Also, the matching method was considered to be questionable, because many parameters could be tweaked and varied to match the FEA-results with those obtained from the external pressure test.

## 6.2 Composite Production

The lower volume fraction of fiber for the SFRP composite samples compared to the CFRP composite samples could be because of the lower winding tension applied to avoid fiber breakage of the steel fiber during winding. Mertiny and Ellyin [35] investigated the influence of the applied winding tension on the physical and mechanical properties of GFRP composite pipes and found that the component strength depends on the degree of tensioning. In general, an increase in winding tension results in an increase in volume fraction of fiber for the finished part. And consequently, an increase in volume fraction of fiber has a beneficial effect on the component strength in the case of a fiber dominated loading. When loaded in hoop compression a slight decrease in the failure strength was obtained by increasing fiber compaction [35].

However, it should be mention that there is a limit to how much tension can be applied before the fiber breaks or can't be compressed anymore. The need for a continuous tension of the fiber is also a problem because fiber breakage and sudden changes in the curvature tend to create resin rich areas. It is highly likely that the high winding tension combined with sharp uncured resin residues caused the fiber to break. Therefore, it is of great importance to make sure that the entire system is clean and free of uncured resin from previous winding sessions. The cleanliness of the wet winding method is a significant disadvantage because of the uncured resin that can stick to the rollers from subsequent winding procedures. The cleanliness in for example prepreg winding is much better because the resin is cured to the B-stage already [19].

The steel fiber loses splits easily without tension (Figure 2.15). Therefore, the steel fibers should be coated with more sizing to make them stick better together for easier handling and production. The unbundling of the fibers can result in misalignment in the composite which is adverse to the compressive strength of the material. Therefore, the winding tension should be high enough for the fibers to align properly on the mandrel, but low enough to avoid breakage of the steel fiber. Any misalignment of the fiber between 2 to 4° can significantly lower the stiffness and strength of the composite due to the low stiffness and yield strength of the epoxy.

During pipe extraction mentioned earlier in section 2.4.5, it was discovered that the pipes would not slip from the mandrel of which they were wound over due to the increased friction caused by the vacuum bag sealant tape and plastic wrapping. A suggestion would be to avoid using any vacuum bag sealant tape and plastic wrapping at all on the mandrel. Instead, more lubricant could be sprayed onto the mandrel to ensure that the mandrel will properly slip from the wound pipes. An alternative to applying grease spray would be to use wax or release film.

For offshore pipelines, longer pipe sections are more likely to be their application. Thus,

filament winding is not recommended due to its limitation to wind longer pipe sections. However, the pultrusion method could be used instead of filament winding. Pultrusion is a manufacturing process used to manufacture constant cross-section pipes of any length. The pultrusion method has the added benefit of having an even cheaper production cost compared to the filament winding process because it achieves direct conversion of continuous fibers and resin into the finished part. The fibers are continuously impregnated and pulled through a heated die, where they are shaped and cured [16].

The volume fraction for the filament wound pipes is not as good as that obtained from other processing methods such as the vacuum infusing in an autoclave. The lower volume fraction could be due to that the resin impregnation of the fibers during winding. A possible cause of this could be because the fibers did not get wetted adequately during impregnation when pulled over the resin roller. A slower winding speed could be used to ensure that the fiber gets well impregnated with resin before it is wound on the mandrel, but this at the cost of reduced production speed. It should be noted that controlling the level of resin impregnation is challenging because of the resin lever. Therefore, it is recommended to replace the existing resin roller and resin lever with another solution that yields better impregnation of the fibers during winding. A suggestion would be to guide the fibers through the tank via a pipe, then straight after the fibers has been impregnated they are then pulled through a small orifice to scrape off excess resin. The suggested method is similar to what Cohen et al. [36] used to produce pressure vessels. He demonstrated a that a higher volume fraction of fiber could be achieved by running the fibers through an orifice after resin impregnation instead of increasing the winding tension. And for the steel fibers, this may be an optimal solution to achieve a better wetting of the steel fibers during resin impregnation, and hence higher volume fraction of fiber in combination with lower winding tension, which reduces the risk of fiber breakage. Figure C.1 in Appendix C illustrates the suggested method to achieve better wetting of the fibers.

## 6.3 Quality Control of the Produced Samples

The fiber volume fraction is an important parameter as the fibers are the main strength and stiffness contributor in a composite material. The volume fraction of fiber calculated from the image analysis is slightly higher than those based on the burn-off test, because, for image analysis, a zone inside the laminate is chosen. Typically, a layer of resin rich area can accumulate on the outside surface of the produced pipe, which decreases the volume fraction of fiber calculated for the composite based on the burn-off method. Consequently, it is important to point out that the specimen surfaces did not receive any enhancement by any means. However, visual inspection of the sample surfaces revealed no inconsistent resin areas. Therefore, the volume fraction of fiber is calculated based on burn-off testing

of specimens. It can be observed that the fiber volume fraction in carbon fiber/epoxy composites is higher than in steel fiber/epoxy composites. The higher tension could explain the higher volume fraction of fiber for the carbon fiber/epoxy pipes applied in winding the pipes, which gave better compaction of the fibers. The burn-off test assumes there are no voids present in the composite. Hence, when assessing void content and volume fraction, a higher void content will give less epoxy content and thus a higher fiber volume fraction in a burn-off test. If a burn-off test's volume fraction from a material with high void content compared to the material data is used, which can result in a high E-modulus. This artificially high E-modulus due to the void content can have detrimental effects on the mechanical behavior of the composite. Also, since there is a considerable difference in the volume fraction of fiber between the CFRP composites and the SFRP composites, the volume fraction of fiber should have been normalized to the same level of fiber content to represent a better comparison.

The overall mean thickness of the CFRP composites was slightly thinner than the SFRP composites, which was expected since the diameter of the carbon fibers and steel fiber has a diameter of 7 $\mu m$ and 8 $\mu m$, respectively. Not surprisingly, the tube wall thickness increases in direct proportion to the number of layers as expected. However, from the thickness measurements, it could be observed that the produced pipe have an uneven thickness along the longitudinal axis, which may have been due to the filament winding process. Thickness measurements of the samples were challenging because of the pronounced unevenness of the sample pipe's outer surface. Not being able to assess a distinct measurement accurately makes them less accurate and can be problematic when the measurements are used to estimate the elastic modulus and buckling pressures.

From the microscopy analysis, it could also be observed that there are voids present in both the SFRP composites and CFRP composites, and can be explained by that the resin was not degassed in a vacuum desiccator to remove the air bubbles inside the resin before winding the pipes. Consequent curing caused the small air bubble to expand and thus forming the voids in the produced composites. Therefore, degassing the resin by using a vacuum pump is recommended before winding. Typically, a void fraction of one percent indicate a high-quality composite, but practical challenges may increase the void content. As suggested by E. Hugaas [38], peel ply could be used on the surface after winding to reduce the void content. He tested this, by applying a sheet of peel ply on a filament wound glass fiber/epoxy tube straight after the pipes had been wound, and found that the presence of voids was reduced to some extent, which could have helped to remove the uneven surface finish of the produced pipes in this thesis. Applying peel-ply to the mandrel is a straightforward and inexpensive solution that should have been considered but was not discovered until after the pipes were produced. Peel-ply could, therefore, be applied to get a smoother surface and reduce the void content of the wound composites.

The timer controlling the electrical curing oven didn't work properly, so the pipes continued to cure long past the recommended 15 hours. It's estimated that the pipes were cured for about 26 hours. Overcuring the pipes could have resulted in a more brittle matrix, but this did not seem much to have an effect on the results for the SFRP6 samples. It is possible that the heat treatment (80°C) during the curing process could give some tempering effects to the non-annealed steel fiber, relieving some of the internal stresses from the bundle drawing process. The tempering effect could have increased the toughness of the fibers, but is unlikely as the temperature was assumed to be too low for tempering effects to occur (tempering is commonly performed above 150°C).

From microscopy analysis of the cross-sections of the sample axis, it was observed that there was a presence of small microcracks in the microstructure which causes some variation in the local volume fraction of fiber. Not to mention, the SFRP composites had more microcracks noticeably in the microstructure compared to the CFRP composites, indicating that there may be a high-stress concentration around the steel fibers. These microcracks were present throughout the thickness of the composite and could have a significant effect on the volume fraction of fiber. Hence, the most critical flaw in influencing the mechanical properties like tensile, compressive and buckling strengths [37]. A hypothesis for SFRP having more microcracks than the CFRP is due to thermally induced stresses. The steel fibers have a larger coefficient of thermal expansion than the carbon fibers, and thus, during curing, the steel fibers causes significant thermal induced stresses in the SFRP composites. The induced thermal stresses in combination with brittle matrix (created by overcuring the SFRP composites) could have generated the microcracks.

## 6.4 Compressive Properties

As observed from the results there is a difference in failure stress in the axial direction between SFRP and CFRP. Axial compressive behavior is mainly dominated by the out-of-plane fiber waviness enabling fiber microbuckling and kink-band formation. While for hoop compression, high compressive stress concentrations at the interface cause the matrix to shear and debond from the fibers, leading to an overall shear failure mode, which indicates a relatively low fiber/matrix interfacial strength.

The results show the compressive hoop strength is almost the same for both the CFRP composites and the SFRP composites; thus, the results indicate that hoop failure of the produced composite is primarily characterized by the matrix compressive properties and state of stress at the fiber/matrix interface. High compressive stress concentrations at the interface cause localized yielding in the matrix, initiating shear failure. The slightly higher hoop strength of the SFRP composites may be because the steel fiber has a more optimal interfacial strength between fiber and the epoxy polymer compared to carbon fiber. During the hoop compression tests, it could be observed that the steel fiber plies

start failing first in a slow continuous manner, followed by delamination of the steel fiber layers and finally sudden drastic failure of the SRPP layers and as a result, failure of the entire composite. Failure damage development is in good agreement with Callens hypothesis for the failure mechanisms in SFRP composites.

It is clear that the SFRP composite has a higher strain-to-failure than the CFRP composite (Table 5.3) and (Table 5.5). The SFRP3 composite shows a lower normalized stress at a given strain compared to the CFRP3 composite. The lower stress is not clearly visible in the linear elastic region due to the higher stiffness of the carbon fiber, however after the yield point, the slope of the stress-strain curve decreases and differences become more pronounced. The SFRP3 samples possess a strain-to-failure of 6.7%, which is almost double of the strain-to-failure of the CFRP3 sample (4.2%). On the other hand, the SFRP6 sample exhibits a higher normalized stress at a given strain compared to the CFRP3 composite combined with a failure strain of 9.4%, which is almost three times greater than the failure strain compared to CFRP6 sample (2.8%). However, the results indicate that the full potential of the strain-to-failure of the steel fibers (20% failure strain) reported in Table 1.3, has not been realized in the composite.

The experimentally measured stiffness in the longitudinal (axial) direction of the produced composites is significantly lower than the one predicted by theoretical models (Table 5.4) and (Table 5.6). An explanation for this could be because the laminate theory and micromechanical models are mainly used to develop the relationships for a flat laminated sample and not for curved structures such as filament wound cylindrical pipes. The model for the longitudinal modulus is considered an accurate model applicable for all standard UD composites, but not for curved structures. When subjected to in-plane loads such as shear and axial forces, bending and twisting moments a flat laminate will not behave the same as for curved structures and therefore the laminate theory is not accurate for this application. In this circumstance, the results indicate that the steel fibers exhibit a non-linear elastic strain-to-failure behavior. Therefore, the assumptions in the classical lamination theory where materials have linear elastic behavior and strains vary linearly through the thickness are not correct.

The effect of the resin is ignored in most cases because the fiber is much stiffer compared to the matrix, but the results indicate that there is some interfacial effect between matrix and fiber. The model for the transverse (hoop) stiffness obtained by Eq. (3.2) is considered to give a rather poor in the majority of cases. A better prediction could have been by using the semi-empirical Halphin-Tsai formula, but the formula requires additional empirical data, which make the formula not useful if the needed material data are not available.

The evaluation of the experiment to find the elastic properties in the axial and hoop direction was based on a formula for an isotropic material. Thus, the predicted results would most probably not very accurate. Nevertheless, this was kept in mind especially

because this parameter had the biggest influence on the results of the theoretical method. Currently available methods which apply conventional laminate theory and failure criteria without allowing for material non-linearity can underestimate the ultimate strength of the filament-wound material. For realistic prediction of ultimate strength, the prediction should take into consideration non-linearity and the effects of progressive damage within the material as suggested by Wang et al. [39].

## 6.5 Shear Properties

The results from the shear stress–strain curve (Figure 5.7b) and (Figure 5.11b) indicates that as the level of stress is increased, a peak shear stress is reached, followed by the realignment of adjacent plies which results in a uniform stress plateau. The realignment of adjacent plies generates interlaminar shearing between the plies and plastic deformation of the ductile epoxy system. In-plane shear failure is governed by the fiber/matrix interfacial strength and matrix properties. Shear deformation triggers fracture by debonding between the fibers and epoxy and the formation of epoxy shear bands between adjacent fiber bundles, resulting in ply delamination. Failure surfaces show evidence of weak fiber/matrix interfacial strength. After functional failure, the matrix increasingly breaks down allowing the fibers to realign in the resultant loading direction and subsequently accompanied by a significant change in length and diameter of the specimen.

## 6.6 Buckling Behavior

The results indicate that the analytical models do not accurately predict buckling pressures, but over-estimate the critical buckling pressures by between 12 to 16%. The layup selected for this thesis has also been employed in some published studies for deep sea applications [40, 41, 22]. Kaddour et al. [42] investigated the behavior of thin and thick helical wound $\pm 55^{\circ}$ composite cylinders under various biaxial loading ratios including external pressure and noted that commonly used analytical models do not accurately predict buckling pressures, but under-estimate critical buckling pressures. Graham [43] studied thin and thick glass and carbon/epoxy wound cylinders ($D/\mathrm{t} = 6$, 9, 16 and 21) subjected to external pressure tests, and found that the experimental results correlated well with predicted the elastic buckling pressure of the thin-walled cylinders. However, in a similar way to [42], Graham did not find good agreement between predicted failure pressure and experimental results for thick-walled cylinders. He concluded that the only reliable method of predicting the collapse of thick composite cylinders due to material failure was by using data from many tests.

The experimental buckling pressures are significantly lower than the one predicted by the Von Mises and DTMB formula; there could be many reasons for this. Firstly, the difference could be due to the misalignment of the fibers caused when the fiber broke during winding

of the SFRP3 pipe. Paor et al. [44] found that geometric imperfections significantly reduces the critical buckling capacity of thin-walled cylindrical pipes subjected to uniform external pressure. Secondly, Eq. (3.8) is an analytical expression for critical buckling pressure $P_{cr}$ of cylindrical shells derived by Windenburg and Trilling for the buckling of a perfect cylinder subjected to uniform external pressure, this is not the case since it was found that the pipes had an uneven thickness along its longitudinal axis. Also, it is worth noting that there are considerable uncertainties concerning both these expressions. For example, in the buckling expression $L_o$ is the tube length, nominally 200 mm, but the presence of the steel end caps which are each 10 mm long at the inner surface and 10 mm at the outer surface, will reduce the effective buckling length to $L$.

It is worth mentioning that it could be observed before testing that all the test specimens had minor defects at the pipe ends from due to the diamond saw cutting. These defects had the form of small delaminations and cracks on the surface, and the affected zones could be approximately measured to be between 5 to 10 mm from the pipe ends for all specimens. These defects should not have any influence on the results as the end caps have shoulders of about 10 mm penetrating into the samples' ends acting as support. Also, after removing the end caps and the vacuum bag sealant tape, some water could be observed in inside the samples, which indicates that there was some initial leakage at low pressures. As the pressure was increased inside the pressure chamber, the leakages were likely stopped as the end caps were pushed into the pipe, sealing off any gaps. Also visible in the pressure graphs is areas with substantial noise caused by operating the compressor. It is hard to tell whether the water inside the tubes post testing came from leakage through the laminate or just from the end caps leaking. The water present in the tubes post testing has therefore no been assessed further when presenting or discussing possible leakage due to material failure.

The results from the external pressure test, indicate that the composite pipes are buckling as expected. It was expected that due to the high ductility of the steel fiber that the samples would buckle elastically, reduce their sensitivity to buckling. Though, this was not the case since both the SFRP3 sample and CFRP3 sample failed by leaving only fragments behind. This type of behavior indicates that a high amount of energy was stored within the structure before failure occurred. On the sample surface of the CFRP3, it can be observed that the sample fractured along the longitudinal axis compared to the SFRP3 sample where the whole mid-section fractured. Variations in the production process can be an explanation for the higher burst pressure of the CFRP3 sample compared to the SFRP3. Another possibility is that the SFRP3 pipe had fiber breakage at the second layer during winding. And therefore, a defect that could have initiated the elastic instability of the component during testing. The failure behavior of the samples seems to follow the trends for shell buckling theory. Where the thin-walled (CFRP3 and SFRP3) samples buckled inelastically and material failure occurred.

Other than this higher pressure, commonly a thicker pipe resulted in a higher buckling pressure, which was anticipated. Since the both the thick-walled samples (CFRP6 and SFRP6) did not buckle during the external pressure test, and there are no other autoclaves available at NTNU that can provide pressures above 50 MPa, it is not possible to tell how they would fail. However, the experimental buckling pressure of the SFRP6 was close to the theoretically predicted buckling pressure of the SFRP6. However, for the CFRP6 there is still a big gap. Hence, it is not definite to conclude that the buckling properties of the CFRP composites perform better than the SFRP composites, or vice versa.

## 6.7 Failure and Damage Mechanisms Analysis

The results indicate that during compressive loading high compressive stress concentrations at the interface cause localized yielding in the matrix, initiating shear failure. Failure by in-plane shear deformation is dominated by the fiber/ matrix interfacial strength and matrix properties [16]. The shear failure surface of unidirectional steel fiber/epoxy composite material is shown in Figure 5.12. As a result of the low fiber/matrix interfacial strength, interlaminar cracks develop between the plies and fiber bundles. Debonding between the layers along with fiber bundle splitting promotes the rotation or scissoring of the fibers ultimately leading to delamination and interlaminar shear over the entire specimen. Further loading of the material increases the rotation of the fiber bundles perpendicular towards the loading axis, resulting in shear dominated failure of the epoxy between adjacent fiber bundles.

The results show that just like for CFRP composites, the mode of failure for the SFRP composites is triggered by fiber microbuckling when individual fibers buckle inside the matrix. However, the SFRP composites exhibits in general a higher strain-to-failure compared to the CFRP composites, even though, the SFRP composites have more microcracks in them than the CFRP composites. A possible explanation may be because the plastically deformed steel fibers make it possible for the steel fibers to bridge the cracks in the matrix [8]. During the plastic deformation, matrix crack density, and fiber/matrix debonding increases, prohibiting deformational stress in the matrix to be transferred to the fibers. Another possible explanation could be that the steel fibers fractured in multiple places and that when the adhesion is high enough, stress transfer can occur through the matrix (assuming that the overcuring of the SFRP composites did not have any effect on the matrix ductility).

The strain concentration resulting from this interfacial failure together with reaching the yield strain of the steel fibers, initiates plastic deformation of the fiber, leading to fiber necking and decreasing of the fiber cross-section. Also, the SFRP composites exhibit similar ductile deformation behavior to that of the dry UD continuous steel fiber, i.e., an initial elastic response, a definite yield point and consecutive plastic and strain hardening

behavior.

Because steel is isotropic, there is a high-stress concentration close to the fibers that can lead to early hoop failure. The stress concentration increases if the difference in stiffness between the polymer and fiber increases [6]. The ratio of the stiffness of the fiber to the stiffness of the polymer is about 60 for steel fibers and 70 for the carbon fibers, while this is only about 20 for glass fibers. It is possible to lower the stress concentration by surface treatment to achieve optimal adhesion strength of the fiber/matrix interface. Research have shown that the fiber/matrix interfacial strength has a significant influence on the overall mechanical properties of the composite [45]. Improving this interfacial strength by chemical surface modification of the fiber could enhance the mechanical properties [6]. It is likely that surface treatment is the way to go when an increase in the strain-to-failure of the composite or even toughness is sought, thus improving the performance of SFRP composites subjected to various loading (i.e. axial compression, hoop compression, and external pressure loading), regarding strength and ductility of the composite [11].

## 6.8 Results Compared to Steel Fiber Laminates

The steel fiber reinforced polymer composites pipe in this thesis are made by the filament winding method and are to the authors' knowledge the first of its kind. Since they are the first of its kind, it is challenging to draw definite conclusions based on the limited characterization tests performed. With this in mind, a brief comparison with recent studies on flat laminated steel fiber reinforced polymer composite will be discussed. Table 6.1 compares the mechanical and specific mechanical properties of the produced UD SFRP composite pipes to what Callens et. al and Allaer et. al found in their study, together with those of other material grades.

It is important to point out that Callens and Allaer used annealed steel fibers in their studies, compared to the non-annealed steel fibers used in this thesis. Also, this thesis used steel fibers with a diameter of 8 $\mu m$, compared to 30 $\mu m$ which they used in theirs. The higher volume fraction of fiber obtained in this study is higher compared to what Callens et al. [6] and Allaer et al. [11] obtained in their study. One of the reasons for the higher volume fraction obtained in this thesis could be explained by that the fibers used in this thesis were thinner compared to theirs, thus enabling the fibers to be more closely packed. Therefore, it's recommended to use the thinnest possible fiber when a higher volume fraction of fiber is desired. Also, another reason or downside of having a larger diameter is because the fibers have a lot less surface area and will lead to a lower adhesion which is unwanted. Etching or mechanically deforming the fibers could be used to increase the surface area. However, this study did not investigate the effect of the fiber diameter and, therefore, it may also be plausible that by using thicker fibers ($\geq 30$ $\mu m$) it's possible to cut down on the extra time and cost of the bundle drawing technique to

make thinner steel fibers.

The density as a function of volume fraction of fiber shows a high slope, due to the high density of steel fibers. And since the volume fraction of fiber is greater for the produced cylindrical SFRP samples the density of the composite is therefore also higher, leading to a lower specific stiffness. The experimental results obtained in this thesis indicate that the produced samples have achieved similar strain-to-failure to those obtained for flat laminated composites, and as such the ductility of the overcuring did not have as much effect on the ductility of the matrix as first anticipated. Table 6.1 show the specific properties of filament wound SFRP composite and SFRP laminates, and other steel materials.

**Table 6.1:** Mechanical properties of UD SFRP composite pipes compared to flat UD SFRP laminates and other structural materials.

| Material | $V_f$ [%] | $\delta$ $[g/cm^3]$ | $E$ $[GPa]$ | $\sigma$ $[MPa]$ | $\epsilon_{failure}$ [%] | $E/\delta$ $[GPa/g/cm^3]$ | $\sigma/\delta$ $[MPa/g/cm^3]$ |
|---|---|---|---|---|---|---|---|
| SFRP3 pipe | 47.1 | 4.41 | 83.2 | 74.5 | 6.7 | 18.9 | 16.9 |
| SFRP6 pipe | 46.5 | 4.36 | 80.5 | 92.7 | 8.0 | 18.5 | 21.3 |
| SFRP/ductile epoxy[a] | 42.0 | 3.94 | 82.5 | 62.1 | 6.73 | 20.9 | 8.1 |
| SFRP/brittle epoxy[b] | 44.0 | 4.19 | 67.0 | 259.6 | 7.3 | 16.0 | 62.0 |
| SFRP/polyamide 6[b] | 41.0 | 4.00 | 73.2 | 265.6 | 12.7 | 18.3 | 66.4 |
| AISI 316L Stainless steel | - | 8.00 | 193 | 660 | 19.5 | 24.1 | 82.5 |
| AISI 1025 Carbon steel | - | 7.80 | 207 | 500 | 25.0 | 26.5 | 64.1 |

[a] K. Allaer et al. [11]. [b] Callens et al. [8].

## 6.9 Evaluation and Further Improvements

It was mentioned earlier that steel combines a high stiffness with a high strain-to-failure. The micromechanical models predicted that steel fiber composites can possess a stiffness that falls in between the stiffness values of carbon fiber and glass fiber composites. More specifically, it is approximately half the stiffness of a typical carbon fiber composite, but double that of a glass fiber composite (with similar fiber volume fractions). For lightweight applications, the mechanical properties per density are more important than the absolute values. CFRP composites have the highest specific stiffness in all cases, and the SFRP composites show either greater or equal specific stiffness as that of GFRP composites and almost comparable to aluminum or titanium. The SFRP composites get outperformed by the CFRP composites, which is not surprising because of their low density. The specific stiffness of the SFRP composite is lower than of the CFRP because the stiffness of the base materials is similar, but the density is four times higher. As a result of this, the specific stiffness of the SFRP is approximately half of the stiffness of CFRP composites.

Since the density of SFRP is very high, its specific properties are low. Therefore, not a competition to carbon fiber composites in lightweight applications, unless the added value of their high ductility and toughness is also taken into account. The trade-off for better strain-to-failure and ductile failure in these composites may be due to their high density and mediocre performance compared to carbon/epoxy.

It should be mentioned that hybrid composites between steel and carbon or even glass fibers could be an attractive solution, where the material can be tuned with the added toughness. A higher content of steel fibers can be used to increase the ductility, hence, the toughness of the composite, while a higher content of carbon or glass fibers is beneficial for the stiffness properties [46]. Or steel fibers can be combined to form hybrid composites with glass or carbon fibers to further lower the cost in combination with density while keeping as much as possible the stiffness, or to increase the toughness of traditional composites without sacrificing the stiffness.

The measured strain-to-failure was higher for the SFRP composites compared to the CFRP composites, which shows that these steel fibers have a substantial capacity for strain hardening. The SFRP composites have a distinct strain hardening behavior much like regular steel, which gives them an extra margin of safety that traditional CFRP composites do not offer. Thus, SFRP composites have pseudo-ductile behavior rather than brittle failure encountered in traditional fiber reinforced composites.

It was shown that the non-annealed steel fibers used in this thesis possess a strain-to-failure up to 20%, but the full potential has not been achieved for the produced SFRP composite pipes in this case. Recent studies [6] has shown that stainless steel fiber composites also have a high strain-to-failure (7%) even when they are combined with brittle matrices like epoxy. The strain-to-failure was further increased to 13% by choosing a more ductile matrix. The study also suggested that the steel fibers could be coated with a substance to achieve an optimal adhesion and obtain an increased strain-to-failure (up to 20%). Further investigation is needed to optimize the interface to utilize the full potential of the steel fibers' ductility.

Is it then possible to utilize stainless steel fiber reinforced polymer composites in the offshore industry in the future? For offshore oil platforms, where weight is crucial, the higher density of the steel fiber compared to carbon will be the limiting factor. It must be mentioned that the density of steel fiber reinforced polymer composites lie in between the density of pure stainless steel and carbon fiber composites. Because the stainless steel fiber has a cost about one-fourth the cost of carbon fiber in combination with lower density compared to regular steel there exists an attractive option to save cost and weight. The stainless steel fiber reinforced polymer composites show that a trade-off between cost/weight and average performance exists.

They are no match to carbon or glass fibers based on strength alone. However, their average yield strength and strain-to-failure could be designed through different heat treatments or drawing steps to improve their performance characteristics. The ability to meet specific needs by tailoring the material could potentially make them highly desirable in a broad area of engineering applications, and not just the offshore oil and gas industry.

From the results currently available, it seems plausible to recommend that steel fiber reinforced polymer composite pipes can potentially be used for offshore pipelines at the seabed, where weight is not as critical as for oil platforms. However, because of strict standards and characterization processes that are required to approve the materials before using them offshore, it's likely to take a long time before they can be utilized in the offshore oil and gas industry. It is probable that the use of steel fiber reinforced composites will continue to increase as the steel fibers become more widely available, and the industry get more experience in fabrication procedures. For now, they need more characterization processes and tests to evaluate their potential application areas.

# 7 Conclusions

## 7.1 Important Results

The primary objective of this work was to investigate the potential of a novel fiber type, annealed stainless steel fiber, for application in filament wound composite pipes. In the present study, this fiber has been used to develop a polymer composite pipe to understand their mechanical behavior and damage development.

The introductory section illustrated that the scientific literature which describes the use of steel fibers as a ductile reinforcing material in filament wound polymer composites is very limited and thus largely unexplored. Therefore, in this work a range of parameters which can influence the mechanical behavior of steel fiber composites was investigated using several different experimental test methods described and analyzed in the various sections of this thesis.

### 7.1.1 Production

The following conclusions can be made for the production process:

- Unidirectional steel fibers embedded in an epoxy polymer matrix composite pipes were created successfully by the filament winding machine.
- No modifications of the filament winding machine is required to be able to wind the SFRP composite pipes. However, the resin roller should be replaced with another solution to achieve a better resin impregnation of the fibers during winding.
- The produced samples have non-uniform wall thickness with minor defects such as delamination on the surface of the pipe ends. Also, the SFRP composites had greater defects compared to the CFRP composites.
- The fiber splits easily and should be coated with more sizing to help them bundle together better.

### 7.1.2 Experimental

The main findings from the experimental tests are listed as follows:

- The axial compressive results show that the full strain capacity of the ductile stainless steel fibers was not achieved in the composite material up to failure. On the other hand, hoop compression exhibits low failure stress and strain, which indicate high compressive stress concentrations at the interface and relatively low fiber/matrix interfacial strength.

- The specific mechanical properties of this stainless steel fiber composite material are comparable to those reported for flat cross-ply laminate samples and their specific stiffness is also similar to a commercial monolithic stainless and carbon steel grades.
- The calculated elastic properties using the micromechanical approach were significantly higher than the experimental values.
- The steel fiber composites exhibit a much greater strain-to-failure than a typical UD carbon and glass fiber composite (almost three times) combined with a high stiffness (about 80 $GPa$). Also, the SFRP composites exhibit similar ductile deformation behavior to that of the dry UD continuous steel fiber, i.e., an initial elastic response, a definite yield point and consecutive plastic and strain hardening behavior.
- Axial compressive behavior is primarily dominated by the out-of-plane fiber waviness enabling fiber microbuckling and kink-band formation, while, in hoop compression, high compressive stress concentrations at the interface cause the matrix to shear and debond from the fibers, leading to an overall shear failure mode.
- In-plane shear failure is dominated by the fiber/matrix interfacial strength and matrix properties. Shear deformation triggers fracture by debonding between the fibers and epoxy and debonding between adjacent plies, resulting in ply delamination. The results indicate that there is a weak fiber/matrix interfacial strength.
- The thin-walled samples failed by inelastic buckling in the areas of thinner wall thickness, which caused higher stress concentrations at these points. The thick-walled test samples reached the maximum operating pressure the autoclave without showing any indication of buckling.
- The results of this study show that stainless steel fiber reinforced polymer composites can offer a reasonable trade-off between cost and average performance for the offshore oil and gas industry.

## 7.2 Recommendations for Further Work

The presented results are only a first investigation of the potential of steel fibers for use in polymer composite pipes. For future work, some recommendations and suggestions are presented below. Suggestions for further study are split up in further optimization and further characterisation of steel fiber composites.

### 7.2.1 Further Optimization

Further optimization should include the following:

- The production method should be optimized to produce samples with a uniform thickness. The optimization could be beneficial regarding quality, cost, and production rate compared to the current production method.
- Apply peel-ply on the surface straight after the pipes have been wound to get a smoother sample surface and reduce the presence of voids. With reduced void content the volume fraction should increase, and hence, strength/stiffness of the composite also increase, as suggested by E. Hugaas [38].
- Study the influence of adhesion between fiber and matrix. With optimized adhesion between the fiber and a stiffer matrix, it is expected that toughness of the steel fiber composites can further be improved as recommended by Callens et al. [6, 45].

### 7.2.2 Further Characterization

Further characterization should include the following:

- More experiments are needed for further testing to validate the obtained results of this thesis. Due to a limited supply of steel fiber, only a few sample has been produced and tested.
- The influence of the respective filament winding process and the change in mechanical behavior needs to be further investigated.
- The theoretical investigation should be extended by using nonlinear material behavior to account for the ductility of the steel fibers as suggested by Wang et al. [39].
- The characterization should be extended for tensile testing to gain a general idea of the tensile behavior of these steel fiber reinforced materials.
- The predicted buckling pressures should be verified with further experiments. Also, the results should be compared to Finite Element software such as Abaqus CAE because it could help solving the problem or probably even show that the predicted buckling pressure are correct.

# Bibliography


[1] S. De Bondt and J. Decrop. Bundle drawn stainless steel fibers, January 23 2007. US Patent 7,166,174.

[2] P. Davies. *Behavior of marine composite materials under deep submergence.* Woodhead Publishing, 2016.

[3] G. Morgan M. Roseman, R. Martin. *Composites in offshore oil and gas applications.* Woodhead Publishing, 2016.

[4] J. Summerscales. *Composites manufacturing for marine structures.* Woodhead Publishing, 2016.

[5] L. Gorbatikh M. G. Callens and I. Verpoest. Tensile behavior of stainless steel fibre/epoxy composites with modified adhesion. *COMPOSITES: PART A*, 2014.

[6] M. G. Callens. *Development of ductile steel fibre composites.* PhD thesis, KU Leuven, Groep Wetenschap & Technologie, 2014.

[7] N. P. Vedvik. *ESSENTIAL MECHANICS OF COMPONENTS.* 2014.

[8] I. Verpoest Michael Callens, Larissa Gorbatikh. Ductile steel fibre composites with brittle and ductile matrices. *COMPOSITES PART A APPLIED SCIENCE AND MANUFACTURING*, 2014.

[9] A. Jain G.H. van Lenthe I. Verpoest Y. Abdin, S.V. Lomov. Geometrical characterization and micro-structural modeling of short steel fiber composites. *Composites: Part A*, 2014.

[10] L. Gorbatikh I. Verpoest M.G. Callens, P. De Cuyper. Effect of fibre architecture on the tensile and impact behaviour of ductile stainless steel fibre polypropylene composites. *Compos Struct, 119 (2015), pp. 528–533*, 2014.

[11] P. Lava W. Van Paepegem J. Degrieck K. Allaer, I. De Baere. On the in-plane mechanical properties of stainless steel fibre reinforced ductile composites. *Composites Science and Technology 100 (2014) 34–43*, 2014.

[12] ASTM D2996. Standard specification for filament-wound “fiberglass” (glass-fiber-reinforced thermosetting-resin) pipe.

[13] Composite components - offshore standard dnv-os-c501, NOVEMBER 2013.

[14] DNV-RP-C205. Environmental conditions and environmental loads.

[15] MAW LS20 MIKROSAM FILAMENT WINDING MACHINE. http://www.mikrosam.com.mk/filament/maw20ls/sl/maw10.06.2016.

[16] Ever J. Barbero. *Introduction to Composite Materials Design Second Edition*. Taylor & Francis Group, 2011.

[17] *Technical Data Sheet: EPIKOTE Resin MGS RIMR 135 and EPIKURE Curing Agent MGS RIMH 134 RIMH 137. Momentive Specialty Chemicals Inc., August 2006.*

[18] Torayca T700S DATA SHEET URL: http://www.toraycfa.com/pdfs/T700SDataSheet.pdf, 10.06.2016.

[19] Daniel Tran. Developing a filament winding process for producing steel-fiber-reinforced polymer composite pressure vessel. Master’s thesis, Norwegian University of Science and Technology, 2015.

[20] Tew BW. Preliminary design of tubular composite structures using netting theory and composite degradation factors. *ASME. J. Pressure Vessel Technol.*, pages 390–394, 1995.

[21] J. T. Evans and A. G. Gibson. Composite angle ply laminates and netting analysis. *Proceedings of the Royal Society of London A: Mathematical, Physical and Engineering Sciences*, 458(2028):3079–3088, 2002.

[22] Wu YS Mistry J, Gibson AG. Failure of composite cylinders under combined external pressure and axial loading. *Composite Structures*, 1992.

[23] Chauchot P Messager T, Gineste B. Optimal laminations of thin underwater composite cylindrical vessels. *Composite Structures*, 2002.

[24] C. T. F. Ross. Pressure vessels: External pressure technology. *Horwood Publishing Limited, Chichester.*, 2001.

[25] G. H. Bryan. Application of the energy test to the collapse of a long thin pipe under external pressure. *Proc. Camb. Philos. Soc. 6, 287–292.*, 1888.

[26] R Von Mises. Der kritische aussendruck für allseits belastete zylindrische rohre, fest zum 70. geburtstag von prof. dr. a. stodola. zürich, pp. 418–430. *Translated and*

*annotated by Windenburg, D. F. (1936). Report No. 366. DTMB, Washington, DC.*, 1929.

[27] D. F. Windenburg and C. Trilling. Collapse by instability of thin cylindrical shells under external pressure. *Trans. ASME 11, 819–825.*, 1934.

[28] ASTM D3171. Standard test methods for constituent content of composite materials.

[29] ASTM D2734. Standard test methods for void content of reinforced plastics.

[30] Leica LeF4. http://www.leica-microsystems.com/products/light-microscopes/industrial-materials/inverted-microscopes/details/product/leica-telatom/, 10.06.2016.

[31] iSolution DT. http://www.imt-digital.com/english/html/solutions.php, 10.06.2016.

[32] ASTM E2954. Standard test method for axial compression test of reinforced plastic and polymer matrix composite vertical members.

[33] ASTM D2924. Standard test method for external pressure resistance of "fiberglass" (glass-fiber-reinforced thermosetting-resin) pipe.

[34] William D. Callister. *Materials Science and Engineering, 8th Edition SI Version.* Wiley, 2010.

[35] F. Ellyin P. Mertiny. Influence of the filament winding tension on physical and mechanical properties of reinforced composites. *Elsevier, Composites: Part A*, 2002.

[36] Zhao L. Cohen D, Mantell SC. The effect of fibre volume fraction on filament wound composite pressure vessel strength. *Composites Part B*, 2001.

[37] S. Gaudham Babu C. Pannererselvann, M. Gopala Krishnan. Evaluation of energy release rate of particle filled gfrp composite laminates. *International Research Journal of Engineering and Technology (IRJET)*, 2015.

[38] Eivind Hugaas. Optimize resistance to buckling under external hydrostatic pressure of thin walled composite tubes. Master's thesis, NTNU, 2014.

[39] S HU HT HAJALI R WANG S. S., SRINIVASAN. Effect of material nonlinearity on buckling and postbuckling of fiber composite laminated plates and cylindrical shells. *Comp. Struct. 33, 7–15*, 1995.

[40] Blake HW Starbuck JM. Failure of composite cylinders subjected to external hydrostatic pressure. *ASTM STP 1185*, 1994.

[41] Y. Haidar A. A. Waheeb C. T. F. Ross, A. P. F. Little. Buckling of carbon/glass

composite tubes under uniform external hydrostatic pressure. *Strain. Volume 47, Issue s1, Pages e156–e174*, 2011.

[42] M. J. Hinton A. S. Kaddour, P. D. Soden. Failure of ± degree filament wound glass/epoxy composite tubes under biaxial compression. *Journal of Composite Materials*, 1998.

[43] Graham D. Composite pressure hulls for deep ocean submersibles. *Comp. Struct. 32:331–43*, 1995.

[44] K. Cronin W.M.D. Wright S.G. McSweeney C. de Paor, D. Kelliher. Prediction of vacuum-induced buckling ppressure of thin-walled cylinders. *Elsevier, Thin-Walled Structures*, 2012.

[45] Yu.A. Gorbatkina. Correlation between the strength of fiber-reinforced plastics and the adhesive strength of fiber "matrix joints. *Mechanics of Composite Materials*, 36(3):169–176, 2000.

[46] Michael R. Wisnomb Gergely Czéla, Meisam Jalalvandb. Design and characterisation of advanced pseudo-ductile unidirectional thin-ply carbon/epoxy–glass/epoxy hybrid composites. *Composite Structures. Volume 143, 20 May 2016, Pages 362–370*, 2016.

[47] Mikrosam. Url: http://www.mikrosam.com/new/article/en/winding-expert/, 10.10.2016.

# Appendix A Software for Filament Winding

## Winding Expert

Winding Expert is a software solution for creating, editing and simulating filament winding programs. It is a user-friendly software which allows the composite designer flexibility to create winding programs that will completely fulfill the product requirements. It has the possibility for circumferential (hoop), helical, transitional and other custom defined winding layers and programs. Features for winding path simulation and winding pattern simulation provide the designer with a powerful tool for natural and precise creation of the composite parts using filament winding technology [47].

## Winding Commander

The Winding Commander software developed by Mikrosam is specially designed to control the MAW LS 20 Filament Winding machine. The PC-based system with latest class CPU running under Windows operating system work parallel with dedicated DSP for smooth, fast and accurate winding process of unlimited program length. The Winding Commander control application is the most advanced and feature rich control for filament winding machines. With the unique graphic interface, it is relatively easy to learn and operate [47].

## Troubleshooting Winding Commander

The following troubleshooting processes can be used to fix the error messages:

**"File access not possible".** This message occurs when Winding Commander sometimes can't find the mandrel-file for some unknown reason. Moving the mandrel-file closer to the root file will fix this.

**"No interpolation for axis tracking".** If the speed is too fast when returning the machine to its reference position, then the machine may jam and give this error message. The only known fix for this so far is by repeatedly pushing the start button, which moves the machine in small steps until the machine frees itself. If this does not work, shutting down the entire system with the main switch and back on may be necessary.

**"Drive shall be moved, but not enabled yet".** The motors are disabled. Enable the motors in the Winding Commander interface.

**"Light barrier activated".** For safety reasons the machine has light sensors that automatically stops the machine when activated. If nothing dangerous has occurred press start to continue the winding process.

# Appendix B Microscopy Pictures

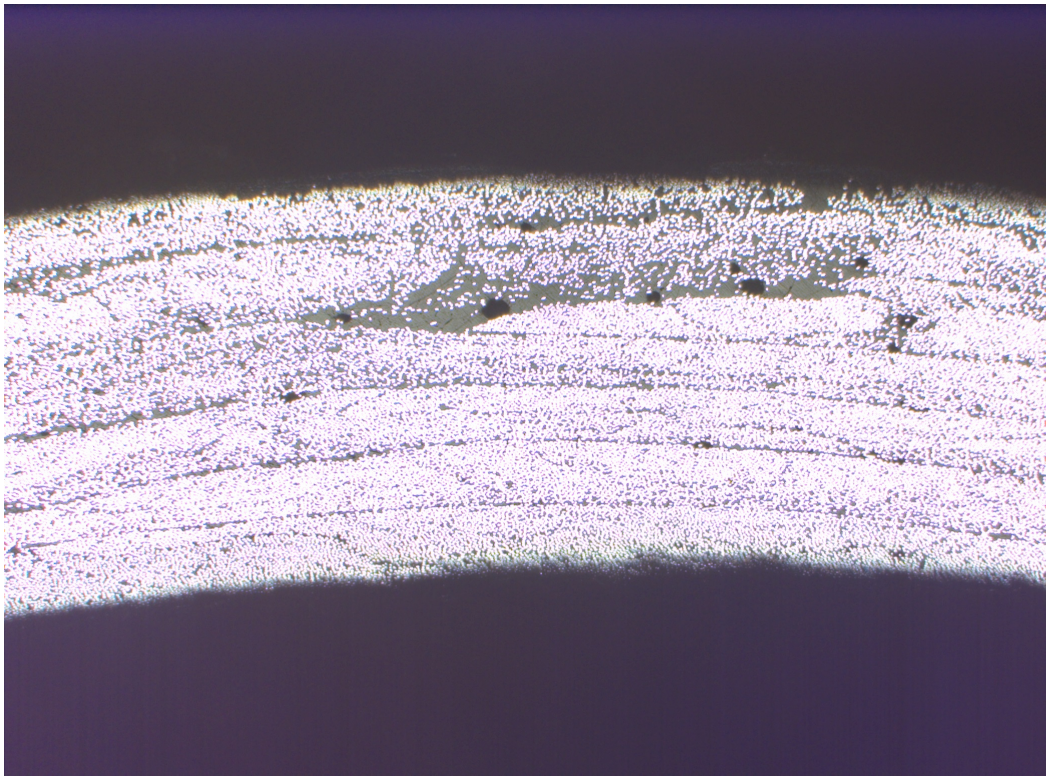

**a**

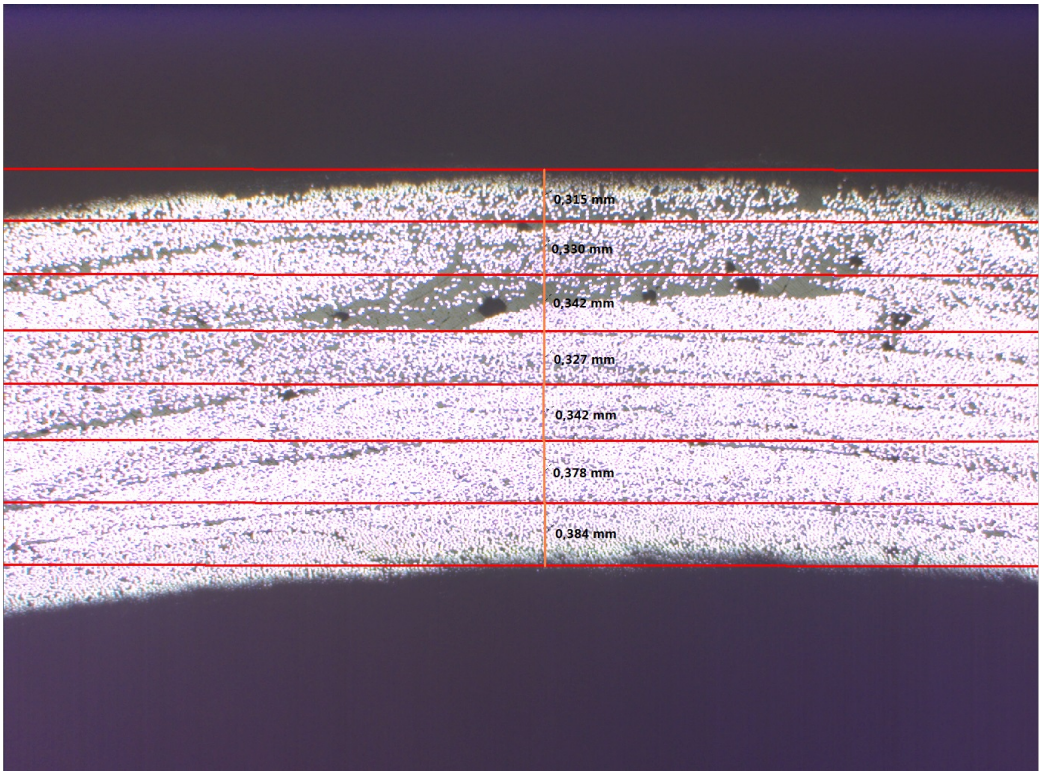


**b**

**Figure B.1:** Microscopy picture number 1 of SFRP3 sample: (a) Original picture. (b) Annotated picture.

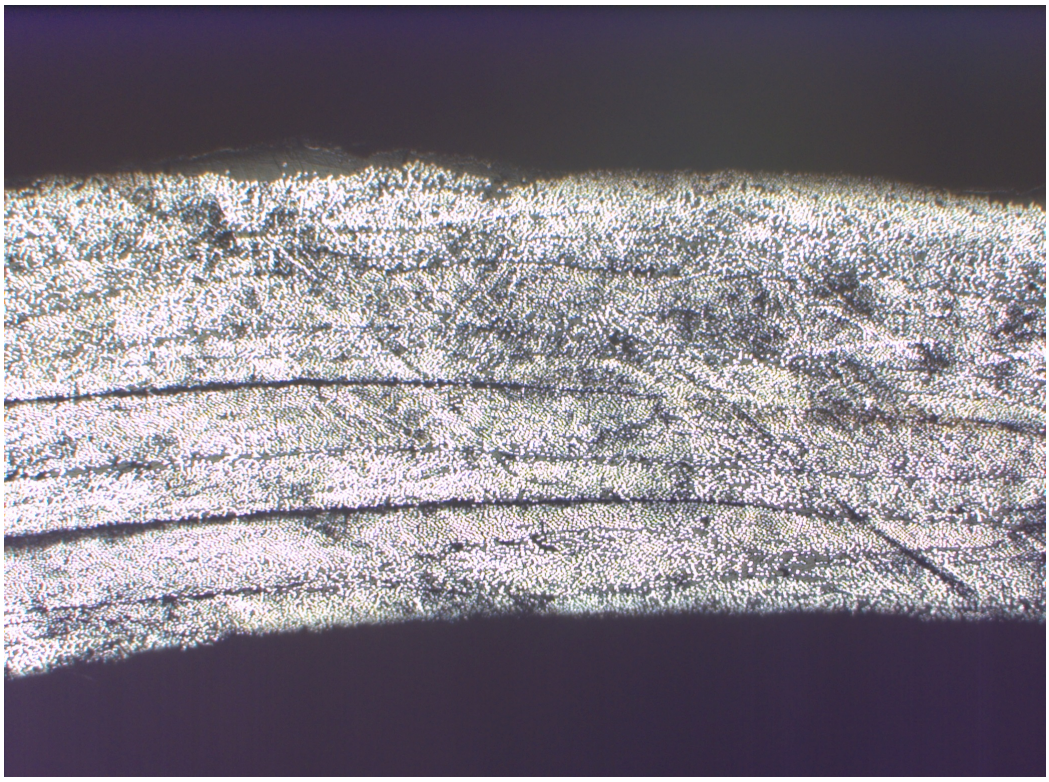

**a**

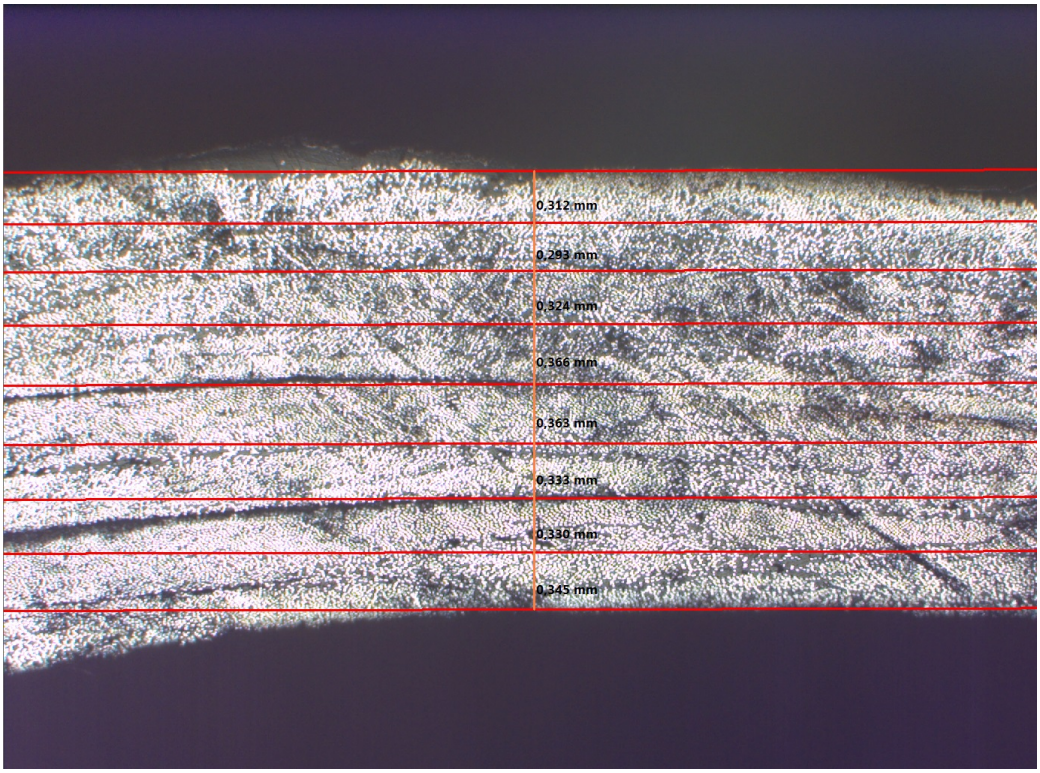


**b**

**Figure B.2:** Microscopy picture number 2 of SFRP3 sample: (a) Original picture. (b) Annotated picture.

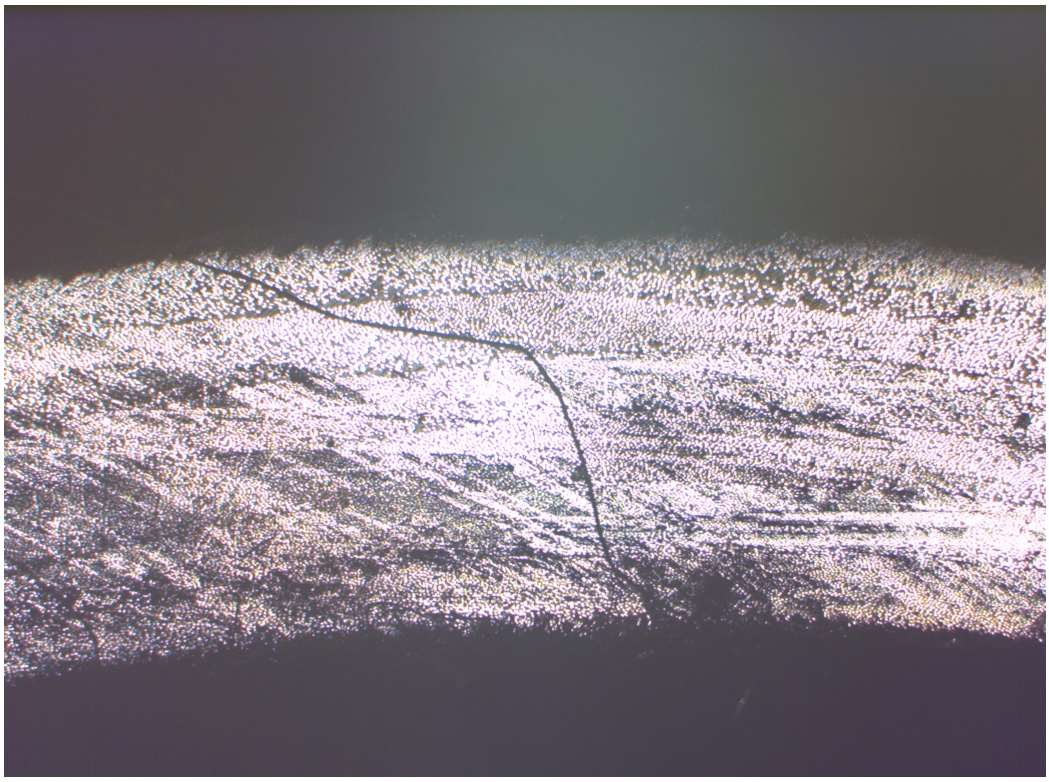

**a**

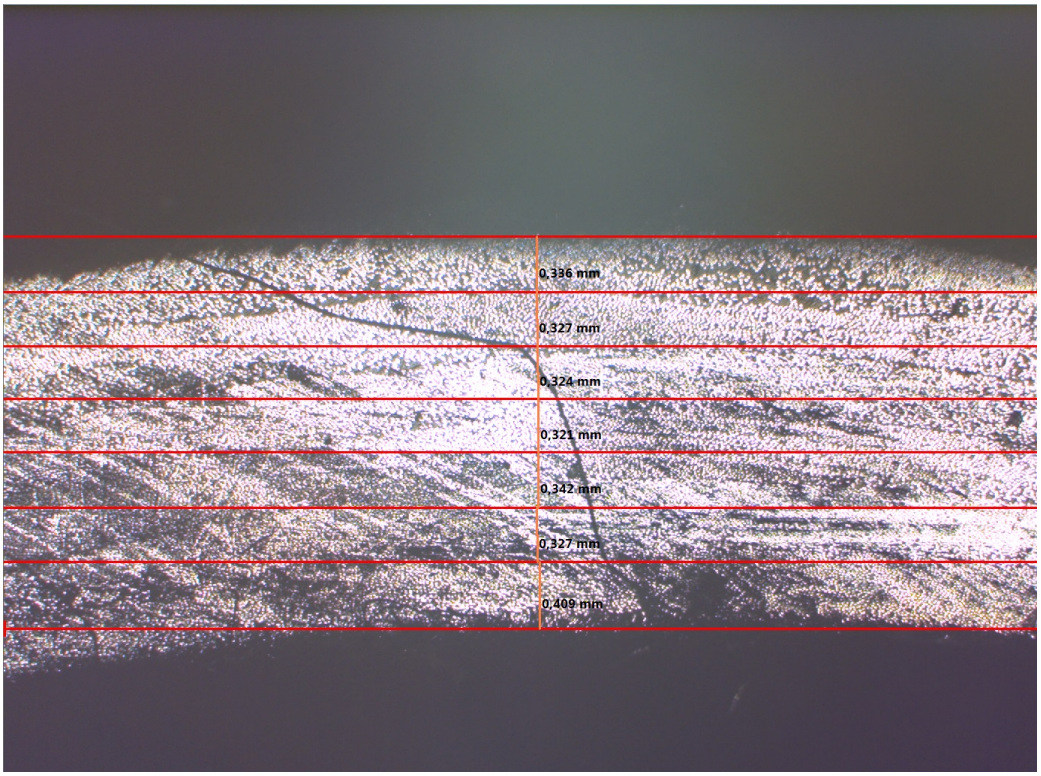


**b**

**Figure B.3:** Microscopy picture number 3 of SFRP3 sample: (a) Original picture. (b) Annotated picture.

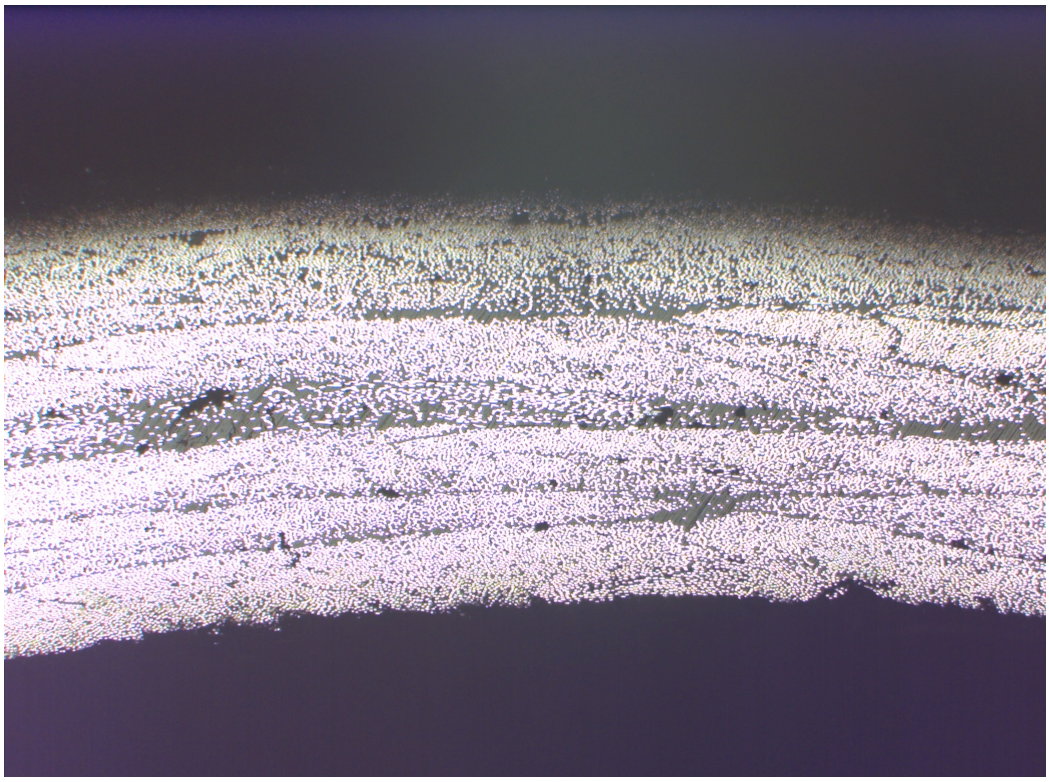

**a**

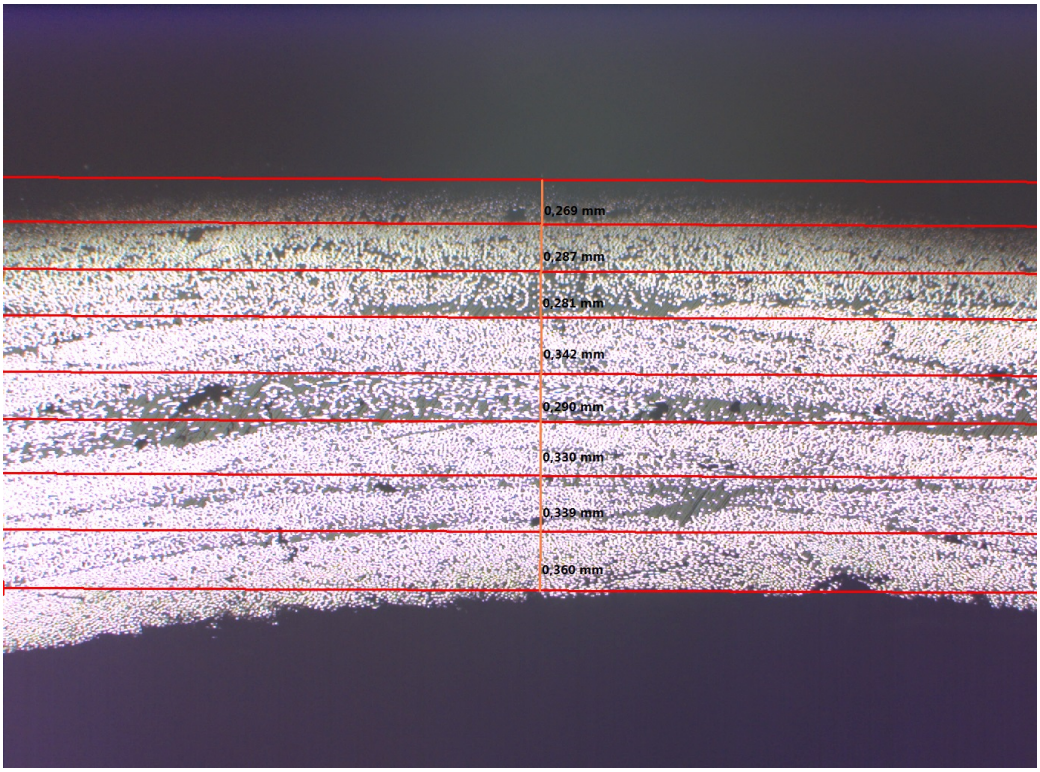


**b**

**Figure B.4:** Microscopy picture number 4 of SFRP3 sample: (a) Original picture. (b) Annotated picture.

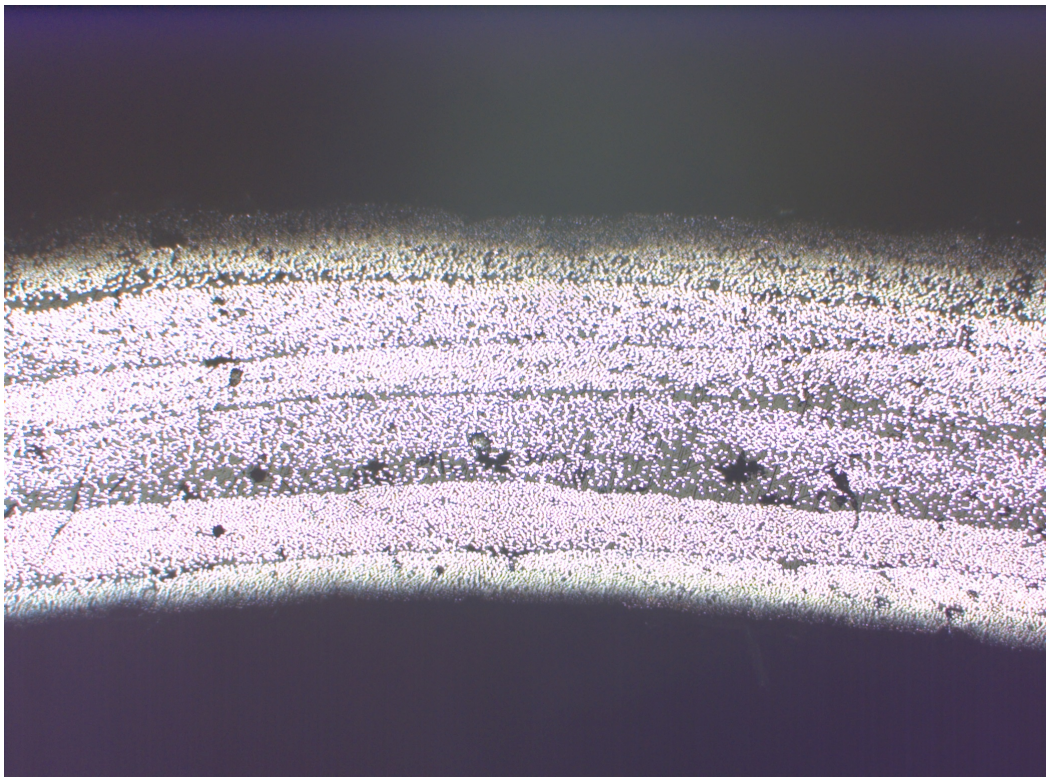

**a**

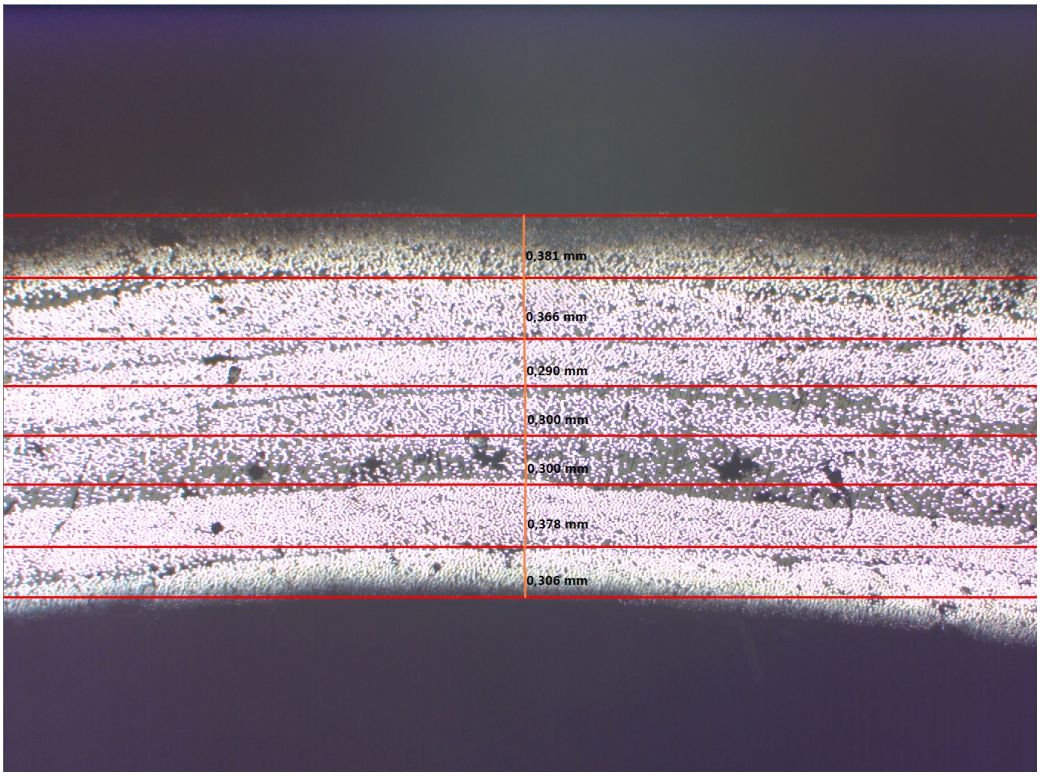


**b**

**Figure B.5:** Microscopy picture number 5 of SFRP3 sample: (a) Original picture. (b) Annotated picture.

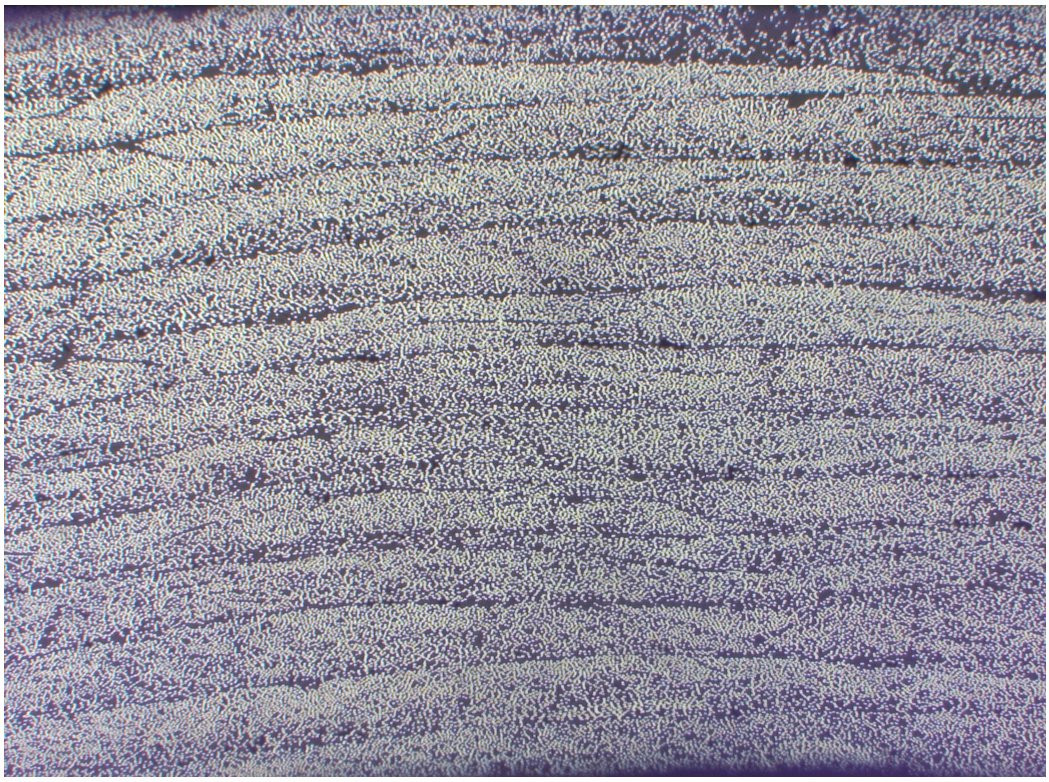

**a**

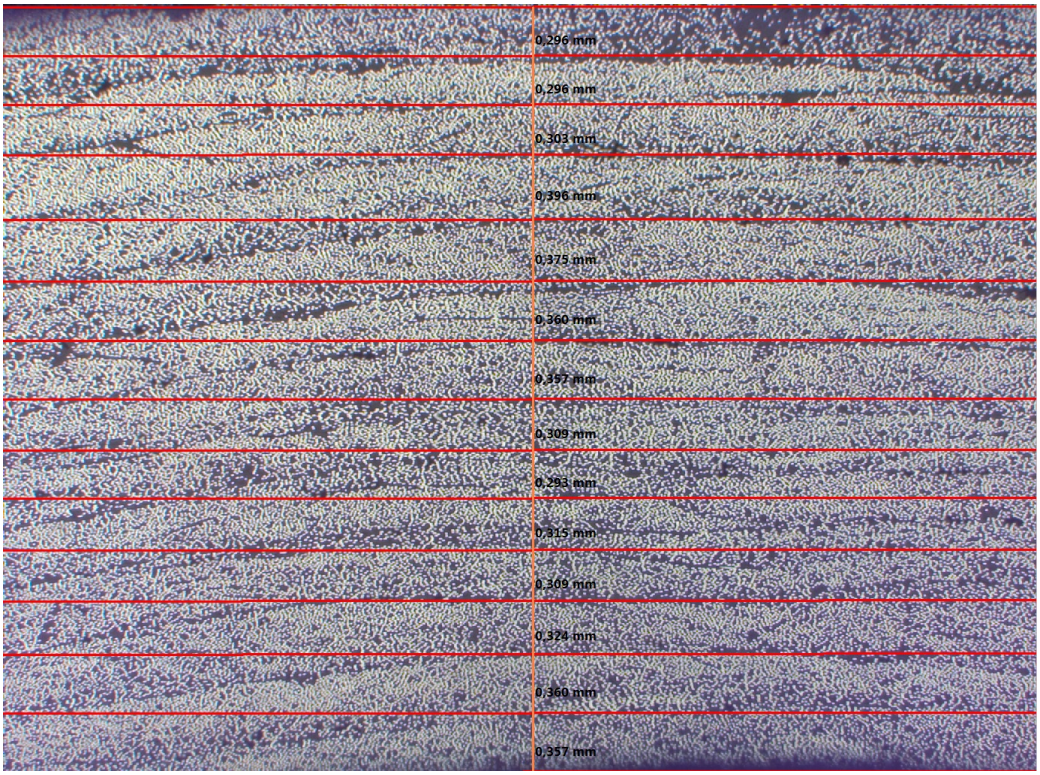


**b**

**Figure B.6:** Microscopy picture number 1 of SFRP6 sample: (a) Original picture. (b) Annotated picture.

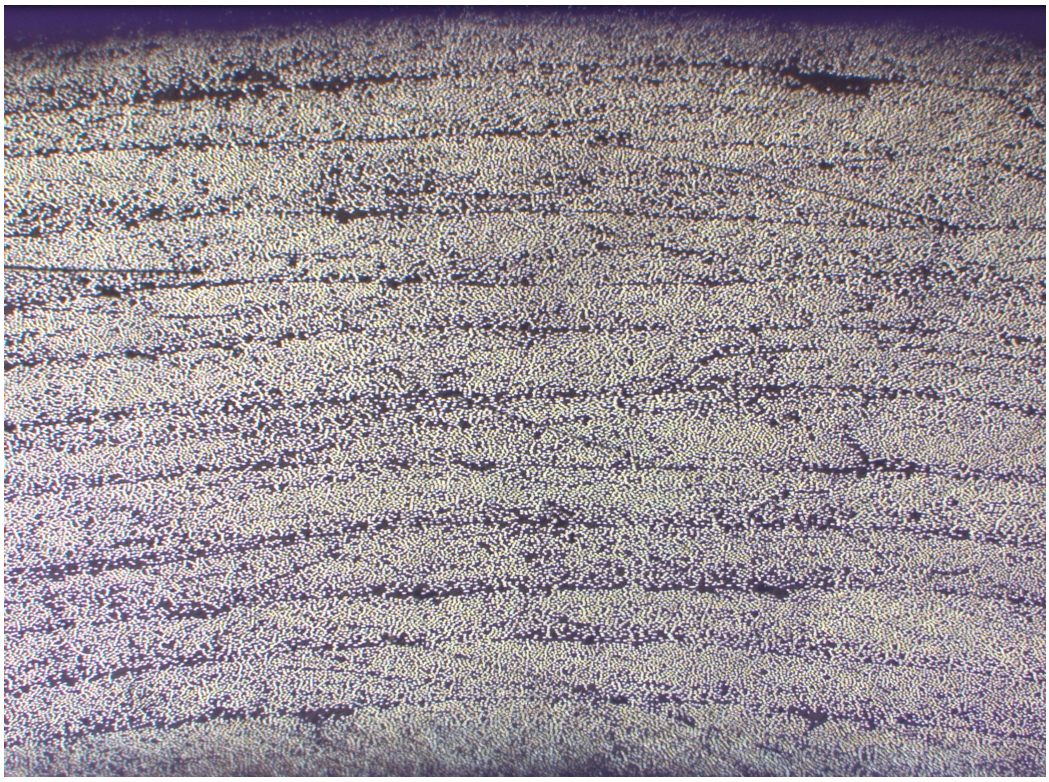

**a**

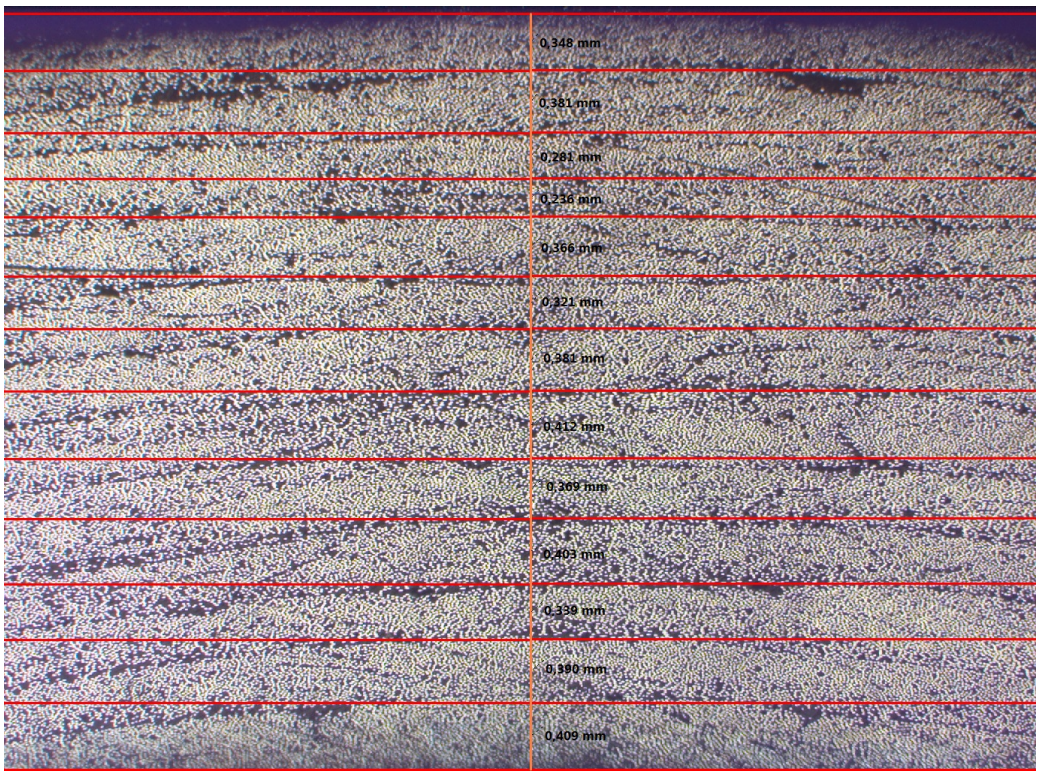


**b**

**Figure B.7:** Microscopy picture number 2 of SFRP6 sample: (a) Original picture. (b) Annotated picture.

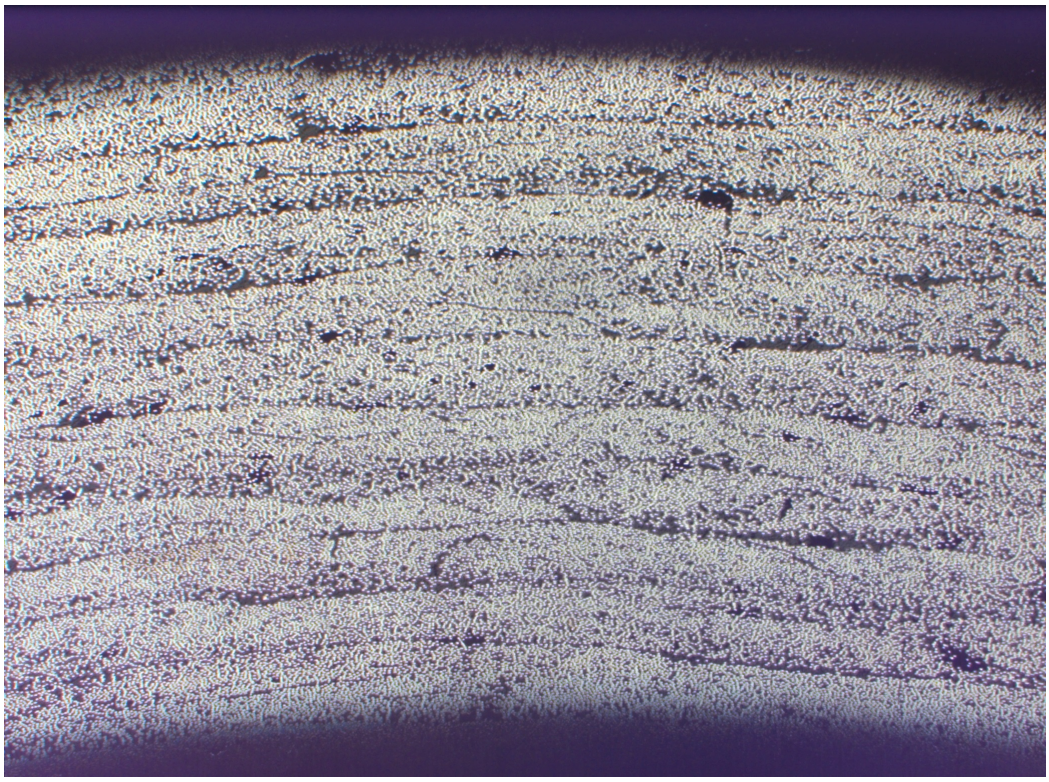

**a**

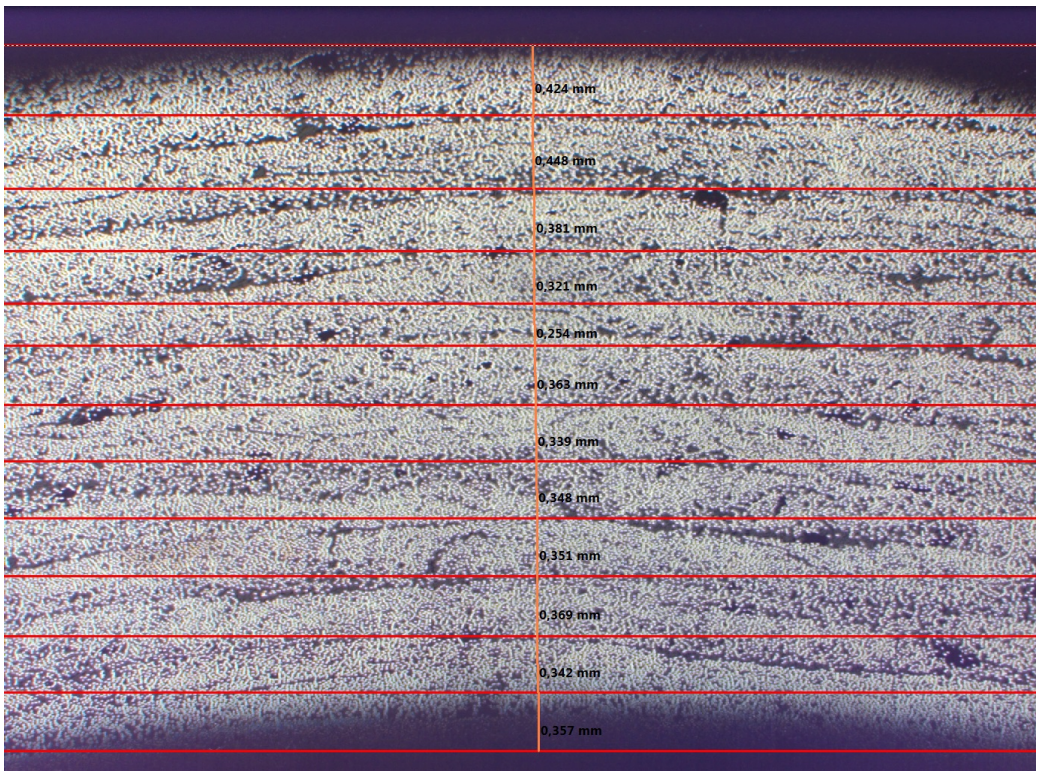


**b**

**Figure B.8:** Microscopy picture number 3 of SFRP6 sample: (a) Original picture. (b) Annotated picture.

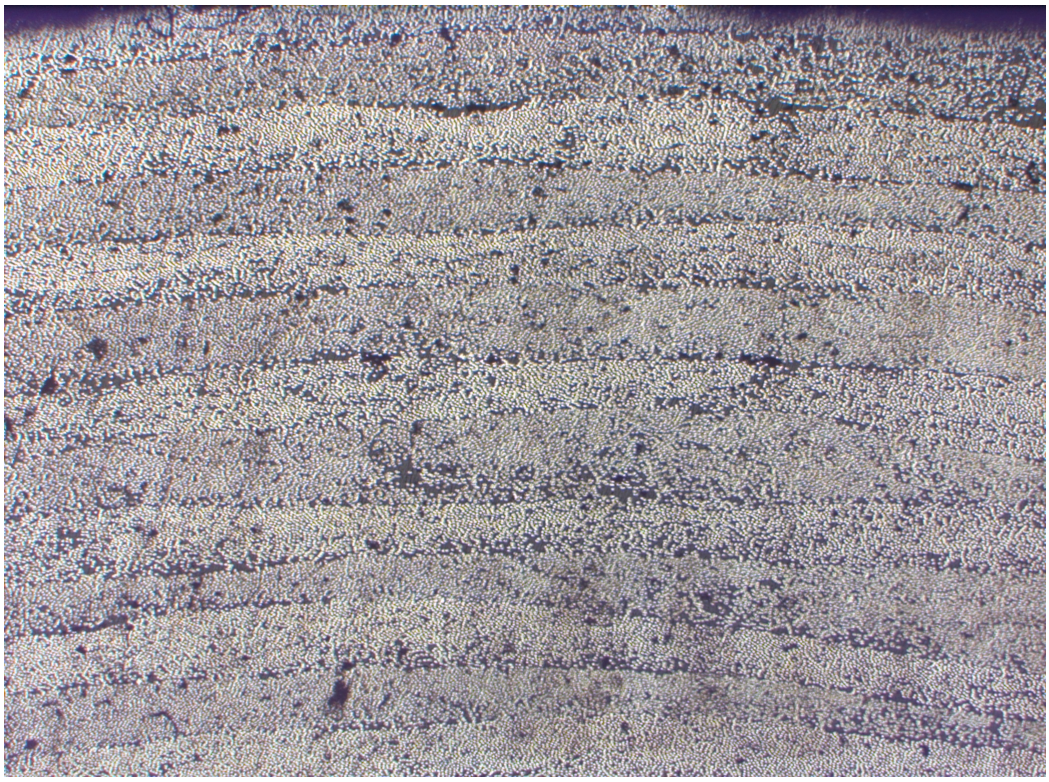

**a**

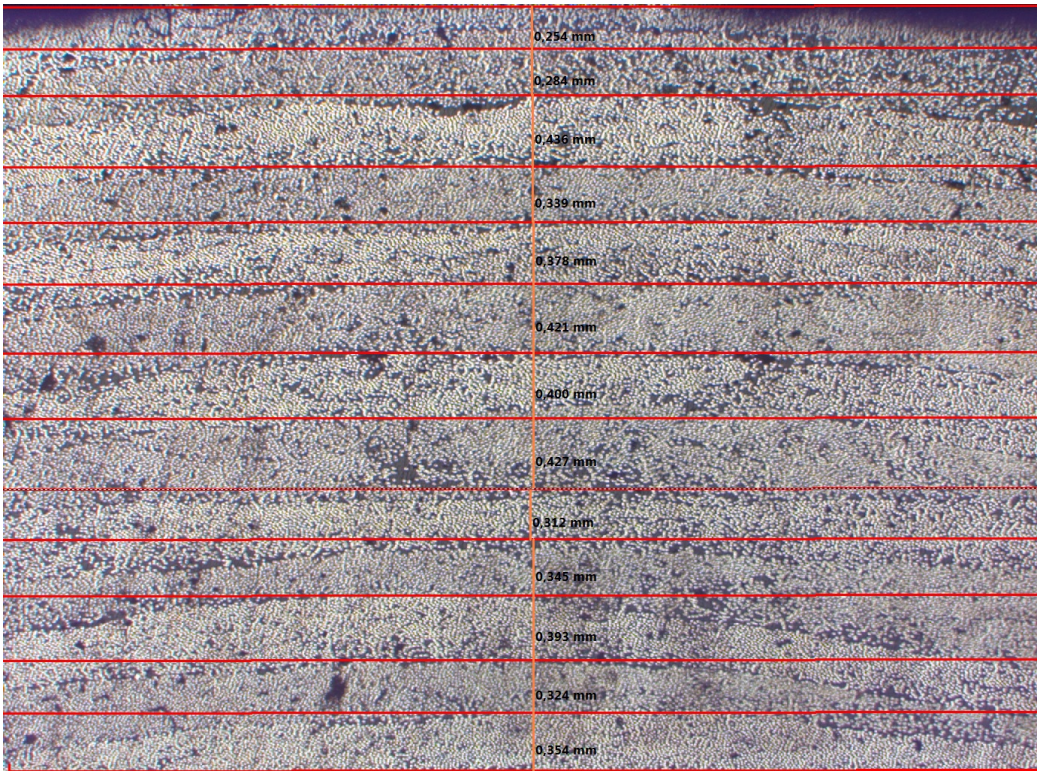


**b**

**Figure B.9:** Microscopy picture number 4 of SFRP6 sample: (a) Original picture. (b) Annotated picture.

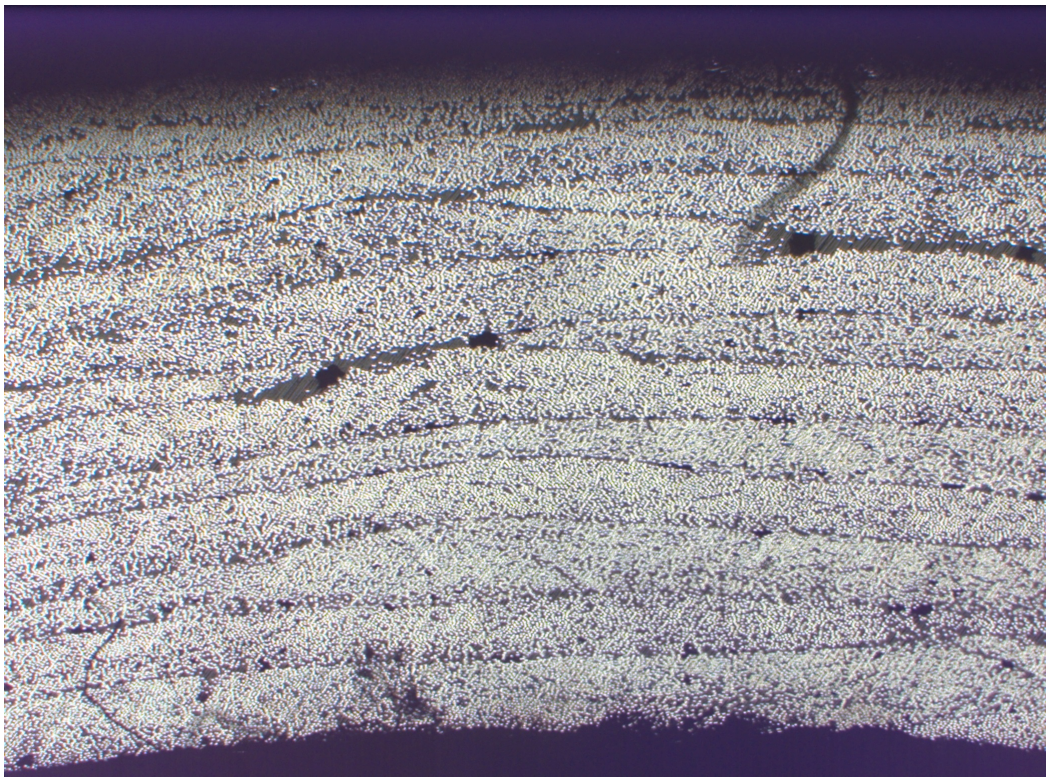

**a**

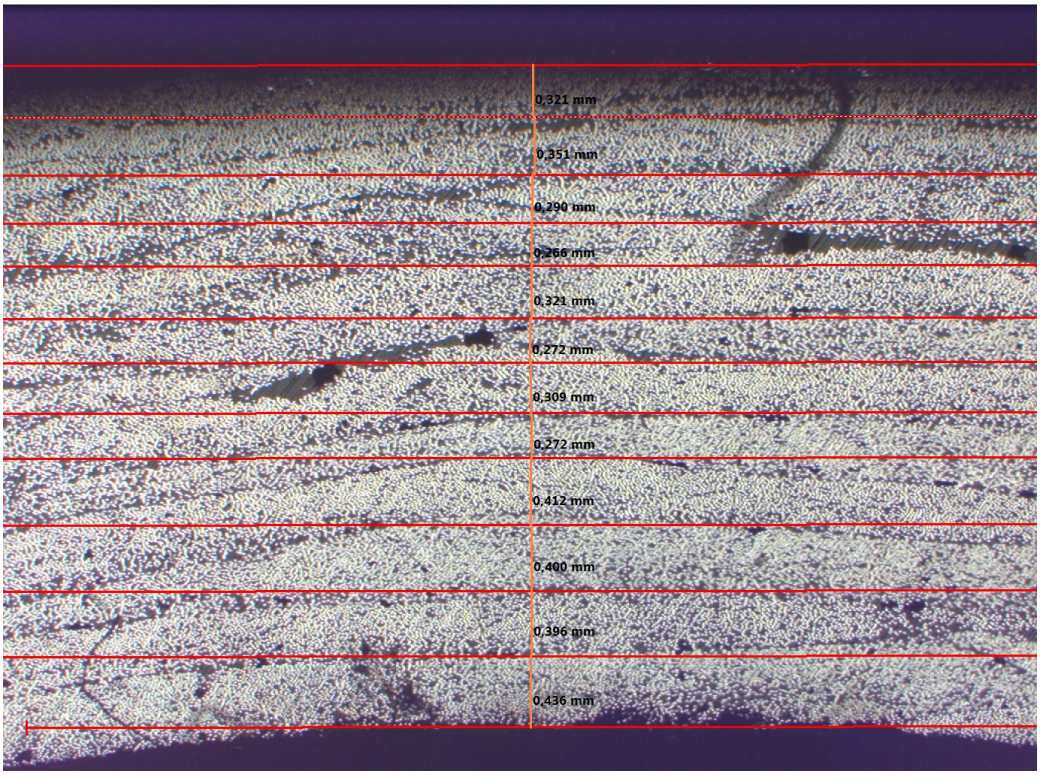


**b**

**Figure B.10:** Microscopy picture number 5 of SFRP6 sample: (a) Original picture. (b) Annotated picture.

**Table B.1:** Thickness measurements of each ply found by microscopy. Numbers in mm.

| Specimen | Ply nr.1 | Ply nr.2 | Ply nr.3 | Ply nr.4 | Ply nr.5 | Ply nr.6 | Ply nr.7 | Ply nr.8 | Ply nr.9 | Ply nr.10 | Ply nr.11 | Ply nr.12 | Ply nr.13 | Ply nr.14 | Average | SD | Total Thickness |
|---|---|---|---|---|---|---|---|---|---|---|---|---|---|---|---|---|---|
| $SFRP_3$ | | | | | | | | | | | | | | | | | |
| Figure B.1b | 0.315 | 0.330 | 0.342 | 0.327 | 0.342 | 0.378 | 0.384 | - | - | - | - | - | - | - | 0.345 | 0.004 | 2.418 |
| Figure B.2b | 0.312 | 0.293 | 0.324 | 0.366 | 0.363 | 0.333 | 0.330 | 0.345 | - | - | - | - | - | - | 0.333 | 0.004 | 2.666 |
| Figure B.3b | 0.336 | 0.324 | 0.321 | 0.342 | 0.327 | 0.409 | - | - | - | - | - | - | - | - | 0.343 | 0.006 | 2.059 |
| Figure B.4b | 0.269 | 0.287 | 0.281 | 0.342 | 0.290 | 0.330 | 0.339 | 0.360 | - | - | - | - | - | - | 0.312 | 0.008 | 2.498 |
| Figure B.5b | 0.381 | 0.366 | 0.290 | 0.300 | 0.300 | 0.378 | 0.306 | - | - | - | - | - | - | - | 0.332 | 0.010 | 2.321 |
| $SFRP_6$ | | | | | | | | | | | | | | | | | |
| Figure B.6b | 0.296 | 0.296 | 0.303 | 0.396 | 0.375 | 0.360 | 0.357 | 0.309 | 0.293 | 0.315 | 0.309 | 0.324 | 0.360 | 0.357 | 0.332 | 0.015 | 4.650 |
| Figure B.7b | 0.348 | 0.381 | 0.281 | 0.236 | 0.366 | 0.321 | 0.381 | 0.412 | 0.369 | 0.403 | 0.339 | 0.390 | 0.409 | - | 0.357 | 0.032 | 4.636 |
| Figure B.8b | 0.424 | 0.448 | 0.381 | 0.321 | 0.254 | 0.363 | 0.339 | 0.348 | 0.351 | 0.369 | 0.342 | 0.357 | - | - | 0.358 | 0.026 | 4.297 |
| Figure B.9b | 0.254 | 0.284 | 0.436 | 0.339 | 0.378 | 0.421 | 0.400 | 0.427 | 0.312 | 0.345 | 0.393 | 0.324 | 0.354 | - | 0.359 | 0.038 | 4.667 |
| Figure B.10b | 0.321 | 0.351 | 0.290 | 0.266 | 0.321 | 0.272 | 0.309 | 0.272 | 0.412 | 0.400 | 0.396 | 0.436 | - | - | 0.337 | 0.040 | 4.046 |
| $CFRP_3$ | | | | | | | | | | | | | | | | | |
| 1 | 0.275 | 0.283 | 0.318 | 0.312 | 0.357 | 0.311 | 0.325 | - | - | - | - | - | - | - | 0.312 | 0.004 | 2.181 |
| 2 | 0.310 | 0.279 | 0.319 | 0.330 | 0.339 | 0.303 | 0.323 | 0.340 | - | - | - | - | - | - | 0.318 | 0.003 | 2.543 |
| 3 | 0.320 | 0.311 | 0.310 | 0.320 | 0.315 | 0.365 | - | - | - | - | - | - | - | - | 0.324 | 0.002 | 1.941 |
| 4 | 0.259 | 0.277 | 0.301 | 0.302 | 0.250 | 0.290 | 0.319 | 0.247 | - | - | - | - | - | - | 0.281 | 0.005 | 2.245 |
| 5 | 0.243 | 0.326 | 0.301 | 0.295 | 0.290 | 0.338 | 0.280 | - | - | - | - | - | - | - | 0.296 | 0.006 | 2.073 |
| $CFRP_6$ | | | | | | | | | | | | | | | | | |
| 1 | 0.276 | 0.296 | 0.303 | 0.336 | 0.355 | 0.432 | 0.317 | 0.309 | 0.273 | 0.304 | 0.309 | 0.324 | 0.360 | 0.357 | 0.325 | 0.022 | 4.551 |
| 2 | 0.328 | 0.321 | 0.243 | 0.226 | 0.346 | 0.311 | 0.331 | 0.412 | 0.349 | 0.363 | 0.329 | 0.310 | 0.361 | - | 0.325 | 0.028 | 4.230 |
| 3 | 0.414 | 0.428 | 0.341 | 0.311 | 0.244 | 0.353 | 0.329 | 0.328 | 0.341 | 0.339 | 0.332 | 0.347 | - | - | 0.342 | 0.024 | 4.107 |
| 4 | 0.244 | 0.254 | 0.416 | 0.329 | 0.318 | 0.401 | 0.390 | 0.327 | 0.312 | 0.335 | 0.363 | 0.324 | 0.344 | - | 0.335 | 0.031 | 4.357 |
| 5 | 0.311 | 0.322 | 0.278 | 0.256 | 0.311 | 0.256 | 0.252 | 0.289 | 0.262 | 0.390 | 0.400 | 0.381 | 0.309 | 0.314 | 0.030 | 0.303 | 3.771 |

# Appendix C Suggested Resin Impregnation Method

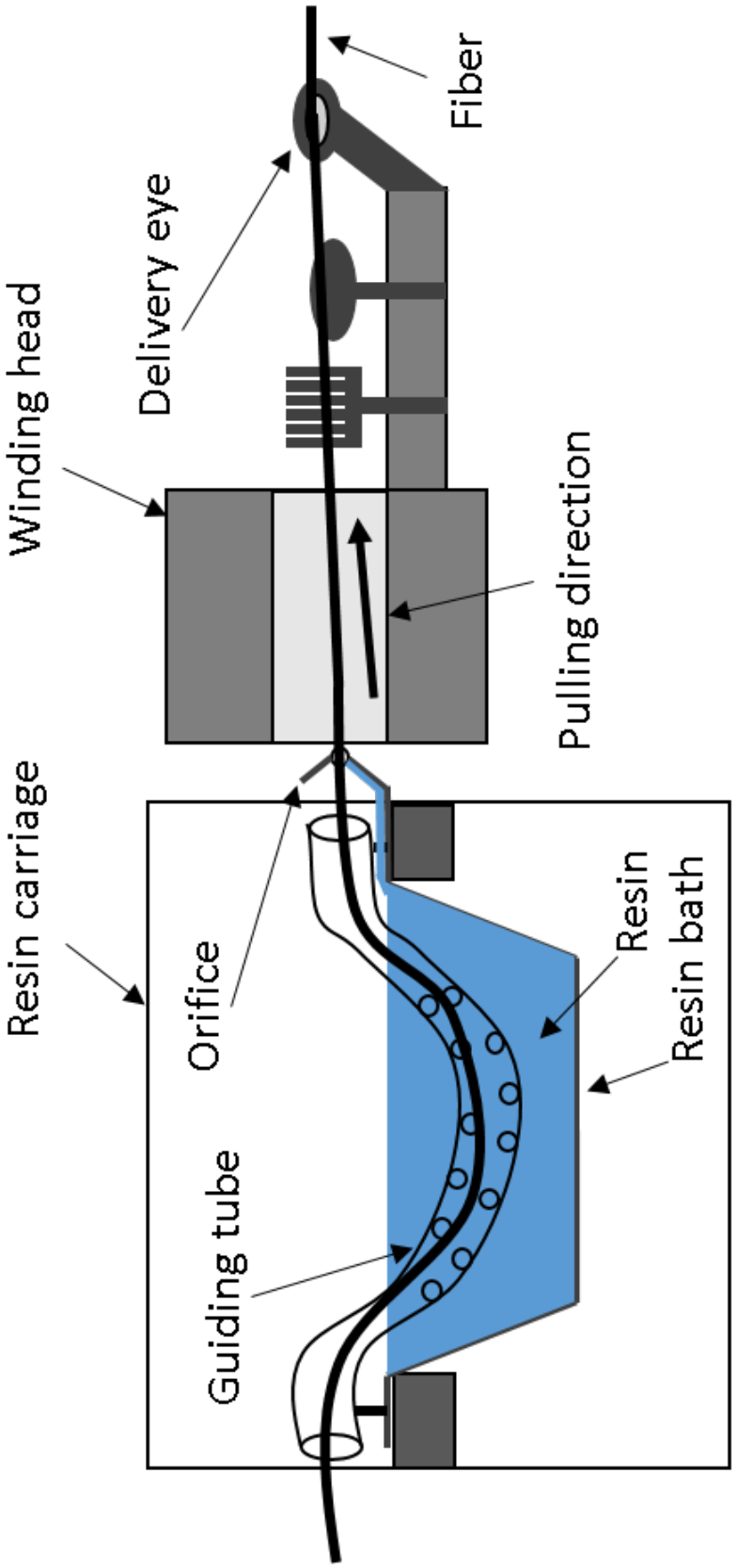


**Figure C.1:** Picture illustrating the new suggestion to how the fiber should be fed through system and impregnated by resin.

# Appendix D Risk Assessment

| NTNU<br>HMS | Kartlegging av risikofylt aktivitet | Utarbeidet av | Nummer | Dato |
|---|---|---|---|---|
| | | HMS-avd. | HMSRV2601 | 22.03.2011 |
| | | Godkjent av | | Erstatter |
| | | Rektor | | 01.12.2006 |

**Enhet: IPM** **Dato: 13.01.2016**

**Linjeleder: Torgeir Welo**

**Deltakere ved kartleggingen** (m/ funksjon)**: Daniel Tran (student), Andreas Echtermeyer (veileder), Nils Petter Vedvik (medveileder)**
*(Ansv. veileder, student, evt. medveiledere, evt. andre m. kompetanse)*

**Kort beskrivelse av hovedaktivitet/hovedprosess:** Masteroppgave student Daniel Tran. "Developing a Filament Winding Process for Producing Steel-Fiber Reinforced Polymer Composite Pressure Vessel"

**Er oppgaven rent teoretisk?** (JA/NEI)**: NEI** *«JA» betyr at veileder innestår for at oppgaven ikke inneholder noen aktiviteter som krever risikovurdering. Dersom «JA»: Beskriv kort aktiviteteten i kartleggingskjemaet under. Risikovurdering trenger ikke å fylles ut.*

**Signaturer:** *Ansvarlig veileder:* *Student:*

| ID nr. | Aktivitet/prosess | Ansvarlig | Eksisterende dokumentasjon | Eksisterende sikringstiltak | Lov, forskrift o.l. | Kommentar |
|---|---|---|---|---|---|---|
| 1a | Viklemaskin | Tran | Romopplæring, HMS kurs | Overbelastningsbryter, lysbrytere | | |
| 1b | Verkstedarbeid | Tran | Romopplæring, HMS kurs | Verneutstyr, skjerming, nødstoppere | | |
| 1c | Trykkprøving | Tran | Ukjent | Skjerming | | |
| 1d | Strekkprøving | Tran | Romopplæring, HMS kurs | Overbelastningsbryter, belastningssperre | | |
| 1e | Bruk av skjæreverktøy | Tran | Ukjent | | | |
| 1f | Bruk av sammenføyningsteknikker | Tran | Brukermanual og datablad | Datablad | Ukjent | |
| 1g | Autoclave | Tran | Romopplæring, HMS kurs | Skjerming | | |
| 2 | Tilstedeværelse ved arbeid utført av andre | Andre | | | | |

| NTNU<br>HMS | Kartlegging av risikofylt aktivitet | Utarbeidet av | Nummer | Dato |
|---|---|---|---|---|
| | | HMS-avd. | HMSRV2601 | 22.03.2011 |
| | | Godkjent av | | Erstatter |
| | | Rektor | | 01.12.2006 |

**Enhet: IPM** **Dato: 13.01.2016**

**Linjeleder: Torgeir Welo**

**Deltakere ved kartleggingen** (m/ funksjon)**: Daniel Tran (student), Andreas Echtermeyer (veileder), Nils Petter Vedvik (medveileder)**
*(Ansv. veileder, student, evt. medveiledere, evt. andre m. kompetanse)*

**Kort beskrivelse av hovedaktivitet/hovedprosess:** Masteroppgave student Daniel Tran. "Developing a Filament Winding Process for Producing Steel-Fiber Reinforced Polymer Composite Pressure Vessel"

**Er oppgaven rent teoretisk?** (JA/NEI)**: NEI** *«JA» betyr at veileder innestår for at oppgaven ikke inneholder noen aktiviteter som krever risikovurdering. Dersom «JA»: Beskriv kort aktiviteteten i kartleggingskjemaet under. Risikovurdering trenger ikke å fylles ut.*

**Signaturer:** *Ansvarlig veileder:* *Student:*

| ID nr. | Aktivitet/prosess | Ansvarlig | Eksisterende dokumentasjon | Eksisterende sikringstiltak | Lov, forskrift o.l. | Kommentar |
|---|---|---|---|---|---|---|
| 1a | Viklemaskin | Tran | Romopplæring, HMS kurs | Overbelastningsbryter, lysbrytere | | |
| 1b | Verkstedarbeid | Tran | Romopplæring, HMS kurs | Verneutstyr, skjerming, nødstoppere | | |
| 1c | Trykkprøving | Tran | Ukjent | Skjerming | | |
| 1d | Strekkprøving | Tran | Romopplæring, HMS kurs | Overbelastningsbryter, belastningssperre | | |
| 1e | Bruk av skjæreverktøy | Tran | Ukjent | | | |
| 1f | Bruk av sammenføyningsteknikker | Tran | Brukermanual og datablad | Datablad | Ukjent | |
| 1g | Autoclave | Tran | Romopplæring, HMS kurs | Skjerming | | |
| 2 | Tilstedeværelse ved arbeid utført av andre | Andre | | | | |

| NTNU<br>HMS | Risikovurdering | Utarbeidet av | Nummer | Dato |
|---|---|---|---|---|
| | | HMS-avd. | HMSRV2601 | 22.03.2011 |
| | | Godkjent av | | Erstatter |
| | | Rektor | | 01.12.2006 |

**Enhet: IPM** **Dato: 13.01.2016**

**Linjeleder: Torgeir Welo**

**Deltakere ved kartleggingen (m/ funksjon): Daniel Tran (student), Andreas Echtermeyer (veileder), Nils Petter Vedvik (medveileder)**
*(Ansv. Veileder, student, evt. medveiledere, evt. andre m. kompetanse)*

**Risikovurderingen gjelder hovedaktivitet:** Prosjektoppgave student Daniel Tran. "Filament winding of steel fiber composite tubes"

**Signaturer:** *Ansvarlig veileder:* *Student:*

| ID nr | Aktivitet fra kartleggings-skjemaet | Mulig uønsket hendelse/ belastning | Vurdering av sannsyn-lighet | Vurdering av konsekvens: | | | | Risiko-Verdi (menn-eske) | Kommentarer/status Forslag til tiltak |
|---|---|---|---|---|---|---|---|---|---|
| | | | (1-5) | Menneske (A-E) | Ytre miljø (A-E) | Øk/ materiell (A-E) | Om-dømme (A-E) | | |
| 1a | Viklemaskin | Innvikling, klemfare, henge seg fast, utvikle allergier | 1 | B | A | A | B | A1 | Skjerming, hansker, briller osv. |
| 1b | Verkstedarbeid | Kuttskader, klemskader, brannskader mm. | 4 | A | A | A | A | A4 | Nødvendig opplæring |
| 1c | Trykkprøving | Sprutakselerasjon, flyvende objekter, vannsprut | 5 | A | B | A | A | A5 | Skjerming, prøving i container, briller og hansker |
| 1d | Strekkprøving | Klemfare, henge seg fast | 1 | B | A | A | B | B1 | Skjerming, belastningssperre |
| 1e | Bruk av skjæreverktøy | Kuttskader | 5 | A | A | A | A | A5 | Hansker, briller |
| 1f | Bruk av sammenføyningsteknikker | Eksploskjonsfare, gasslekkasje, brannskader | 3 | C | C | C | B | C3 | Sammenføyningsutstyr, sveisebriller/hansker |
| 1g | Autoclave | Sprutakselerasjon, flyvende objekter, vannsprut | 4 | A | B | A | A | A4 | Skjerming, vernebriller, nødvendig opplæring |

| NTNU<br>HMS | Risikovurdering | Utarbeidet av | Nummer | Dato |
|---|---|---|---|---|
| | | HMS-avd. | HMSRV2601 | 22.03.2011 |
| | | Godkjent av | | Erstatter |
| | | Rektor | | 01.12.2006 |

| | | | | | | | | | |
|---|---|---|---|---|---|---|---|---|---|
| 2 | Tilstedeværelse ved arbeid utført av andre | Ukjent og avhengig av aktivitet | 4 | B | A | A | A | B4 | Verneutstyr og briller |

## Sannsynlighet vurderes etter følgende kriterier:

| Svært liten<br>1 | Liten<br>2 | Middels<br>3 | Stor<br>4 | Svært stor<br>5 |
|---|---|---|---|---|
| 1 gang pr 50 år eller sjeldnere | 1 gang pr 10 år eller sjeldnere | 1 gang pr år eller sjeldnere | 1 gang pr måned eller sjeldnere | Skjer ukentlig |

## Konsekvens vurderes etter følgende kriterier:

| Gradering | Menneske | Ytre miljø<br>Vann, jord og luft | Øk/materiell | Omdømme |
|---|---|---|---|---|
| **E**<br>**Svært Alvorlig** | Død | Svært langvarig og ikke reversibel skade | Drifts- eller aktivitetsstans >1 år. | Troverdighet og respekt betydelig og varig svekket |
| **D**<br>**Alvorlig** | Alvorlig personskade.<br>Mulig uførhet. | Langvarig skade. Lang restitusjonstid | Driftsstans > ½ år<br>Aktivitetsstans i opp til 1 år | Troverdighet og respekt betydelig svekket |
| **C**<br>**Moderat** | Alvorlig personskade. | Mindre skade og lang restitusjonstid | Drifts- eller aktivitetsstans < 1 mnd | Troverdighet og respekt svekket |
| **B**<br>**Liten** | Skade som krever medisinsk behandling | Mindre skade og kort restitusjonstid | Drifts- eller aktivitetsstans < 1uke | Negativ påvirkning på troverdighet og respekt |
| **A**<br>**Svært liten** | Skade som krever førstehjelp | Ubetydelig skade og kort restitusjonstid | Drifts- eller aktivitetsstans < 1dag | Liten påvirkning på troverdighet og respekt |

**Risikoverdi = Sannsynlighet x Konsekvens**
Beregn risikoverdi for Menneske. Enheten vurderer selv om de i tillegg vil beregne risikoverdi for Ytre miljø, Økonomi/materiell og Omdømme. I så fall beregnes disse hver for seg.

**Til kolonnen "Kommentarer/status, forslag til forebyggende og korrigerende tiltak":**
Tiltak kan påvirke både sannsynlighet og konsekvens. Prioriter tiltak som kan forhindre at hendelsen inntreffer, dvs. sannsynlighetsreduserende tiltak foran skjerpet beredskap, dvs. konsekvensreduserende tiltak.

| NTNU | Risikomatrise | utarbeidet av | Nummer | Dato | |
|---|---|---|---|---|---|
| | | HMS-avd. | HMSRV2604 | 08.03.2010 | |
| HMS/KS | | godkjent av | | Erstatter | |
| | | Rektor | | 09.02.2010 | |

## MATRISE FOR RISIKOVURDERINGER ved NTNU

| KONSEKVENS | | | | | | |
|---|---|---|---|---|---|---|
| | Svært alvorlig | E1 | E2 | E3 | E4 | E5 |
| | Alvorlig | D1 | D2 | D3 | D4 | D5 |
| | Moderat | C1 | C2 | C3 | C4 | C5 |
| | Liten | B1 | B2 | B3 | B4 | B5 |
| | Svært liten | A1 | A2 | A3 | A4 | A5 |
| | | Svært liten | Liten | Middels | Stor | Svært stor |
| | | SANNSYNLIGHET | | | | |

**Prinsipp over akseptkriterium. Forklaring av fargene som er brukt i risikomatrisen.**

| Farge | | Beskrivelse |
|---|---|---|
| Rød | | Uakseptabel risiko. Tiltak skal gjennomføres for å redusere risikoen. |
| Gul | | Vurderingsområde. Tiltak skal vurderes. |
| Grønn | | Akseptabel risiko. Tiltak kan vurderes ut fra andre hensyn. |

Appendix D Risk Assessment

# Appendix E Safety and Evaluation of Activities in the Laboratory and Workshop

| **Sikkerhets- og kvalitetsgjennomgang av laboratorietester og verkstedsarbeid**<br>***Safety and Quality Evaluation of Activities in the Laboratory and Workshop*** | NTNU<br>**Perleporten** |
|---|---|

| **1 Identifikasjon - *Identification*** | **Dokumentnr. – *Document no.*:** | |
|---|---|---|
| Kundenavn – *Customer name*<br>Daniel Tran | Prosjektnavn – *Project name*<br>Producing steel-fiber-reinforced polymer composite pipes | Projektnr. – *Project no.* |
| Beskrivelse av arbeid – *Description of job*<br>Bearbeide og vikling av kompositrør<br>Kompressiontesting av kompositrør<br>Ekstern trykktesting av kompositrør | | Dato – *Date*<br>*19.02.2016 - 10.06.2016* |

| **2 Projekt - *Team*** | | | |
|---|---|---|---|
| Prosjektleder og organisasjon – *Project manager and organisation* | Daniel Tran | Ansvarlig for instrumentering – *Responsible for instrumentation.* | Daniel Tran |
| Leiestedsansvarlig – *Laboratory responsible* | Daniel Tran | Operatør – *Operator* | Daniel Tran |
| Auditør for sikkerhets og kvalitetsgjennomgang – *Auditer for safety check* | Carl Magnus Midtbø | Ansvarlig for styring av forsøk – *Responsible for running the experiment.* | Daniel Tran |
| Ansvarlig for eksperimentelt faglig innhold – *Responsible for experimental and scientific content* | Daniel Tran | Ansvarlig for logging av forsøksdata – *Responsible for logging and storing experimental data* | Daniel Tran |
| Ansvarlig for dimensjonering av last og trykkpåkjente komponenter – *Reponsible for dimensioning load bearing and pressurized components* | Daniel Tran | Ansvarlig for montering av testrigg – *Responsible for building the rig* | Daniel Tran |

| **3 Viktig!! – *Important!!*** | J: Ja – *Yes* / N: Nei - *No* |
|---|---|
| Er arbeidsordren signert? – *Is the work order signed?* | J |
| Har operatøren nødvendig kurs/trening i bruk av utstyret? - *Has the operator the required courses/training on the equipment?* | J |
| Har operatøren sikkerhetskurs? (påbudt) – *Has the operator followed the safety courses? (mandatory)* | J |
| Kan jobben gjøres alene? - *Can the work be done alone?* | N |
| - Dersom ja, er det med visse forbehold (for eksempel, må bruke alarm, ha avtale med noen som kommer innom med jevne mellomrom eller lignende). Dette må vurderes i Seksjon 5.<br>*If yes, the work may have to be done under special conditions (e. g. must use the alarm, have agreement with somebody coming back periodically or similar). This shall be evaluated in Section 5.* | |

| **4.1 Sikkerhet – *Safety*** (Testen medfører – *The test contains*) | | | J: Ja – *Yes* / N: Nei - *No* |
|---|---|---|---|
| Stor last – *Big loads* | N | Brannfare – *Danger of fire* | N |
| Tunge løft – *Heavy lifting* | J | Arbeid i høyden – *Working at heights* | N |
| Hengende last – *Hanging load* | N | Hydraulisk trykk – *Hydraulic pressure* | J |
| Gasstrykk – *Gas pressure* | N | Vanntrykk – *Water pressure* | J |
| Høy temperatur – *High temperature* | N | Lav temperatur – *Low temperature* | N |
| Deler i høy hastighet – *Parts at high velocity* | J | Farlige kjemikalier – *Dangerous chemicals* | N |
| Sprutakselerasjon ved brudd – *Sudden acceleration at fracture/failure* | J | Forspente komponenter – *Pre-tensioned components* | J |
| Farlig støv – *Dangerous dust* | N | Kraftig støy – *Severe noise* | J |
| Klemfare – *Danger of pinching* | J | Roterende deler – *Rotating parts* | J |

| **4.2 Påkrevet verneustyr – *Required safety equipment*** | | | J: Ja – *Yes* / N: Nei - *No* |
|---|---|---|---|
| Briller (påbudt) – *Glasses (mandatory)* | J | Vernesko – *Safety shoes* | J |
| Hjelm – *Helmet* | N | Hansker – *Gloves* | J |
| Skjerm – *Screen* | J | Visir – *Visir* | N |
| Hørselsvern – *Ear protection* | J | Løfteredskap – *Lifting equipment* | J |

| | | | |
|---|---|---|---|
| Yrkessele, fallsele, etc. – *Harness ropes, other measures to prevent falling down.* | N | | |

# Sikkerhets- og kvalitetsgjennomgang av laboratorietester og verkstedsarbeid

NTNU
Perleporten

**5.1 Beskrivelse av aktivitet – *Description of the activity (see Appendix)***

| | |
|---|---|
| Vurdering skal være basert på en skriftlig prosedyre for bruk av maskinen. I enkelte tilfeller kan prosedyre bli beskrevet direkte i tabellen nedenfor. | *The evaluation shall be based on a written operating procedure for the machine. For simple cases the procedure can be directly described in the tables below.* |

| Nr. | Beskrivelse av aktivitet – *Description of activity* | Fare - *Danger* | Lov, forskrift o.l. – *Legal requirements* | Prosedyre nr. – *Procedure no.* | Sannsynlighet – *Probability* | Konsekvens –*Consequence* | Risiko – *Risk* |
|---|---|---|---|---|---|---|---|
| 1 | Bruk av sirkelsag | Skade på kropp | HMS-regler v/NTNU | 1 | 3 | C | 3C |
| 2 | Verkstedarbeid (både mellom 08-16 og 16-08) | Sprutakselerasjon, kuttskader, klemskader, skade på maskiner | HMS-regler v/NTNU | 2 | 2 | B | 2B |
| 3 | Kompresjonstesting av karbonrør og stålrør (både mellom 08-16 og 16-08) | Sprutakselerasjon ved brudd, skade på kropp/maskiner | HMS-regler v/NTNU | 3 | 2 | C | 2C |
| 4 | Håndtering av epoxy, bearbeiding og påføring av release agent/wax (både mellom 08-16 og 16-08) | Uønsket reaksjon mellom epoxy og kropp/miljø | MSDS for oppgitt epoxy | 4 | 3 | C | 3C |
| 5 | Sette opp viklemaskin for forsøk + nedrigging (både mellom 08-16 og 16-08) | Skade på kropp/maskiner | HMS-regler v/NTNU | 5 | 2 | B | 2B |
| 6 | Utføre viklejobb (både mellom 08-16 og 16-08) | Skade på kropp/maskiner, uønsket reaksjon mellom epoxy og kropp/miljø | HMS-regler v/NTNU | 6 | 3 | C | 3C |
| 7 | Postcuring (både mellom 08-16 og 16-08) | Skade på kropp/maskiner | MSDS for oppgitt epoxy | 7 | 1 | B | 1B |
| 8 | Bruk av propangassbrenner på metall og epoxy (både mellom 08-16 og 16-08) | Skade på kropp/miljø | HMS-regler v/NTNU | 8 | 2 | B | 2B |
| 9 | Løftekran (både mellom 08-16 og 16-08) | Skade på kropp, klemskader, skade på maskiner | HMS-regler v/NTNU | 9 | 2 | B | 2B |
| 10 | Eksternt trykktest (både mellom 08-16 og 16-08) | Sprutakselerasjon ved brudd, skade på kropp/maskiner | HMS-regler v/NTNU | 10 | 2 | C | 2C |
| | | | | | | | |
| | | | | | | | |
| | | | | | | | |

**5.2 Korrigerende Tiltak – *Corrective Actions***

| Nr. | Korrigerende tiltak – Corrective action | Sannsynlighet | Konsekvens | Risiko | Utført dato |
|---|---|---|---|---|---|

| | | – *Probability* | – *Consequence* | – *Risk* | – *Date of action* |
|---|---|---|---|---|---|
| 1 | Holde avstand til sagblad, bruke hørselvern og vernebriller.<br>Være minst 2 personer tilstede under bruk. | 1 | A | 1A | *19.02.2016* |
| 2 | Bruke vernebriller, forhøre deg med verkstedpersonell ved nye aktiviteter, ikke bruk tykke hansker. | 1 | A | 1A | *19.02.2016* |
| 3 | Bruke skjerm og vernbriller, bruk passende grenseverdier på Instron. Sette opp klare sperrer som hindrer andre i å forstyrre prosessen. Gi beskjed til verkstedpersonell om test så de vet hva som foregår til en hver tid. Gi også beskjed til andre om at test pågår. | 1 | A | 1A | *19.02.2016* |
| 4 | Bruk åndedrettsvern og hansker. Kast påføringsverktøy i ett lisensert avfallsdepot. Være minst 2 personer tilstede ved håndtering. | 1 | A | 1A | *19.02.2016* |
| 5 | Vær fokusert. Unngå brå bevegelser. Være minst 2 personer tilstede ved håndtering. | 1 | A | 1A | *19.02.2016* |
| 6 | Ha en operatør uten hansker og en med hansker, med klare arbeidsfordelinger.<br>Start maskin i lav hastighet. | 1 | A | 1A | *19.02.2016* |
| 7 | Sette opp klare sperrer som hindrer andre i å forstyrre prosessen. | 1 | A | 1A | *19.02.2016* |
| 8 | Bruke hansker og evt. tang/tvinge til håndtering, bruk gassmaske ved brenning av epoxy.<br>Vit hvor brannslukkingsapparat befinner seg. | 1 | A | 1A | *19.02.2016* |
| 9 | Ha en operatør uten hansker og en med hansker, med klare arbeidsfordelinger.<br>Start kran i lav hastighet. Kurs fra verkstedansvarlig. | 1 | A | 1A | *19.02.2016* |
| 10 | Bruke skjerm og vernbriller, bruk passende trykk, ikke overstig makstrykk grense for trykktank. Sette opp klare sperrer som hindrer andre i å forstyrre prosessen. Gi beskjed til verkstedpersonell om test så de vet hva som foregår til en hver tid. Gi også beskjed til andre om at test pågår. | 1 | A | 1A | *19.02.2016* |
| | | | | | |

# Sikkerhets og kvalitetsgjennomgang av laboratorietester og verkstedsarbeid

NTNU
Perleporten

## 5.3 Feilkilder – *Reasons for mistakes/errors*

***Sjekkliste: Er følgende feilkilder vurdert? – Check list: Is the following considered?*** J: Ja – *Yes* / N: Nei - *No*

| | | | |
|---|---|---|---|
| Tap av strøm – *Loss of electricity* | **J** | Overspenning – *Voltage surge* | **J** |
| Elektromagnetisk støy – *Electromagnetic noise* | **J** | Manglende aggregatkapasitet av hydraulikk – *Insufficient power of the machine* | **J** |
| Jordfeil – *Electrical earth failure* | **J** | Vannsprut – *Water jet* | **J** |
| Ustabilt trykk av hydraulikk/kraft – *Unstable pressure or hydraulic force* | **J** | Tilfeldig avbrudd av hydraulikk/kraft – *Unintended interruption of power supply* | **J** |
| Last-/ forskyvnings grenser etablert ? – *Are load and displacement limits established?* | **J** | Lekkasjer (slanger/koblinger, etc.) – *Leakage of pipes, hoses, joints, etc.* | **J** |
| Mulige påvirkninger fra andre aktiviteter – *Possible interference from other activities* | **J** | Mulige påvirkninger på andre aktiviteter – *Possible interference towards other activities* | **J** |
| Problemer med datalogging og lagring – *Troubles in loading and storage* | **J** | Brann i laboratoriet – *Fire in the laboratory* | **J** |

## 6 Kalibreringsstatus for utstyr – *Calibration of equipment*

***(ex: load cell, extensometer, pressure transducer, etc)***

| I.D. | Utstyr - *Equipment* | Gyldig til (dato) – *Valid until (date)* |
|---|---|---|
| 1 | Pressure transducer | |
| 2 | Schlenk 250 kN | |
| | | |
| | | |
| | | |
| | | |
| | | |

## 7 Sporbarhet – *Tracebility*

| Eksisterer – Is there | J: Ja – *Yes* / N: Nei - *No* |
|---|---|
| Er alle prøvematerialene kjente og identifiserbare? – *Are all experimental materials known and traceable?* | J |
| Eksisterer det en plan for markering av alle prøvene? – *Is there a plan for marking all specimens?* | J |
| Er dataloggingsutstyret identifisert? – *Is the data aquisition equipment identified?* | J |
| Er originaldata lagret uten modifikasjon? – *Are the original data stored safely without modification?* | J |
| Eksisterer det en backup-prosedyre? – *Is there a back-up procedure for the data (hard disk crash)?* | J |
| Eksisterer det en plan for lagring av prøvestykker etter testing? – *Is there a plan for storing samples after testing?* | J |
| Eksisterer en plan for avhending av gamle prøvestykker? – *Is there a plan for disposing of old samples?* | J |

## 8 Kommentarer – *Comments*

## 9 Signaturer – *Signatures*

***Godkjent (dato/sign) – Approved (date/signature)***

| Prosjektleder – *Project leader* | Verifikatør – *Verifier* | Godkjent – *Approved by* |
|---|---|---|
| Daniel Tvan | | Carl Magnus M |

| **Sikkerhets og kvalitetsgjennomgang av laboratorietester og verkstedsarbeid** | NTNU Perleporten |
|---|---|
| **APPENDIX** Bakgrunn - Background | |

## Sannsynlighet vurderes etter følgende kriterier:

*Probability shall be evaluated using the following criteria:*

| **Svært liten**<br>Very unlikely<br>**1** | **Liten**<br>Unlikely<br>**2** | **Middels**<br>Probable<br>**3** | **Stor**<br>Very Probable<br>**4** | **Svært stor**<br>Nearly certain<br>**5** |
|---|---|---|---|---|
| 1 gang/50 år eller sjeldnere<br>*– Once per 50 years or less* | 1 gang/10 år eller sjeldnere<br>*– Once per 10 years or less* | 1 gang/år eller sjeldnere<br>*– Once a year or less* | 1 gang/måned eller sjeldnere<br>*– Once a month or less* | Skjer ukentlig<br>*– Once a week* |

## Konsekvens vurderes etter følgende kriterier:

*Consequence shall be evaluated using the following criteria:*

| **Gradering**<br>*– Grading* | **Menneske**<br>*– Human* | **Ytre miljø, Vann, jord og luft**<br>*– Environment* | **Øk/materiell**<br>*– Financial/Material* | **Omdømme**<br>*– Reputation* |
|---|---|---|---|---|
| **E**<br>**Svært Alvorlig**<br>***– Very critical*** | Død – Death | Svært langvarig og ikke reversibel skade<br>*– Very prolonged, non-reversible damage* | Drifts- eller aktivitetsstans >1 år.<br>*– Shutdown of work >1 year.* | Troverdighet og respekt betydelig og varig svekket<br>*– Trustworthiness and respect are severely reduced for a long time.* |
| **D**<br>**Alvorlig**<br>***– Critical*** | Alvorlig personskade. Mulig uførhet.<br>*– May produce fatality/ies* | Langvarig skade. Lang restitusjonstid<br>*– Prolonged damage. Long recovery time.* | Driftsstans > ½ år<br>Aktivitetsstans i opp til 1 år<br>*– Shutdown of work 0,5-1 year.* | Troverdighet og respekt betydelig svekket<br>*– Trustworthiness and respect are severely reduced.* |
| **C**<br>**Moderat**<br>***– Dangerous*** | Alvorlig personskade.<br>*– Permanent injury, may produce serious health damage/sickness* | Mindre skade og lang restitusjonstid<br>*– Minor damage. Long recovery time* | Drifts- eller aktivitetsstans < 1 mnd<br>*– Shutdown of work < 1 month.* | Troverdighet og respekt svekket<br>*– Troverdighet og respekt svekket.* |
| **B**<br>**Liten**<br>***– Relatively safe*** | Skade som krever medisinsk behandling<br>*– Injury that requires medical treatment* | Mindre skade og kort restitusjonstid<br>*– Minor damage. Short recovery time* | Drifts- eller aktivitetsstans < 1uke<br>*– Shutdown of work < 1 week.* | Negativ påvirkning på troverdighet og respekt<br>*– Negative influence on trustworthiness and respect.* |
| **A**<br>**Siker**<br>**- Safe** | Injury that requires first aid | Insignificant damage. Short recovery time | Shutdown of work < 1day | |
| | | | | |

**Risikoverdi = Sannsynlighet X Konsekvenser**

Beregn risikoverdi for menneske. IPM vurderer selv om de i tillegg beregner risikoverdi for ytre miljø, økonomie/ material og omdømme. I så fall beregnes disse hver for seg.

**Risk = Probability X Consequence**

Calculate risk level for humans. IPM shall evaluate itself if it shall calculate in addition risk for the environment, economic/material and reputation. If so, the risks shall be calculated separately.

## Risikomatrisen
*Risk Matrix*

I risikomatrisen er ulike grader av risiko merket med rød, gul eller grønn:

Rød: Uakseptabel risiko. Tiltak skal gjennomføres for å redusere riskoen.

Gul: Vurderingsområde. Tiltak skal vurderes.

Grønn: Akseptabel risiko. Tiltak kan vurderes ut fra andre hensyn.

Når risikoverdien havner på rødt felt, skal altså enheten gjennomføre tiltak for å redusere risikoen. Etter at tiltak er iverksatt, skal dere foreta ny risikovurdering for å se om risikoen har sunket til akseptabelt nivå.

For å få oversikt over samlet risiko: Skriv risikoverdi og aktivitetens IDnr. i risikomatrise (docx) / risikomatrise (odt). Eksempel: Aktivitet med IDnr. 1 har fått risikoverdi 3D. I felt 3D i risikomatrisen skriver du IDnr. 1. Gjør likedan for alle aktiviteter som har fått en risikoverdi. En annen måte å skaffe oversikt på, er å fargelegge feltet med risikoverdien i skjemaet for risikovurdering. Dette tydeliggjør og gir samlet oversikt over riskoforholdene. Ledelse og brukere får slik et godt bilde av risikoforhold og hva som må prioriteres.

In the risk matrix different degrees of risk are marked with red, yellow or green;

Red: Unacceptable risk. Measures shall be taken to reduce the risk.

Yellow: Assessment Area . Measures to be considered.

Green: Acceptable risk. Measures can be evaluated based on other considerations.

When a risk value is red, the unit shall implement measures to reduce risk. After the action is taken, you will make a new risk assessment to see if the risk has decreased to acceptable levels.

To get an overview of the overall risk: Write the risk value and the task ID no . the risk matrix ( docx ) / risk matrix ( odt ) . Example : Activity with ID no . 1 has been risk value 3D. In the field of 3D risk matrix type ID no . 1 Do the same for all activities that have been a risk . Another way to get an overview is to color the field of risk value in the form of risk assessment . This clarifies and gives overview of the risk factors . Management and users get such a good picture of the risks and what needs to be prioritized.

| KONSEKVENS | | | | | | |
|---|---|---|---|---|---|---|
| | Svært alvorlig | E1 | E2 | E3 | E4 | E5 |
| | Alvorlig | D1 | D2 | D3 | D4 | D5 |
| | Moderat | C1 | C2 | C3 | C4 | C5 |
| | Liten | B1 | B2 | B3 | B4 | B5 |
| | Svært liten | A1 | A2 | A3 | A4 | A5 |
| | | Svært liten | Liten | Middels | Stor | Svært stor |
| | | SANNSYNLIGHET | | | | |

**Prinsipp over akseptkriterium. Forklaring av fargene som er brukt i risikomatrisen.**

| Farge | | Beskrivelse |
|---|---|---|
| Rød | | Uakseptabel risiko. Tiltak skal gjennomføres for å redusere risikoen. |
| Gul | | Vurderingsområde. Tiltak skal vurderes. |
| Grønn | | Akseptabel risiko. Tiltak kan vurderes ut fra andre hensyn. |

---

**Til Kolonnen "Korrigerende Tiltak":**

Tiltak kan påvirke både sannsynlighet og konsekvens. Prioriter tiltak som kan forhindre at hendelsen inntreffer, dvs sannsynlighetsreduserende tiltak foran skjerpende beredskap, dvs konsekvensreduserende tiltak.

**For Column "Corrective Actions"**

Corrections can influence both probability and consequence. Prioritize actions that can prevent an event from happening.

---

**Oppfølging:**

Tiltak fra risikovurderingen skal følges opp gjennom en handlingsplan med ansvarlige personer og tidsfrister.

**Follow Up**

Actions from the risk evaluation shall be followed through by an action plan with responsible persons and time limits.

Etterarbeid #

- Gå gjennom aktiviteten/prosessen på nytt.
- Foreta eventuell ny befaring av aktiviteten/prosessen for enten a) å få bekreftet at risikoverdiene er akseptable eller b) for å justere risikoverdiene.
- Gå gjennom, vurder og prioriter tiltak for å forebygge uønskede hendelser. Først skal dere prioritere tiltak som reduserer sannsynlighet for risiko. Dernest skal dere ta for dere tiltak som reduserer risiko for konsekvenser.
- Tiltakene skal føres inn i handlingsplanen. Skriv fristen for å gjennomføre tiltaket (dato, ikke tidsrom) og navn på den / de som har ansvar for tiltakene.
- Foreta helhetsvurdering for å avgjøre om det nå er akseptabel risiko.
- Ferdig risikovurdering danner grunnlag for å utarbeide lokale retningslinjer og HMS-dokumenter, opplæring og valg av sikkerhetsutstyr.
- Ferdig risikovurdering og eventuelle nye retningslinjer gjøres kjent/tilgjengelig for alle involverte.
- Sett eventuelt opp kostnadsoverslag over planlagte tiltak.